THE HIGGS BOSON H^0

Revised October 2013 by M. Carena (Fermi National Accelerator Laboratory and the University of Chicago), C. Grojean (ICREA at IFAE, Universitat Autònoma de Barcelona), M. Kado (LAL and CERN), and V. Sharma (University of California San Diego).

I. Introduction

The announcement on 4th July 2012 of the observation by ATLAS [1] and CMS [2] of a new boson with a mass of about 125 GeV decaying into $\gamma\gamma$, WW and ZZ bosons and the subsequent studies of the properties of this particle have provided an important leap forward in the understanding of the mechanism that breaks electroweak symmetry and generates the masses of the known elementary particles[1], one of the most fundamental problems in particle physics. The Brout–Englert–Higgs mechanism [3] provides a general framework to keep untouched the structure of the gauge interactions at high energy and still generate the observed masses of the $W^{\pm}$ and Z gauge bosons by means of charged and neutral Goldstone bosons that manifest themselves as the longitudinal components of the gauge bosons in the ultraviolet. For several decades, the origin of these Goldstone bosons remained unclear. The discovery of ATLAS and CMS [1,2] now strongly suggests that these three Goldstone bosons combine with an extra elementary scalar field to form a weak doublet. This picture matches very well with the Standard

[1] In the case of neutrinos, it is possible that the Higgs mechanism plays a role but is not entirely responsible for the generation of their observed masses.

Model (SM)) [4] which describes the electroweak interactions by a gauge field theory invariant under the $SU(3) \times SU(2)_L \times U(1)_Y$ symmetry group. The Brout–Englert–Higgs mechanism posits a self-interacting complex doublet of scalar fields, and renormalizable interactions are arranged such that the neutral component of the scalar doublet acquires a vacuum expectation value (VEV) $v \approx 246$ GeV, which sets the scale of electroweak symmetry breaking (EWSB). Three massless Goldstone bosons are generated, which are absorbed to give masses to the $W^{\pm}$ and Z gauge bosons. The remaining component of the complex doublet becomes the Higgs boson — a new fundamental scalar particle. The masses of all fermions are also a consequence of EWSB since the Higgs doublet is postulated to couple to the fermions through Yukawa interactions. However, the true structure of newly discovered boson and the exact dynamics at the origin of the Higgs VEV and its ultraviolet completion are still unsolved. Even if the discovered boson has weak coupling to all known SM degrees of freedom, it is not impossible that it emerges from a light resonance of a strongly coupled sector. And it should be established whether the Higgs boson is solitary or whether other states, possibly a full second weak doublet, populate the EWSB sector.

The main reason to expect new physics beyond the recently discovered Higgs boson is the Higgs boson itself. The Higgs boson is special, because without it the calculability power of the SM would have been spoiled. In particular, without a Higgs boson, pertubative unitarity [5,6] would be lost at high energies since the longitudinal W boson scattering amplitude would grow as the center of mass energy increases, and loops involving the longitudinal component of the gauge bosons contributing to the self energies, for example, would not be finite. With the discovery of the Higgs, it has been experimentally established that the SM is based on a gauge theory that can be consistently extrapolated to the Planck scale. The Higgs must have couplings to W/Z gauge bosons and fermions precisely as those in the SM to recover consistency of the theory, hence, from the calculability point of view there is no need for new physics at the EW scale. However, the SM Higgs boson is a scalar field,

hence its mass is not protected by any symmetry and at the quantum level has sensitivity to the physics in the ultraviolet

$$m_H^2(Q) = m_H^2(\mu) + \delta_{m_H}^2,$$

$$\delta_{m_H}^2 = \frac{3m_{F,B}^2}{8\pi^2}\lambda_{F,B}^2(-1)^{2S}\ln\left(\mu^2/Q^2\right) \quad (1)$$

Given the value of the Higgs mass (or equivalently the Higgs mass parameter in the scalar potential) at a scale μ as input, the value of the Higgs mass at another scale Q, e.g. the electroweak scale, receives contributions that depend quadratically on all the masses $m_{F,B}$ of the particles that interact with the Higgs with couplings $\lambda_{F,B}$, respectively, with the sign depending on the spin of the particle. Hence, in general, light scalars like the Higgs boson cannot naturally survive in the presence of heavy states at the GUT, String or Planck scales. This is known as the hierarchy or naturalness problem of the SM [7].

There are two possible, preferred solutions to the naturalness problem:one is based on a new fermion-boson symmetry in nature called Supersymmetry (SUSY) [8,9,10]. This is a weakly coupled approach to EWSB and in this case the Higgs boson remains elementary but its mass is protected by the new fermion-boson symmetry. These theories predict at least five Higgs particles [11] [2], and one of the neutral Higgs bosons, most often the lightest CP-even Higgs, has properties that resemble those of the SM Higgs boson. We refer to this Higgs boson as a SM-like Higgs, meaning that this is the Higgs responsible for EWSB, and hence has SM-like couplings to the W and Z gauge bosons. It is also possible to have extensions of the SM without low energy Supersymmetry, but with extended Higgs sectors. The most commonly studied alternatives are two Higgs Doublets Models (2HDM's) that can have different types of coupling structure to fermions that are restricted by experimental constraints related to flavor changing neutral and charged current effects. The other approach invokes the existence of

[2] Except in exotic susy scenarios where the Higgs boson is identified as a sneutrino, the scalar partner of a neutrino [12], in which case the gauge anomalies cancel without the need for a second Higgs doublet.

strong interactions at a scale of order a TeV or above and induces strong breaking of the electroweak symmetry [13]. In the original incarnation of this second approach, dubbed technicolor, the strong interactions themselves were triggering EWSB without the need of a Higgs boson. Another possibility, more compatible with the ATLAS and CMS discovery, is that the strong interactions produce 4 light resonances identified with the Higgs doublet and EWSB proceeds through vacuum misalignement [14]. Both approaches can have important effects on the phenomenology of the Higgs boson associated to EWSB. Also, in each case the Higgs role in unitarization is shared by other particles: additional Higgs bosons in supersymmetry or 2HDM's, or new particles in the strong sector. In Section V we will discuss in detail some of the most interesting models proposed in these two categories.

The naturalness problem has been the prime argument for new physics at the TeV scale. But the absence of any direct signal of new dynamics and the appalling compliance of the Higgs couplings with the SM prediction together with the strong bounds inherited from precision electroweak and flavor data might suggest that the light Higgs mass is not natural and that the Higgs boson is after all elementary, weakly coupled and solitary till the Planck scale. Such a scenario, if established experimentally, will force the theorists to rethink the basic concepts of high energy physics, starting with the original principles of quantum mechanics and special relativity.

II. The Standard Model and the Brout–Englert–Higgs Mechanism

As mentioned above, In the SM [4], the Brout–Englert–Higgs Mechanism [3] is responsible for generating mass for the W and Z gauge bosons rendering the weak interactions short range. The SM scalar potential reads:

$$V(\Phi) = m^2 \Phi^\dagger \Phi + \lambda \left(\Phi^\dagger \Phi \right)^2 \tag{2}$$

with the Higgs field ϕ being a self interacting $SU(2)$ complex doublet (four real degrees of freedom) with weak hypercharge Y=1 (the hypercharge is normalized such that $Q = T_{3L} + Y/2$):

$$\Phi = \frac{1}{\sqrt{2}} \begin{pmatrix} \phi^+ \\ \phi^0 + ia^0 \end{pmatrix}.$$

$V(\Phi)$ is the most general renormalizable scalar potential and if the quadratic term is negative the neutral component of the scalar doublet acquires a non-zero vacuum expectation value (vev)

$$\langle \phi \rangle = \frac{1}{\sqrt{2}} \begin{pmatrix} 0 \\ v \end{pmatrix},$$

defining $\phi^0 = H + v$, inducing the spontaneous breaking of the SM gauge symmetry $SU(3)_C \times SU(2)_L \times U(1)_Y$ into $SU(3)_C \times U(1)_{\rm em}$. The global minimum of the theory defines the ground state, and spontaneous symmetry breaking implies that there is a symmetry of the system (Lagrangian) that is not respected by the ground state. The Higgs potential describes the energetics of turning on the Higgs field, that permeates all the universe and through its self-interactions can cause spontaneous electroweak symmetry-breaking (EWSB) in the vacuum without picking a preferred frame or direction. From the 4 generators of the $SU(2)_L \times U(1)_Y$ gauge group, three are spontaneously broken, implying that they lead to non-trivial transformations of the ground state and indicate the existence of three massless Goldstone bosons identified with three of the four Higgs field degrees of freedom. The Higgs field couples to the W_μ and B_μ gauge fields associated to the $SU(2)_L \times U(1)_Y$ local symmetry, respectively, through the covariant derivative, $D_\mu \Phi = (\partial_\mu + igW_\mu + ig' \frac{Y}{2} B_\mu)\Phi$ appearing in the kinetic term of the Higgs Lagrangian

$$\mathcal{L}_{\rm Higgs} = (D_\mu \Phi)^\dagger (D^\mu \Phi) - V(\Phi),$$

where g_1 and g_2 are the corresponding gauge couplings. As a result, the neutral and the two charged massless Goldstone degrees of freedom mix with the gauge fields corresponding to the broken generators of $SU(2)_L \times U(1)_Y$ and become the longitudinal components of the Z and W physical gauge bosons,

respectively. The fourth generator remains unbroken since it is the one associated to the conserved $U(1)_{\rm em}$ gauge symmetry, and its corresponding gauge field, the photon, remains massless. Similarly the eight color gauge bosons, the gluons, corresponding to the conserved $SU(3)_C$ gauge symmetry with 8 unbroken generators, also remain massless. Hence, from the initial 4 degrees of freedom of the Higgs field, 2 are absorded by the $W^{\pm}$ gauge bosons and one by the Z gauge boson that become massive:

$$M_W^2 = \frac{g^2 v^2}{4} \qquad M_Z^2 = \frac{\left(g'^2 + g^2\right) v^2}{4}.$$

There is one remaining degree of freedom, H, that is the physical Higgs boson — a new scalar particle. The Higgs boson is neutral under the electromagnetic interactions and transforms as a singlet under $SU(3)_C$ and hence it does not couple at tree level to the massless photons and gluons. The fermions of the SM acquire mass through a new type of renormalizable interaction between the Higgs field and the fermions: the Yukawa interaction

$$\mathcal{L}_{\rm Yukawa} = -\left(h_d\right)_{ij} \bar{q}_{L_i} \Phi \; d_{R_j} - \left(h_u\right)_{ij} \bar{q}_{L_i} \tilde{\Phi} u_{R_j} - \left(h_l\right)_{ij} \bar{l}_{L_i} \Phi \; e_{R_j} + h.c.$$

that respect the symmetries of the SM but generate fermion masses once EWSB occur. In the above, $\tilde{\phi} = i\sigma_2 \phi^*$ and q_L (l_L) and u_R, d_R (e_R) are the quark (lepton) $SU(2)_L$ doublets and singlets, respectively, while each term is parametrized by a 3x3 matrix in family space. We have omitted a mass term for neutrinos that could be added in analogous manner to the up type quarks when right-handed neutrinos are supplementing the SM particle content. Once the Higgs acquires a vev, all fermions acquire a mass given by $m_f = h_f v/\sqrt{2}$.

II.1. The SM Higgs boson mass, couplings and quantum numbers

The SM Higgs boson is a CP-even scalar of spin 0. Its mass is given by $m_H = \sqrt{2\lambda}\; v$, where λ is the Higgs self-coupling parameter in $V(\Phi)$. The expectation value of the Higgs field, $v = (\sqrt{2} G_F)^{-1/2} \approx 246$ GeV, is fixed by the Fermi coupling G_F, which is determined with a precision of 0.6 ppm from muon

decay measurements [15]. The quartic coupling λ, instead, is a free parameter in the SM, and hence there is a priori no prediction for the Higgs mass. Moreover the mass parameter $\mu^2 = -\lambda v^2$. Therefore, if the newly discovered particle is indeed the SM Higgs with $m_H \simeq$125.5 GeV, that implies that $\lambda \simeq 0.13$ and $|\mu| \simeq 88.8$ GeV. It is interesting to observe that in the SM one needs to assume that the mass term in the potential is negative to trigger EWSB. In other theories Beyond the SM (BSM), such as Supersymmetry, instead, the analogous of the Higgs mass parameter is rendered negative dynamically.

The Higgs boson couples to all particles proportionally to their masses. This is a new type of interaction, very weak for ordinary particles, such as up, down quarks and electrons but strong for heavy particles such as the W and Z bosons and the top quark. In particular, the SM Higgs couplings to fundamental fermions are proportional to the fermion masses, and the couplings to bosons are proportional to the square of the boson masses. The SM Higgs boson couplings to gauge bosons, Higgs bosons and fermions are summarized in the following Lagrangian:

$$\mathcal{L} = -g_{Hff}\bar{f}fH + \frac{g_{HHH}}{6}H^3 + \frac{g_{HHHH}}{24}H^4$$

$$+\delta_V V_\mu V^\mu \left(g_{HVV}H + \frac{g_{HHVV}}{2}H^2\right)$$

with

$$g_{Hf\bar{f}} = \frac{m_f}{v}, \quad g_{HVV} = \frac{2m_V^2}{v}, \quad g_{HHVV} = \frac{2m_V^2}{v^2}$$

$$g_{HHH} = \frac{3m_H^2}{v} \quad g_{HHHH} = \frac{3m_H^2}{v^2}$$

where $V = \mathrm{W}^\pm$ or Z and $\delta_W = 1, \delta_Z = 1/2$. As a result, the dominant mechanisms for Higgs boson production and decay involve the coupling of the H to the $\mathrm{W}^\pm$, Z and/or the third generation quarks and leptons. The Higgs boson's coupling to gluons, is induced at leading order by a one-loop graph in which the H couples to a virtual $t\bar{t}$ pair. Likewise, the Higgs boson's coupling to photons is also generated via loops, although in this case the one-loop graph with a virtual W^+W^- pair provides the dominant contribution [11] and the one involving a virtual

$t\bar{t}$ pair is subdominant. Reviews of the SM Higgs boson's properties and phenomenology, with an emphasis on the impact of loop corrections to the Higgs boson decay rates and cross sections, can be found in Refs. [16,17,18,19,20,21].

II.2. The SM custodial symmetry

The SM Higgs Lagrangian, $\mathcal{L}_{\rm Higgs}$, is by construction $SU(2)_L \times U(1)_Y$ gauge invariant, but it also has and approximate global symmetry. One can show that in the limit $g' \to 0$ and $h_f \to 0$, the Higgs sector has a global $SU(2)_R$ symmetry, and hence in such limit it is invariant under a global $SU(2)_L \times SU(2)_R$ symmetry, with $SU(2)_L$ just being the global variant of the SM chiral gauge symmetry. The $U(1)_Y$ group is a subgroup of $SU(2)_R$ and given that g' is naturally very small, it follows that $SU(2)_R$ is an approximate, accidental symmetry of the SM Higgs sector. Once the Higgs acquires a vev, then both the $SU(2)_L$ and $SU(2)_R$ symmetry groups are broken but the subgroup $SU(2)_{L+R}$ remains unbroken and is the subgroup that defines the custodial symmetry of the SM [22].

We explained above that the W and Z gauge boson masses are given in term of the gauge couplings, thus

$$\frac{M_W^2}{M_Z^2} = \frac{g^2}{g'^2 + g^2} = \cos^2\theta_W \qquad \text{or} \qquad \rho = \frac{\mathrm{M_W^2}}{\mathrm{M_Z^2}\cos^2\theta_\mathrm{W}} = 1$$

at tree level. In the limit $g' \to 0$ ($\sin^2\theta_W \to 0$), the W and Z gauge bosons have equal mass and form a triplet of the $SU(2)_{L+R}$ unbroken global symmetry. This in turn implies that radiative corrections to the ρ parameter involving the Higgs are proportional to g'^2 and the custodial symmetry guards the tree level relation between W and Z gauge boson masses from radiative corrections. There are also some radiative corrections generated by massive fermions. They are proportional to $m_t^2 + m_b^2 - 2(m_t^2 m_b^2)\,\log(m_t^2/m_b^2)/(m_t^2 - m_b^2)$ and vanish in the custodial limit $m_t = m_b$ [23].

One can conceive BSM theories in which the Higgs is a pseudo-Nambu–Goldstone boson of a strongly interacting sector [24], and/or where there are additional degrees of freedom that may contribute to the W and Z mass via virtual loops, but inasmuch as the electroweak sector has a manifest

custodial symmetry, the theory will be protected from large radiative corrections. Precision measurement observables are powerful in constraining such large radiative corrections. Hence, the custodial isospin symmetry is a powerful probe of BSM physics. For a pedagogical discussion see Ref. [25].

II.3. Stability of the Higgs Potential

The discovery of a scalar particle with mass $m_H \approx 125.5$ GeV has far reaching consequences within the SM framework. Such a low value of the Higgs mass is in perfect agreement with the upper bound on the Higgs boson mass from perturbative unitarity constraints [5,6]. Moreover, the precise value of m_H determines the value of the quartic coupling λ at the electroweak scale and makes it possible to investigate its behavior up to high energy scales. If m_H were too large then the Higgs self-coupling would become non-perturbative at some scale Λ that could be well below the Planck scale. Considering the measured values of the Higgs mass, the top quark mass, the W and Z boson masses, and the strong gauge coupling, all within their experimental uncertainties, it follows that, the same as the SM gauge and Yukawa couplings, the Higgs quartic coupling remains perturbative all the way up to M_{Planck} [26]. The recently measured Higgs mass value, however, generates an EW Higgs potential in which the vacuum state is at the edge between being absolute stable and metastable. Indeed, for $m_H = 125.7 \pm 0.3$ GeV and allowing all relevant SM observables to fluctuate within their experimental and theoretical uncertainties, the metastability condition seems to be favored. The high energy evolution of λ shows that it becomes negative at energies $\Lambda = \mathcal{O}(10^{10} - 10^{12})$ GeV, with a slightly broader range if a 3σ fluctuation in the top quark mass value is allowed, as shown in Fig. 1 [28]. When this occurs, then the Higgs potential develops a second (global) minimum at a large value of the magnitude of the scalar field of order Λ. In the SM the new minimum is beyond the scale of quantum gravity, but already below M_{Planck} the Higgs potential becomes deeper that at the EWSB minimum. This behavior may call for new physics at an intermediate scale below M_{Planck}, so that the global minimum of the theory corresponds to the observed $\mathrm{SU}(2)_L \times \mathrm{U}(1)_Y$

broken vacuum with $v \approx 246$ GeV. Otherwise, if no new physics occurs below M_{Planck}, the electroweak vacuum remains metastable [27]. Therefore, within the SM framework, the relevant question is related to the lifetime of the EW metastable vacuum that is determined by the rate of quantum tunneling from this vacuum into the true vacuum of the theory. It turns out that, a coincidence or not, the running of the Higgs self coupling slows down at high energies with a cancellation of its β-function at energies just one to two orders of magnitude below the Planck scale. This slow evolution of the quartic coupling is responsible for saving the EW vacuum from premature collapse allowing it to survive much longer times than those relevant from astrophysical considerations. The peculiar behavior of the quartic coupling leaves open the possibility that the SM might be all what is there up to the quantum gravity scale or it could be the result of a special dynamics or a new symmetry at high energies, such as Supersymmetry with possible flat directions. A more exciting picture would be to have new physics at a smaller energy scale, what could be desirable to explain other mysteries of the universe such as dark matter. At the moment the LHC Higgs discovery leaves all these options equally open.

II.4. Production and decay mechanisms at colliders

II.4.1. Production mechanisms at an electron-positron collider

The main Higgs boson production cross sections at an e^+e^- collider are the Higgs-strahlung process $e^+e^- \to ZH$ [6,29], and the WW fusion process [30] $e^+e^- \to \bar{\nu}_e\nu_e W^*W^* \to \bar{\nu}_e\nu_e H$. As the center-of-mass energy $\sqrt{s}$ is increased, the cross-section for the Higgs-strahlung process decreases as s^{-1} and is dominant at low energies, while the cross-section for the WW fusion process grows as $\ln(s/m_H^2)$ and dominates at high energies [31,32,33]. The ZZ fusion mechanism, $e^+e^- \to e^+e^-Z^*Z^* \to e^+e^-H$, also contributes to Higgs boson production, with a cross-section suppressed by an order of magnitude with respect to that of WW fusion. The process $e^+e^- \to t\bar{t}H$ [34,35] becomes relevant for large $\sqrt{s} \geq 500$ GeV. For a more detailed discussion of Higgs production properties at lepton colliders see for example

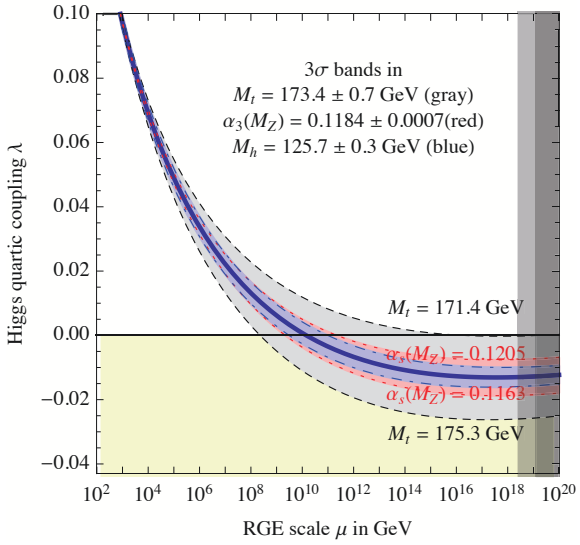

Figure 1: Renormalization group evolution of the Higgs self coupling λ, for the central values of $m_H = 125.7$ GeV, $m_t = 173.4$ GeV and $\alpha_S(M_Z) = 0.1184$ (solid curve), and variation of these central values by $\pm$ 3 σ for the blue, gray and red, dashed curves, respectively. For negative values of λ, the lifetime of the SM vacuum due to quantum tunneling at zero temperature is longer than the age of the universe. The grey shadings cover values of the RG scale above the Planck mass $M_{\rm Pl} = 1.2 \times 10^{19}$ GeV, and above the reduced Planck mass $\bar{M}_{\rm Pl} = M_{\rm Pl}/\sqrt{8\pi}$ From Ref. 28. See full-color version on color pages at end of book.

Refs. [17] and [18], and references therein. Table 1, from Ref. [90], summarizes the dominant Higgs boson production cross sections at various e^+e^- collision energies.

II.4.2. Gluon Fusion production mechanisms at hadron colliders

At high-energy hadron colliders, the Higgs boson production mechanism with the largest cross section is $gg \to H + X$. At leading order (LO) [36] this process is governed by a top quark loop proportional to its Yukawa coupling to the Higgs boson and to the squared of the QCD coupling constant. QCD radiative corrections are very important and have been studied in much detail in the literature. This process is known at

Table 1: Dominant Higgs boson production cross sections at various e^+e^- collision energies. From Ref. [90] (where the polarization fractions used for the cross section computations can be found).

cross section in fb $m_H = 125$ GeV							
Mode		$\sqrt{s}$ (GeV)					
		250	350	500	1000	1400	3000
ZH	unpolar.	211	134	64.5	16.1	8.48	2.00
	polar.	318	198	95.5	22.3	10.0	2.37
$\nu_e\bar{\nu}_e H$	unpolar.	20.8	34.1	71.5	195	278	448
	polar.	36.6	72.5	163	425	496	862
e^+e^-H	unpolar.	7.68	7.36	8.86	20.1	27.3	48.9
	polar.	11.2	10.4	11.7	24.7	32.9	56.5

next-to-leading order (NLO) in QCD in the large top mass limit [37], that turns out to be an excellent approximation at the level of a few percent, as well as for arbitrary top and bottom mass dependence [38,39]. The QCD next-to-next-to-leading order (NNLO) corrections have been computed in the large top-mass limit [40]. The NLO QCD corrections approximately double the leading-order prediction, and the NNLO QCD corrections add approximately 50% to the NLO prediction. NLO electroweak corrections have been computed and they increase the LO term by about 5% for $m_H \simeq 125$ GeV [41]. Mixed QCD-electroweak corrections $O(\alpha\alpha_s)$ are computed in Ref. [42]. Although there are delicate issues related to how to combine the EW and QCD corrections precisely, the mentioned results considered an effective Lagrangian approach and support the factorization hypothesis that suggests that EW corrections become multiplicative factors of the full QCD expansion. This is expected to be a good approximation for Higgs boson masses below several hundred GeV. Electroweak effects for Higgs production at finite transverse momentum have also been studied [43] and they are at most at the percent level.

In addition, the NNLO QCD calculations have been improved by resumming the soft-gluon contributions to the cross

sections at next-to-leading logarithmic (NLL), NNLL and partial NNNLL accuracy [44]. Much progress has been made in the past several years in the computation of radiative corrections and in the evaluation of uncertainties. The validity of the large top-quark mass limit approximation in NNLO calculations have been established [45] at the percent level for Higgs masses below a few hundred GeV. Updated predictions for the gluon fusion cross sections at NNLO or through soft-gluon resummation up to next-to-next-to-leading logarithmic accuracy (NNLL), and two-loop electroweak effects as well as the inclusion of using the most recent parametrizations of parton distribution functions at next-to-next-to-leading order can be found in Refs. [42,46,47]. An alternative discussion of the evaluation and uncertainties of the Higgs gluon fusion mechanism can be found in Refs. [48]. A cross section calculation based on an effective field theory leads to a better perturbative convergence achieved by resumming the enhanced contributions arising from the analytic continuation of the gluon form factor [49]. Updated predictions to compute the gluon fusion cross sections at NNNLL in renormalization group improved perturbation theory and incorporating two-loop electroweak effects can be found in Ref. [50]. An additional enhancement of the cross section is obtained when soft-gluon resummation is extended to NNNLL order and a resummation of the kinematically enhanced terms in the time-like gluon form factor is performed [49]. For a detailed discussion and tables of gluon fusion cross sections and uncertainties, as a function of the Higgs boson mass and the LHC center of mass energy, see Ref. [19].

In understanding the Higgs bosons properties, besides considering the inclusive cross sections it is relevant to consider differential distributions. The experimental analysis must impose cuts on the final state in order to improve the signal to background ratio. The benchmark cuts need to be defined, and the differential distributions compared at various levels of theoretical accuracy, i.e., at NLO/NNLO and with Monte Carlo (MC) generators. Many search modes for the Higgs boson are carried out in the exclusive mode, i.e., by separating

the events according to number of jets or the transverse momentum of the Higgs boson. In the heavy top quark mass limit, the Higgs boson production in association with one jet is considered in Refs. [51,52,53,54] and in association with two jets in Refs. [55,56]. Moreover, a first calculation of Higgs-boson production in association with a jet at NNLO in the infinite top mass limit is considered in Ref. [57]. Most recently there has been much activity in computing Higgs plus jet(s) production processes [21,58] as well as on focusing on the transverse-momentum spectrum of the SM Higgs (see Ref. [20] and references therein).

II.4.3. Vector boson fusion production mechanisms at hadron colliders

The next most relevant production mechanism of a SM Higgs boson at the LHC is in association with two hard jets in the forward and backward regions of the detector and is dubbed Vector Boson Fusion (VBF). At the Tevatron, VBF is also relevant, but for $m_H \simeq 125$ GeV the Higgs production in association with W as well as with a Z gauge boson are more important. The vector boson fusion process $qq \to qqH + X$ receives two type of contributions at hadron colliders: the genuine VBF channel where the Higgs couples to a W or Z gauge boson that connects two quark lines via t-and u-channel diagrams, and the contribution to WH and ZH production with the gauge bosons decaying hadronically. In the genuine VBF production mechanism the hard jet pairs have a strong tendency to be forward-backward directed in contrast to other jet-production mechanisms. This allows to implement cuts to suppress backgrounds, including the Higgs +2 jet production via gluon fusion that becomes a background to this production mechanism. The VBF cuts also suppress importantly the s-channel production in the hadronic WH and ZH channels as well as its interference with the t-and u-channels. The VBF channel is not only relevant for Higgs searches but it also provides an important handle in the determination of Higgs-gauge boson couplings at the LHC [59].

The total cross section for electroweak Higgs production via VBF: $qq \to qqH + X$, has been computed in approximations

and in full considering the NLO EW and QCD corrections [60]. Approximate NNLO QCD corrections to the total inclusive cross section for VBF have been presented in Ref. [61]. After including these NNLO QCD corrections the remaining theoretical uncertainties in the inclusive cross section are approximately 2%. The uncertainties due to parton distributions are estimated to be at the same level. For a detailed discussion and tables of VFB Higgs production cross sections and uncertainties as a function of the Higgs boson mass and the LHC center of mass energy, see Ref. [19].

Theoretical predictions for cross sections with cuts and distributions are particularly interesting for the VBF production mechanism since cuts on the tagging jets are used to suppress events from Higgs + 2 jet production via gluon fusion as well as other backgrounds. At present, differential distributions or cross sections with cuts, are only available at NLO level. The uncertainties are larger if jets are required or vetoed [20].

II.4.4. WH and ZH associated production mechanisms at hadron colliders

The next most relevant Higgs boson production mechanisms after gluon fusion and VBF at the LHC, and the most relevant ones after gluon fusion at the Tevatron, are associated production with W and Z gauge bosons. The cross sections for the associated production processes $q\overline{q} \to \mathrm{W}^{\pm}H + X$ and $q\overline{q} \to \mathrm{Z}H + X$ receive contributions at NLO given by NLO QCD corrections to the Drell–Yan cross section [62,63,64] and from NLO EW corrections, that unlike the QCD corrections do not respect the factorization into Drell–Yan production since there are irreducible box corrections to $q\overline{q} \to VH$ (V=W,Z) already at one loop [65]. At NNLO, the QCD corrections to WH production can be readily derived for the Drell–Yan part and for the bulk of the ZH production [66]. For ZH production there are, however, gluon-gluon induced contributions that do not involve a virtual Z gauge boson but are such that the Z gauge boson and H boson couple to gluons via top quark loops [67]. In addition both WH and ZH production receive non Drell–Yan-like corrections in the $q\overline{q}$ initiated channels at the NNLO level where the Higgs is radiated off top quark loops [68]. In

summary, the most updated NNLO QCD corrections and the NLO EW corrections for the total inclusive VH production cross section are available in Ref. [69]. The residual uncertainty is less than 5%. For a detailed discussion and tables of WH and ZH associated production cross sections and uncertainties, as a function of the Higgs boson mass and the LHC center of mass energy see Ref. [19].

The WH and ZH associated productions together with the Higgs boson production in association with top pairs are the only processes where the Higgs decay into bottom pairs can be studied, since the other available processes are swamped by QCD background. Moreover to overcome SM QCD background it is important to consider the full kinematical information of the process and the W/Z leptonic decays. The NNLO QCD corrections to the fully differential observables for WH and ZH are available [70], while the EW NLO corrections have been generalized for the processes $pp \to WH \to \nu_l l H$ and $pp \to ZH \to l^- l^+ H / \nu_l \bar{\nu}_l H$ [20,21].

II.4.5. Higgs production in association with $t\bar{t}$ at hadron colliders

Higgs radiation off top quarks $pp \to Ht\bar{t}$ is an important production process at the LHC, in particular in the search for Higgs decays into bottom quark pairs. Moreover, the measurement of the $t\bar{t}H$ production rate can provide relevant information on the top-Higgs Yukawa coupling. The LO cross section was computed in Ref. [72]. Later on the NLO in QCD corrections [73] were evaluated yielding a moderate increase in the total cross section of at most 20%, but reducing significantly the scale dependence of the inclusive cross section. The total theoretical errors estimated combining the uncertainties from scale dependence, strong gauge coupling dependence, and PDF dependence, for low Higgs-boson masses, amount to 10–15% of the corresponding cross sections. For a detailed discussion and tables of $Ht\bar{t}$ associated production cross sections and uncertainties, as a function of the Higgs boson mass and the LHC center of mass energy, see Ref. [19].

A detailed study of the interface of the NLO QCD calculation of $t\bar{t}H$ with parton shower Monte Carlo programs

Table 2: $m_H = 125$ GeV Higgs boson production cross sections together with their relative theory uncertaintities at the LHC operating at $\sqrt{s} = 7, 8$ and14 TeV. From Refs. [19] and [21].

$\sqrt{s}$	cross section in pb $m_H = 125$ GeV					
(TeV)	ggF	VBF	WH	ZH	$t\bar{t}$H	total
7	$15.1^{+15\%}_{-15\%}$	$1.22^{+3\%}_{-2\%}$	$0.58^{+4\%}_{-4\%}$	$0.33^{+6\%}_{-6\%}$	$0.09^{+12\%}_{-18\%}$	17.4
8	$19.3^{+15\%}_{-15\%}$	$1.58^{+3\%}_{-2\%}$	$0.70^{+4\%}_{-5\%}$	$0.41^{+6\%}_{-6\%}$	$0.13^{+12\%}_{-18\%}$	22.1
14	$49.8^{+20\%}_{-15\%}$	$4.18^{+3\%}_{-3\%}$	$1.50^{+4\%}_{-4\%}$	$0.88^{+6\%}_{-5\%}$	$0.61^{+15\%}_{-28\%}$	57.0

provides a state-of-the-art tool to obtain theoretical predictions and theoretical uncertainties on total and differential cross sections, including experimental cuts and vetos on the final-state particles and their decay products [74]

II.4.6. Results of Higgs production cross sections at Hadron colliders

The cross sections for the production of SM Higgs bosons are summarized in Fig. 2 for $p\overline{p}$ collisions at the Tevatron [75], and in Fig. 3 for pp collisions at $\sqrt{s} = 8$ TeV at the LHC [76]. A more detailed discussion, including uncertainties in the theoretical calculations due to missing higher order effects and experimental uncertainties on the determination of SM parameters involved in the calculations can be found in Refs. [19,20,21]. These references also contain state of the art discussions on the relevance of PDF's uncertainties, QCD scale uncertainties and uncertainties due to different matching procedures when including higher order corrections matched to parton shower simulations as well as uncertainties due to hadronization and parton-shower events.

Table 2, from Refs. [19] and [21], summarizes the Higgs boson production cross sections at the various operating LHC energies.

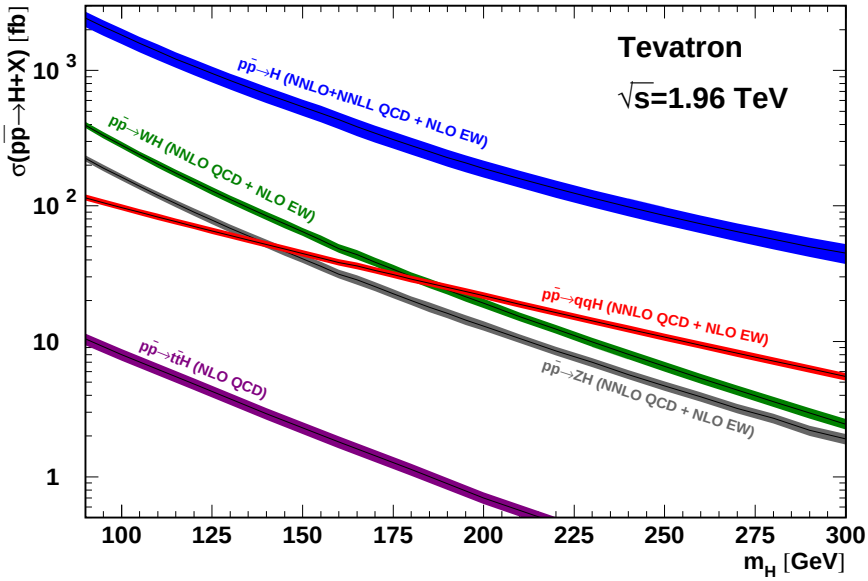

Figure 2: SM Higgs boson production cross sections for $p\overline{p}$ collisions at 1.96 TeV, including theoretical uncertainties [75]. See full-color version on color pages at end of book.

II.4.7. SM Higgs Branching Ratios and Total Width

For the understanding and interpretation of the experimental results, the computation of all the relevant Higgs decay widths is essential, including an estimate of their uncertainties and, when appropriate, the effects of Higgs decays into off-shell particles with successive decays into lighter SM ones. Given the value of the Higgs boson mass, it is a good approximation to compute the partial widths for the on-shell Higgs boson, and then use them to compute the branching ratios. A Higgs mass of 125.5 GeV provides an excellent opportunity to explore the Higgs couplings to many of the SM particles. In particular the dominant decay modes are into $H \to b\bar{b}$ and $H \to WW^*$, followed by $H \to gg$, $H \to \tau^+\tau^-$, $H \to c\bar{c}$ and $H \to ZZ^*$. With much smaller rates follow the Higgs decays into $H \to \gamma\gamma$, $H \to \gamma Z$ and $H \to \mu_+\mu_-$, with the decay into two photons being of particular relevance due to the small SM backgrounds involved. Since the decays into gluons, diphotons and $Z\gamma$ are loop induced, they provide indirect information on the Higgs to WW, ZZ and $t\bar{t}$ couplings in different combinations. In practice,

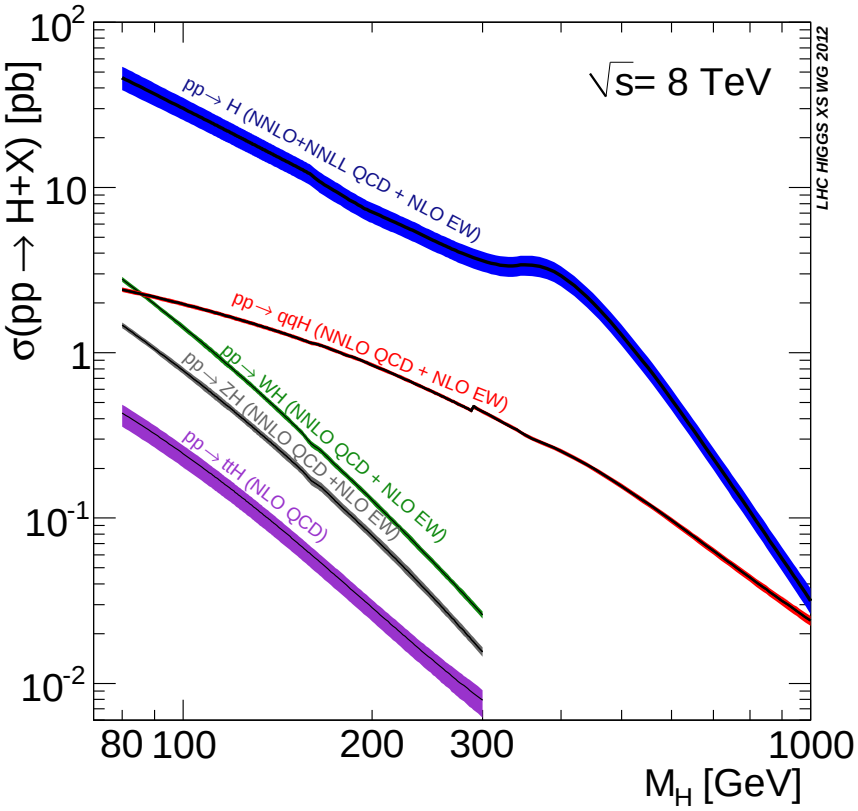

Figure 3: SM Higgs boson production cross sections for pp collisions at 8 TeV, including theoretical uncertainties [76]. See full-color version on color pages at end of book.

the $H \to t\bar{t}$ coupling is mainly probe in the gluon fusion Higgs production and $Ht\bar{t}$ associated production processes discussed previously. The Higgs decays into WW^* and ZZ^* effectively need to be studied considering the decays of the gauge bosons into 4 fermions, considering the leptonic, semi-leptonic and full hadronic final states. The uncertainties in the branching ratios include the missing higher order corrections in the theoretical calculations as well as the errors in the SM input parameters, in particular fermions masses and gauge couplings, involved in the calculations. In the following we will briefly discuss the state of the art of the theoretical calculations and refer the reader to Refs. [19,20] for further details.

The evaluation of radiative corrections of fermionic decays of the SM Higgs at different levels of accuracy are available in the literature and are implemented in HDECAY [77]. The decays $H \to b\bar{b}$ and $H \to c\bar{c}$ are computed including the complete massless QCD corrections up to and including NNNNLO, with

a corresponding scale dependence of about 0.1% [78]. Both the electroweak corrections to $H \to b\bar{b}$, $c\bar{c}$ as well as $H \to \tau^+\tau^-$ are known at NLO [79] with an accuracy of about 1-2% for $m_H \simeq$125.5 GeV. In the case of $H \to t\bar{t}$, the radiative QCD corrections are computed at NLO [80] while the electroweak corrections due to self interactions of the Higgs bosons are available at NLO.

The loop induced decays of the SM Higgs are known at NLO and partially beyond that approximation. For $H \to gg$, the QCD corrections are known up to NNNLO in the limit of heavy top quarks [81,39] and the uncertainty from the scale dependence is about 3%. For the $H \to \gamma\gamma$, the full NLO QCD corrections are available [39,82]. The NLO electroweak corrections to $H \to gg$ and $H \to \gamma\gamma$ have been computed in Ref. [83]. Missing higher orders corrections are estimated to be below 1%. All these corrections are implemented in HDECAY. In addition the contribution of the $H \to \gamma e^+e^-$ decay via virtual photon conversion has been computed in Ref. [84]. The partial decay width $H \to Z\gamma$ has been computed at NLO in QCD [85] and electroweak corrections but it is only implemented at LO in HDECAY, including the virtual W, top, bottom, and τ loop contributions. The remaining contributions are less than 5%, an accuracy that will be hard to achieve in measurements at the LHC.

The evaluation of the decays $H \to WW/ZZ \to 4f$ are based on PROPHECY4F [86], a Monte Carlo event generator which considers the LO and NLO partial widths for any possible 4- fermion final state. It includes the complete NLO QCD and electroweak corrections and all interferences at LO and NLO, meaning that it takes into account both the corrections to the decays into intermediate WW and ZZ states as well as their interference for all possible 4 fermion final states. The calculation is consistently performed with off-shell gauge bosons without any on-shell approximation, hence, it is valid above, near, and below the gauge-boson pair thresholds. The treatment of the LO and NLO gauge-boson widths ensures that the effective W and Z branching ratios add up to one. For the SM Higgs boson mass the missing higher-order corrections are estimated

to roughly 0.5%. Such uncertainties will have to be combined with the parametric uncertainties, in particular those associated to the bottom quark mass and the strong gauge coupling, to arrive at the full theory uncertainties. When discussing differential distributions for $H \to WW/ZZ \to 4f$ it is important to emphasize the impact of NLO corrections and in particular the impact of interference effects on such distributions. These effects are included in PROPHECY4F which is based on the full $H \to 4f$ matrix elements including all interferences between different Feynman diagrams. A more detailed treatment of the differential distributions for a Higgs decay with four charged leptons in the final state is presented in Ref. [21].

The branching ratios for the most relevant decay modes of the SM Higgs boson as functions of m_H, including the most recent theoretical uncertainties, are shown in Fig. 4. The total decay width as function of m_H is shown in Fig. 5. Further details of these calculations can be found in Refs. [17,18,19,20,21].

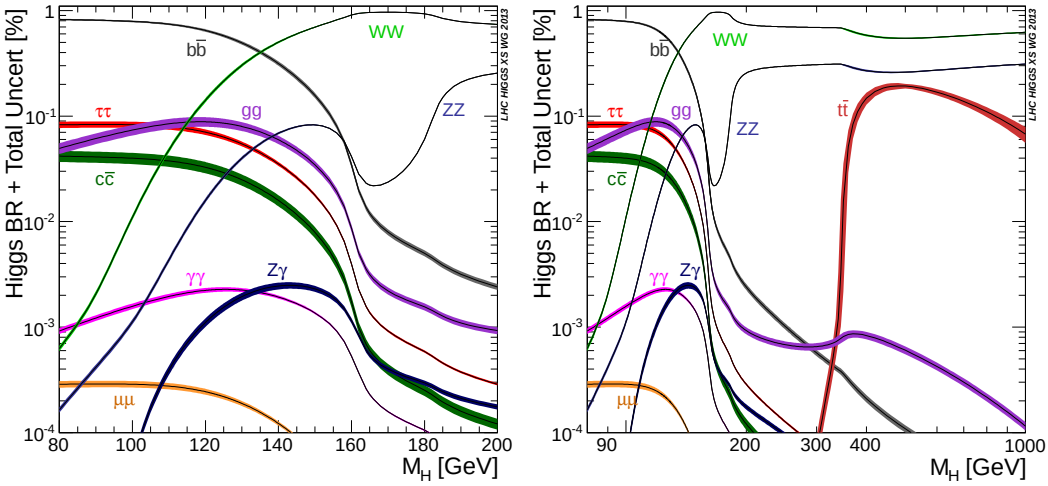

Figure 4: Branching ratios for the main decays of the SM Higgs boson, including theoretical uncertainties [21]. See full-color version on color pages at end of book.

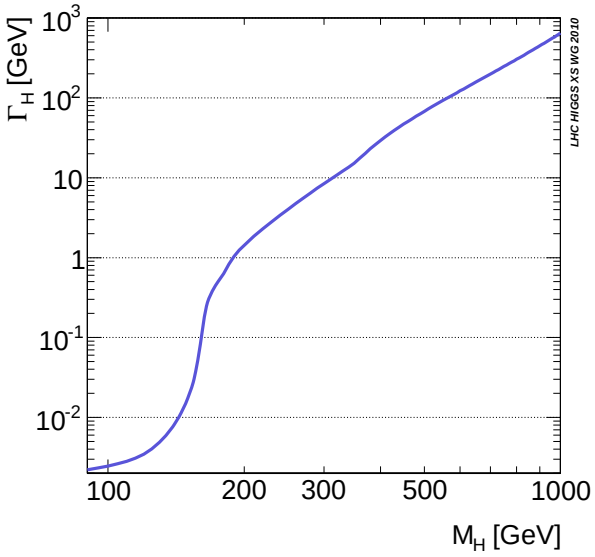

Figure 5: The total decay width of the SM Higgs boson, shown as a function of m_H [19].

III. Searches For the Standard Model Higgs boson

Indirect experimental bounds for the SM Higgs boson mass can be obtained from fits to precision measurements of electroweak observables. The Higgs boson contributes to the $W^{\pm}$ and Z vacuum polarization through loop effects, leading to a logarithmic sensitivity of the ratio of the $W^{\pm}$ and Z gauge boson masses on the Higgs boson mass. A global fit to the precision electroweak data accumulated in the last two decades at LEP, SLC, the Tevatron, and elsewhere, suggests $m_H = 94^{+29}_{-24}$ GeV, or $m_H < 152$ GeV at 95% C.L. [91].

Direct and model-independent searches for the Higgs boson were conducted by the ALEPH, DELPHI, L3, and OPAL experiments at LEP e^+e^- collider. The combination of LEP data collected near the Z resonance and at center-of-mass energies up to 209 GeV yielded a 95% Confidence level (CL) lower bound [95] of 114.4 GeV for the mass of the SM Higgs boson. Following the shutdown of the LEP collider in 2000, the direct search for the Higgs boson was picked up at Fermilab's Tevatron $p\overline{p}$ collider. The combined results [115] from approximately

10 fb^{-1} recorded by the CDF and DØ experiments excluded two ranges in m_H: between 90 GeV and 109 GeV, and between 149 GeV and 182 GeV. In addition, a broad excess in data was seen in the mass range 115 GeV $< m_H <$ 140 GeV with a local significance[3] of 3 standard deviations. The commissioning in 2010 and the high intensity running of the LHC pp collider at CERN at $\sqrt{s}$ =7 TeV in 2011 followed by an energy boost to $\sqrt{s}$ =8 TeV in 2012 opened up a new landscape where the Higgs boson could be searched for, quickly and effectively, in the 110-1000 GeV mass range.

The announcement on 4th July 2012 of the observation [1–2] at the LHC of a narrow resonance with a mass of about 126 GeV has provided an important new direction in the decades long search for the SM Higgs boson. The analyzed data corresponded to integrated luminosities of up to 4.8 (5.1) fb^{-1} at $\sqrt{s}$ = 7 TeV in 2011 and 5.9 (5.3) at $\sqrt{s}$ = 8 TeV in 2012 recorded by the ATLAS and CMS experiments respectively. The observed decay channels indicated that the new particle is a boson. The evidence was strong that the new particle decays to $\gamma\gamma$ and ZZ with rates consistent with those predicted for the Standard Model (SM) Higgs boson. There were indications that the new particle also decays to W^+W^-. While the decays to $b\bar{b}$ and $\tau^+\tau^-$ were searches for, no statistically significant signal was found in that data.

The significance of such an observation can be quantified by a p-value [97], which is the probability to observe an upward fluctuation of the background which gives a result at least as signal-like as that observed in the data. For example, a p-value of 2.87×10^{-7} corresponds to a five standard deviation excess over the background-only prediction. Fig. 6 shows the p-values reported by the ATLAS and CMS experiments for each analysis channel and their combination. ATLAS observed the largest excess with a local significance of 5.0σ at a mass m_H = 126.5 GeV, with an expected significance of 4.6σ if a SM Higgs boson were present at such mass. CMS observed an

[3] In this review, we use the phrase "local significance" to indicate a calculation of the significance not corrected for the look-elsewhere effect [96].

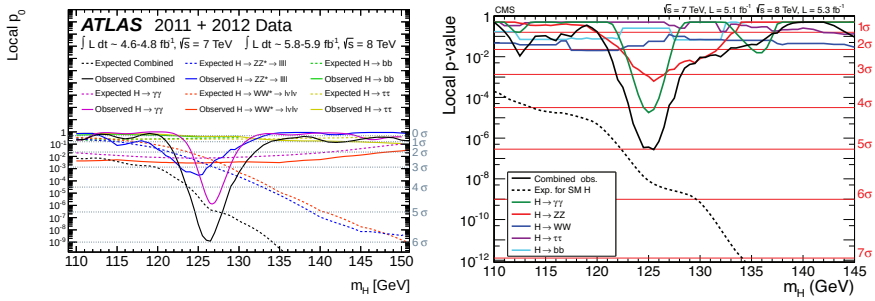

Figure 6: Local p-values for the ATLAS SM Higgs boson search (left), and the CMS SM Higgs boson search (right), separately for each decay channel. The solid lines show the observed p-values and the dashed lines show the expected p-values, assuming a SM Higgs boson is present, computed at each value of m_H.

excess with a local significance of 4.9σ at a mass of 125.5 GeV, with an expected significance of 5.9σ, and measured the mass of the new boson as $m_H = 125.3 \pm 0.6$ GeV.

Even as this discovery was being announced, ATLAS and CMS continued to accumulate pp collision data as $\sqrt{s} = 8$ TeV recording a total of about 20 fb^{-1} each at this energy. Fig. 7 shows four snapshots of the evolution of the p-value Vs m_H with increasing datasets.

In the remainder of this section we focus on the recent major results. Unless explicitly mentioned, all measurements are based on the full data set recorded by the Tevatron and the LHC experiments.

III.1. The Discovery channels

The discovery channels of the SM Higgs boson depend on its mass m_H. For a given m_H the sensitivity of the search channel depends on the production cross section of the Higgs bosons, its decay branching fraction, reconstructed mass resolution, selection efficiency and the level of background in the final state. For a low mass Higgs boson ($110 < m_H < 150$ GeV) where the natural width of the Higgs boson is only a few MeV, the five modes that play an important role are listed in Table 3. In the $H \to \gamma\gamma$ and $H \to ZZ \to 4\ell$ channels all final state particles can be very precisely measured and the reconstructed m_H resolution

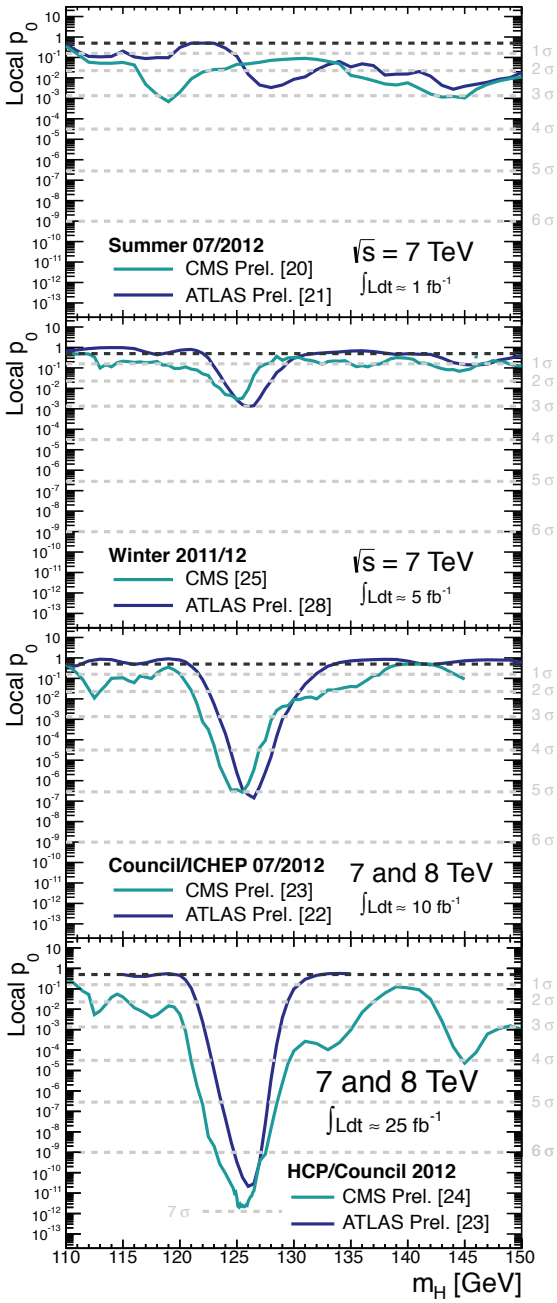

Figure 7: Evolution of the signal significance observed by the ATLAS and CMS experiments (a) Summer'11 ($\approx 1\text{fb}^{-1}$/expt) (b) Winter'12 ($\approx 5\text{fb}^{-1}$/expt) (c) Summer'12 ($\approx 10\text{fb}^{-1}$/expt) and (d) Winter'12 ($\approx 25\text{fb}^{-1}$/expt).

is excellent. While the $H \to W^+W^- \to \ell^+\nu_\ell\ell'^-\bar{\nu}_{\ell'}$ channel has relatively large branching fraction, the m_H resolution is poor due to the presence of neutrinos. The $H \to b\bar{b}$ and the $H \to \tau^+\tau^-$ channels suffer from large backgrounds and a poor mass resolution. For $m_H > 150$ GeV, the discovery channels are $H \to WW$ & $H \to ZZ$ where the W or Z boson decays into a variety of leptonic and hadronic final states.

Table 3: The five low mass Higgs boson discovery channels.

Decay channel	m_H range (GeV)	m_H resolution (approximate)
$H \to \gamma\gamma$	110 – 160	1-2%
$H \to ZZ \to \ell^+\ell^-\ell'^+\ell'^-$	110 – 1000	1-2%
$H \to W^+W^- \to \ell^+\nu_\ell\ell'^-\bar{\nu}_{\ell'}$	110 – 1000	20%
$H \to b\bar{b}$	110 – 140	10 %
$H \to \tau^+\tau^-$	110 – 145	15 %

III.1.1. $H \to \gamma\gamma$

In the $H \to \gamma\gamma$ channel a search is performed for a narrow peak over a smoothly falling background in the invariant mass distribution of two high p_T photons. The background in this channel is high and stems from prompt $\gamma\gamma$, γ+jet and dijet processes. In order to optimize search sensitivity and also to separate the various Higgs production modes, ATLAS and CMS experiments split events into several mutually exclusive categories. Diphoton events containing a high p_T muon, electron. dijets or missing energy (E_T^{miss}) consistent with the decay of a W or Z boson are tagged in the VH production category, those containing energetic dijets with a large mass and psuedorapidity difference are assigned to the VBF production category and the remaining events ($\approx 99\%$ of the total) are considered in the gluon fusion production category. The VH and VBF categories have significant contamination from the gluon fusion channel. Untagged events are further categorized according to their expected $m_{\gamma\gamma}$ resolution and signal-to-background

ratio. Categories with good m_H resolution and largeer signal-to-background ratio contribute most to the sensitivity of the search.

In each category, $Z \to e^+e^-$ and $Z \to \mu^+\mu^-\gamma$ events from data are used to construct a parametric signal model. The functional form of the background is determined by a fit to the full $m_{\gamma\gamma}$ distribution in each category. All categories are fitted simultaneously to determine the signal yields. In the full dataset, the $M_{\gamma\gamma}$ distribution after combining all categories are shown for the ATLAS experiment in Fig. 8 and for the CMS experiment in Fig. 9 . ATLAS observes [101] an enhancement at $m_H = 126.5$ GeV with a significance of 7.4σ compared with 4.3σ expected for SM Higgs boson at that mass. CMS observes [106] its largest excess at $m_H = 125.4$ GeV with a significance of 3.2σ compared with 4.2σ expected for SM Higgs boson of that mass.

The signal strength $\mu = (\sigma \cdot \mathcal{B})_{\rm obs}/(\sigma \cdot \mathcal{B})_{\rm SM}$ which is the observed product of the Higgs boson production cross (σ) section and its branching ratio ($\mathcal{B}$) in units of the corresponding SM values, is $1.65^{+0.34}_{-0.30}$ for ATLAS and 0.78 ± 0.27 for CMS at their reported masses.

CMS has also searched for $H \to \gamma\gamma$ in the $t\bar{t}$H production mode and set a 95% CL upper limit of on the signal strength $\mu_{\rm t\bar{t}H} < 5.4$ for $m_H = 125$ GeV [103].

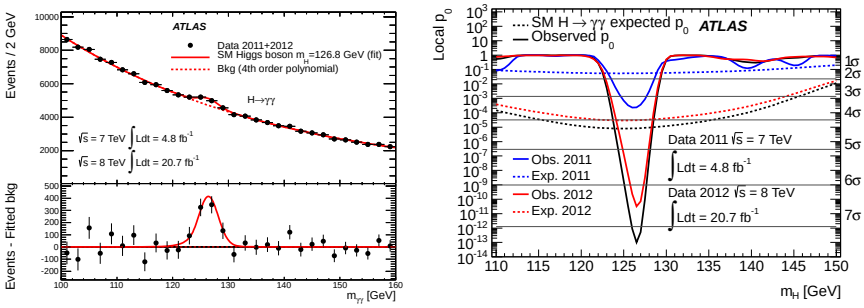

Figure 8: (Left) The combined invariant mass distribution of diphoton candidates observed by ATLAS. The residuals of the data with respect to the fitted background are displayed in the lower panel. (Right) The observed and expected local p-value and significance as a function of m_H.

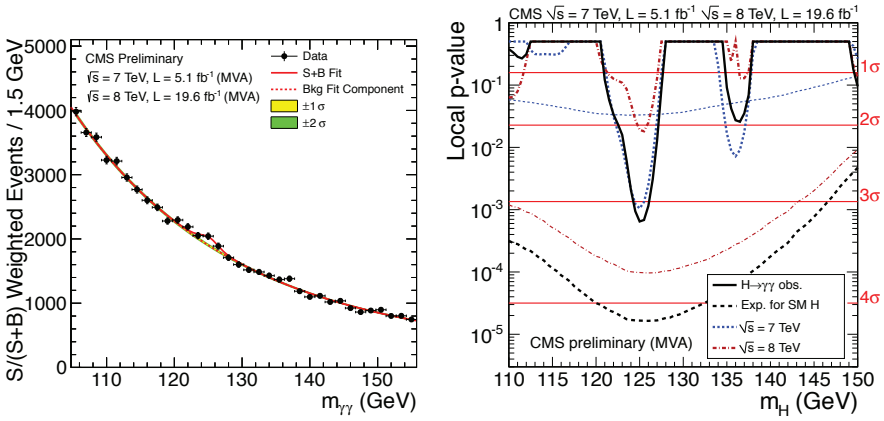

Figure 9: (Left) The combined CMS $M_{\gamma\gamma}$ distribution with each event weighted by the ratio of signal-to-background in each event category. (Right) Observed and expected local p-values and significance as a function of m_H.

III.1.2. $H \to ZZ^{(*)} \to \ell^+\ell^-\ell'^+\ell'^-$, $(\ell, \ell' = e, \mu)$

In the $H \to ZZ^{(*)} \to \ell^+\ell^-\ell'^+\ell'^-$ channel a search is performed for a narrow mass peak over a small continuous background dominated by non-resonant $ZZ^{(*)}$ production from gg fusion and $q\overline{q}$ annihilation processes. The contribution and the shape of this background is taken from simulated events. The subdominant and reducible backgrounds stem from $Z + b\bar{b}$, $t\bar{t}$ and Z+jets events and their yield is estimated from data.

To help distinguish the Higgs signal from the dominant non-resonant $ZZ^{(*)}$ background, CMS uses a matrix element likelihood approach [2] to construct a kinematic discriminant built for each 4ℓ event based on the ratio of complete leading-order matrix elements $|\mathcal{M}_{sig}{}^2/\mathcal{M}_{bkg}{}^2|$ for the signal ($gg \to H \to 4\ell$) and background($q\overline{q} \to ZZ \to 4\ell$) hypotheses. The signal matrix element $\mathcal{M}_{sig}$ is computed assuming $m_H = m_{4\ell}$.

To enhance the sensitivity to VBF and VH production processes, ATLAS and CMS experiment divide 4ℓ events into mutually exclusive categories. Events containing dijets with a large mass and psuedorapidity difference populate the VBF category. ATLAS requires presence of an additional lepton in the VH category. In events with less than two jets, CMS uses the $p_T^{4\ell}$ to distinguish between production via gluon fusion and VH/VBF processes.

Since the $m_{4\ell}$ resolutions and the reducible background levels are different in the 4μ, $4e$ and $2e2\mu$ sub-channels, they are analyzed separately and the results combined.

The combined ATLAS $m_{4\ell}$ distribution is shown in Fig. 10(left). The largest deviation from the SM background-only expectation is observed at $m_H = 124.3$ GeV where the significance of the observed peak is 6.6σ in the full 7 & 8 TeV data. The expected significance for the SM Higgs boson at that mass is 4.4σ.As shown in Fig. 11, the CMS experiment observes its largest excess at $m_H = 125.8$ GeV with a observed significance of 6.6σ to be compared with an expected significance of 7.2σ at that mass. Both experiments also observe a clear peak at $m_{4\ell} = 91$ GeV from Z/γ^* production at the expected rate.

The signal strength μ for the inclusive $H \to 4\ell$ production measured by the ATLAS and CMS experiments are $1.7^{+0.5}_{-0.4}$ and $0.91^{+0.30}_{-0.24}$ respectively.

III.2. Mass & Width Measurements

In order to measure the mass of the observed state, ATLAS and CMS experiments combine the measurements from the $\gamma\gamma$ and ZZ channels which have excellent mass resolution and where excesses with large significance are observed. For a model-independent mass measurement, the signal strengths

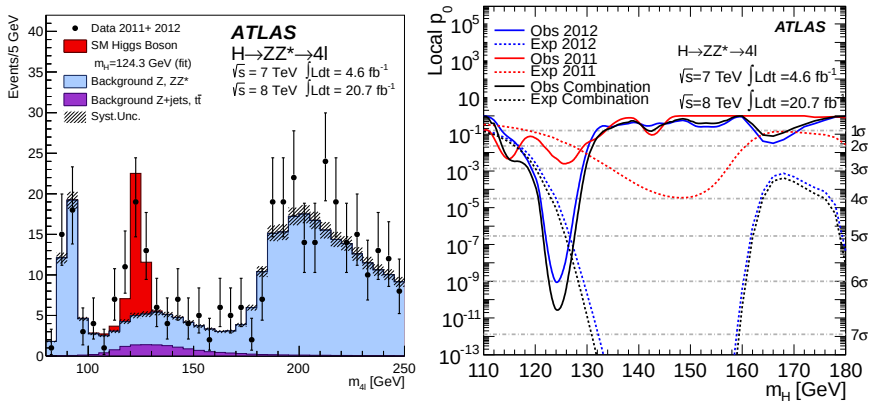

Figure 10: (Left) The combined $m_{4\ell}$ distribution from ATLAS. (right) The observed and expected local p-value and significance as a function of m_H.

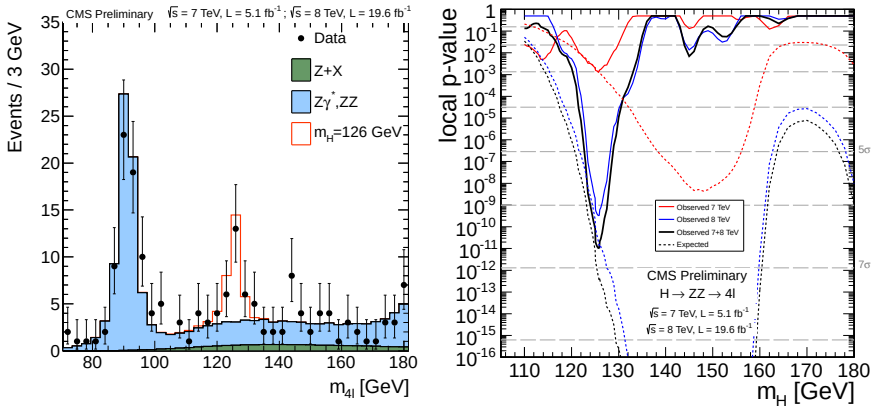

Figure 11: (Left) The combined $m_{4\ell}$ distribution from CMS. (right) The observed and expected local p-value and significance as a function of m_H for the sum of 4μ, $4e$ and $2e2\mu$ channels.

in the $\gamma\gamma$ and ZZ channels are assumed to be independent and not constrained to the expected rate ($\mu = 1$) for the SM Higgs boson. The combined mass measured by ATLAS [101] and CMS [100] are $125.5 \pm 0.2(\text{stat.}) \,^{+0.5}_{-0.6}(\text{syst.})$ GeV and $125.7 \pm 0.3(\text{stat.}) \pm 0.3(\text{syst.})$ GeV respectively. In both experiments the systematic uncertainty is dominated by the imprecision in the knowledge of the photon energy and the lepton momentum scale. Fig. 12 summarizes these measurements

and our combination of the two results assuming uncorrelated systematic uncertainties.

The natural width of a SM Higgs boson with a mass of 125 GeV is about 4 MeV, much smaller than the mass resolution obtainable with the most precisely measured photons and leptons in ATLAS and CMS. Nevertheless, 95 % CL bounds on the width of the Higgs boson of $\Gamma_H < 6.9$ GeV [104] and $\Gamma_H < 3.4$ GeV [107] have been placed from the investigations in the $\gamma\gamma$ and ZZ channels respectively by CMS.

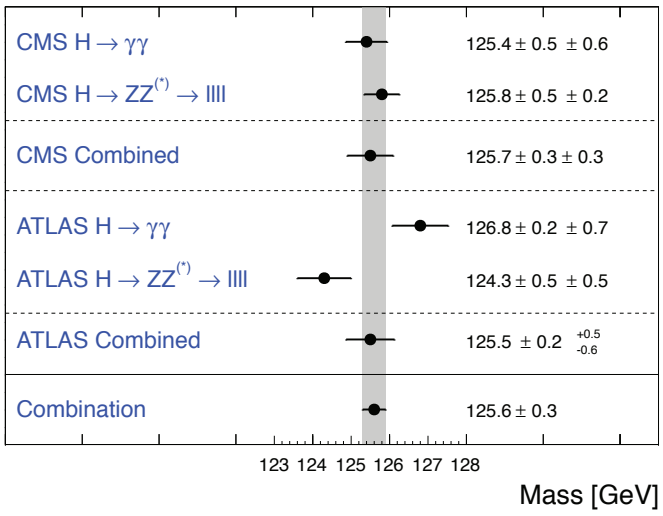

Figure 12: A compilation of the CMS and ATLAS mass measurements in the $\gamma\gamma$ and ZZ channels, the combined result from each experiment and our average of the combinations.

III.3. $H^0 \to W^+W^- \to l^+\nu l^-\overline{\nu}$

While the production rate in this channel is large, due to the presence of two neutrinos in the decay, in the $H \to W^+W^- \to \ell^+\nu\ell^-\bar{\nu}$ channel the m_H resolution is quite poor ($\approx 20\%$ m_H) so the search is reduced to a counting experiment of event yield in broad bins in m_H.

Experiments search for an excess of events with two leptons of opposite charge accompanied by missing energy and up to two jets. Events are divided into several categories depending on

the lepton flavor combination (e^+e^-, $\mu^+\mu^-$and $e^\pm\mu^\mp$) and the number of accompanying jets ($N_{jet} = 0, 1, \geq 2$). The $N_{jet} \geq 2$ category is optimized for VBF production process by selecting two leading jets with a large pseudorapidity difference and with a large mass ($m_{jj} > 500$ GeV). Backgrounds contributing to this channel are numerous and vary by the category of selected events. Reducing them and accurately estimating the remainder is major challenge in this analysis. For events with opposite flavor lepton and no accompanying high p_T jets, the dominant background stems from non-resonant WW production. Events with same flavor leptons suffer from large Drell–Yan contamination. $t\bar{t}$, Wt and W+jets (with the jet misidentified as a lepton) contaminate all categories. Non-resonant WZ, ZZ and Wγ processes also contribute to the background at a sub-leading level.

A requirement of large missing energy ($E_T^{\rm miss}$) is used to reduce the Drell–Yan and multi-jet backgrounds. In the e^+e^-& $\mu^+\mu^-$ categories events with m_{ll} consistent with the Z mass are vetoed. The $t\bar{t}$ background is suppressed by a veto against identified b-jets or low p_T muons (assumed to be coming from semileptonic b-hadron decays within jets) and tight isolation requirements diminish the W+jets background. The scalarity of the Higgs boson and the V-A nature of the W boson decay implies that the two charged leptons in the final state are emitted at small angles. Therefore the dilepton invariant mass ($m_{\ell\ell}$) and the azimuthal angle difference between the leptons ($\Delta\phi_{\ell\ell}$) are used to discriminate between the signal and non-resonant WW events. The transverse mass constructed from the dilepton p_T ($p_T^{\ell\ell}$) , $E_T^{\rm miss}$ and the azimuthal angle between $E_T^{\rm miss}$ and $p_T^{\ell\ell}$ and defined as $m_T = \sqrt{2p_T^{\ell\ell}E_T^{\rm miss}(1 - cos\Delta\phi_{E_T^{\rm miss}\ell\ell})}$ serves as an effective discriminant against backgrounds.

All residual background rates except for the small contributions from non-resonant WZ, ZZ and Wγ are evaluated from control samples devised from data.

The m_T distributions of selected events is shown in Fig. 13 and Fig. 14 for the ATLAS and CMS experiments respectively. The 0-jet category is dominated by non-resonant WW background while $t\bar{t}$ dominates the the 1 & 2 jet categories. Both

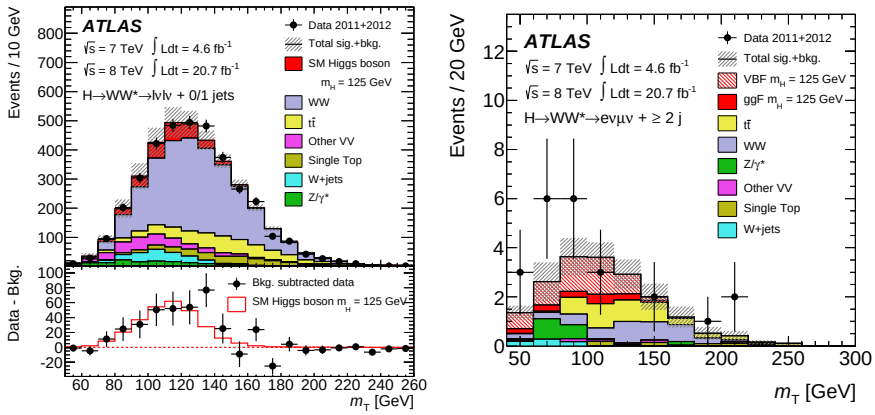

Figure 13: (Left) The m_T distribution for selected events summed over all lepton flavors and with ≤ 1 associated jets. The contributions from various background sources and a 125 GeV SM Higgs are stacked together. The difference between data and estimated SM background and the expectation from a SM Higgs boson with $m_H = 125$ GeV are shown in the lower panel. (right) The m_T distribution for selected $e^{\pm}\mu^{\mp}$ events and with ≥ 2 associated jets. The signal yield from the VBF and gluon fusion processes are indicated.

experiments see a clear excess over background expectation in the 0 & 1 jet categories. ATLAS fits the m_T distributions and observes [101,108] the most significant excess for $m_H = 140$ GeV. The significance of the observed excess for $m_H = 125.5$ GeV is 3.8σ, the same as expected. The measured inclusive signal strength $\mu = 1.01 \pm 0.31$. In the VBF category an excess with a significance of 2.5σ corresponding to a signal strength of $\mu_{\rm VBF} = 1.66 \pm 0.67 \pm 0.43$ is observed for $m_H = 125$ GeV. The CMS analysis of 0 & 1 jet categories, using all lepton flavor combinations, shows [110] an excess with an observed significance of 4σ consistent with the expected significance of 5.1σ for a 125 GeV Higgs boson. A separate analysis optimized for the VBF mode reports [111] no significant excess and sets a 95% CL upper limit of $\mu_{\rm VBF} < 1.7$ for $m_H = 125$ GeV

The ATLAS and CMS experiments have also searched for associated Higgs boson production (VH) in this channel and have set 95% CL limits on $\mu_{\rm VH}$ of 7.2 [109] and 5.0 [112] respectively for $m_H = 125$ GeV.

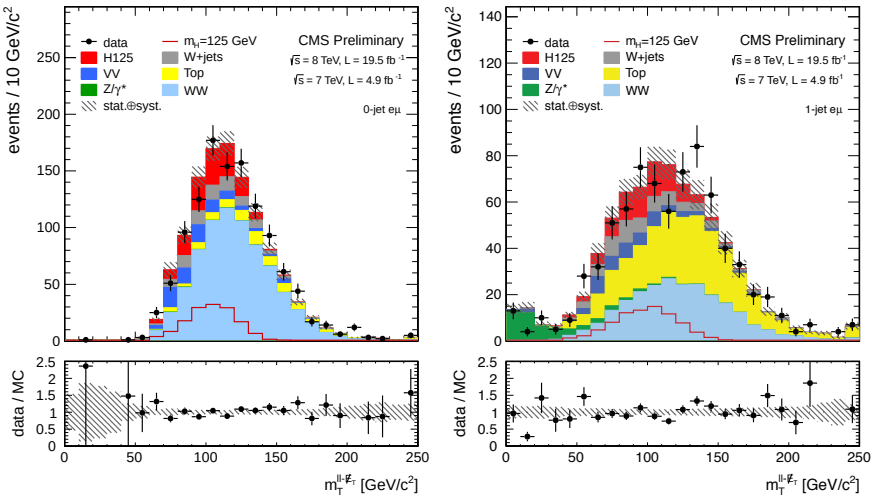

Figure 14: (Left) The m_T distribution for events, selected with a cut-based analysis, summed over all lepton flavors and with zero associated jets (left) and 1-jet (right). The contributions of all SM background sources and a SM Higgs with m_H=125 GeV are stacked together.

III.4. Decays to fermions

As described in **III.I**, significant signals for the decay of the observed boson in the the $\gamma\gamma$, ZZ and W^+W^- channels have been observed by the ATLAS and CMS experiments. The measured signal strengths in these channels are consistent with this boson playing a role in electroweak symmetry breaking. However the nature of its interaction with fermions and whether this Higgs-like boson serves also as a source of mass generation for quarks and leptons via Yukawa interactions is a topic of active investigation.

At the Hadron colliders, the most promising channel for probing the coupling of the Higgs field to the quarks and leptons are $H \to b\bar{b}$ and $H \to \tau^+\tau^-$ respectively. For a Higgs boson with $m_H \approx 125$ GeV, the branching fraction to $b\bar{b}$ is about 57% and to $\tau^+\tau^-$ is about 6%. Nevertheless the presence of overwhelming backgrounds makes the isolation of a Higgs boson signal in these channels quite challenging.

III.4.1. $H^0 \to b\bar{b}$

The dominant production mode $gg \to H \to b\bar{b}$ is overwhelmed by the background from the inclusive production of

$p\bar{p} \to b\bar{b} + X$ via the strong interaction. The associated production modes $\mathrm{W}^{\pm}H$ and $\mathrm{Z}H$ (collectively termed VH modes) allow use of the leptonic W and Z decays to purify the signal and reject QCD backgrounds. W bosons are reconstructed via their leptonic decay $\mathrm{W}^{\pm} \to \ell\bar{\nu}_{\ell}$ where $\ell = e, \mu$ or τ. The Z bosons are reconstructed via their decay into $e^+e^-, \mu^+\mu^-$or $\nu\bar{\nu}$. The Higgs boson candidate mass is reconstructed from two b-tagged jets in the event. Backgrounds arise from production of W & Z bosons in association with gluon, light and heavy-flavored jets (V+jets), $t\bar{t}$, non-resonant diboson (ZZ & WZ with $\mathrm{Z} \to b\bar{b}$) and QCD multijet processes. Due to the limited $m_{b\bar{b}}$ mass resolution, a SM Higgs boson signal is expected to appear as a broad enhancement in the reconstructed dijet mass distribution. The crucial elements in this search are b-jet tagging with high efficiency and low fake rate, accurate estimate of b-jet momentum and estimate of backgrounds from various signal depleted control samples constructed from data.

CDF and DØ collaborations use multivariate analysis (MVA) techniques that combine several discriminating variables into a single final discriminant used to separate signal from background. Each channel is divided into exclusive subchannels according to various lepton, jet multiplicity, and b-tagging characteristics in order to group events with similar signal-to-background ratio and thus optimize the overall search sensitivity. The combined CDF & DØ data shows [114,115] an excess of events with respect to the predicted background in the most sensitive bins of the discriminant distributions suggesting the presence of a signal. Fig. 15 (left) shows the best-fit cross section times branching ratio $(\sigma_{\mathrm{WH}} + \sigma_{\mathrm{ZH}}) \times \mathrm{B}(H \to b\bar{b})$ as well as the SM prediction as a function of m_H. The p-value, the observed and expected significance as a function of m_H are shown in Fig. 15(right). A significant excess of events is observed in the 115-140 GeV mass range. At $m_H = 125$ GeV the local significance of the excess is 3.0 standard deviations. At that mass, the observed signal strength $\mu = 1.59^{+0.69}_{-0.72}$.

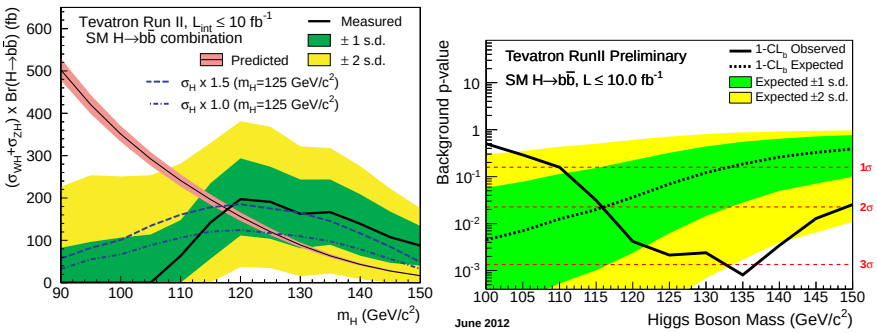

Figure 15: Result from the Tevatron: (Left) The best-fit cross section times branching ratio $(\sigma_{\rm WH} + \sigma_{\rm ZH}) \times {\rm B}(H \to b\bar{b})$ as well as the SM prediction as a function of m_H. The dark and light-shaded regions indicate the 1 and 2 standard deviations measurement uncertainties, and the SM prediction is shown as the smooth, falling curve. The expected cross section fit values assuming a SM Higgs boson with $m_H = 125$ are shown with dot-dashed lines for the expected SM rate (dark blue) and the best fitted rate from data (light magenta). (right) The p-value as a function of m_H under the background-only hypothesis. Also shown are the median expected values assuming a SM Higgs signal for different m_H. The associated dark and light-shaded bands indicate the 1 and 2 standard deviations fluctuations of possible experimental outcomes.

To reduce the dominant V+jets background, following [113], the LHC experiments select a region in VH production phase space where the vector boson is significantly boosted and recoils from the $H \to b\bar{b}$ candidate with a large azimuthal angle $\Delta\phi_{\rm VH}$. For each channel, events are categorized into different p_T(V) regions with varying signal/background ratios. Events with higher p_T(V) have smaller backgrounds and better $m_{b\bar{b}}$ resolution. CMS uses [116] MVA classifiers based on kinematic, topological and quality of b-jet tagging and trained on different values of m_H to separate Higgs boson signal in each category from backgrounds. MVA output for all categories are then fit simultaneously. Fig. 16(left) shows the combined MVA output of all channels where events are gathered in bins of similar expected signal-to-background ratios as predicted by the MVA

discriminants. The excess of events observed in bins with the largest signal-to-background ratios is consistent with the production of a 125 GeV SM Higgs boson with a significance of 2.1 standard deviations. The observed signal strength at 125 GeV is $\mu = 1.0 \pm 0.5$. Fig. 16(right) shows the $m_{b\bar{b}}$ distribution for all categories combined, weighted by signal to background ratio in each category, with all backgrounds except dibosons subtracted. The data also show the presence of a diboson ($W/Z + Z \to b\bar{b}$ signal with a rate consistent with the standard model prediction together with an excess consistent with the production of the SM Higgs boson with $m_H = 125$ GeV.

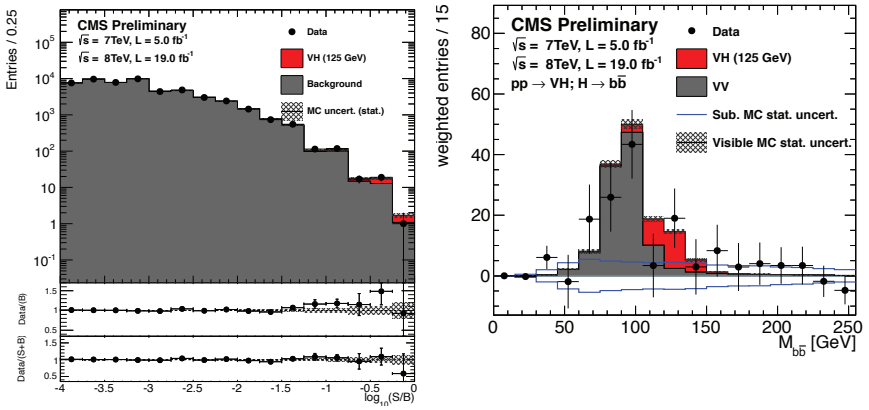

Figure 16: CMS results: (left) The combination of all channels into a single distribution. The two bottom insets show the ratio of the data to the background-only prediction (above) and to the predicted sum of background and SM Higgs boson signal with a mass of 125 GeV(below). (right) The $m_{b\bar{b}}$ distribution with all backgrounds, except dibosons, subtracted. The solid histograms for the backgrounds and the signal are summed cumulatively. The line histogram for signal and for VV backgrounds are also shown superimposed.

ATLAS performs a cut based analysis [120], with selected events divided into a large number of categories in $p_T(V)$. $m_{b\bar{b}}$ is used as the discriminating variable, and customized control samples devised from data are used to constrain the contributions of the dominant background processes. Fig. 17(left) shows the $m_{b\bar{b}}$

distribution where the contributions from signal regions in all categories are summed weighted by the expected-Higgs-boson-signal over background ratio. No significant excess is observed (see Fig. 17(right)). The signal strength for $m_H = 125$ GeV is measured to be $^- \mu = 0.2 \pm 0.5(\text{stat.}) \pm 0.4(\text{syst.})$.

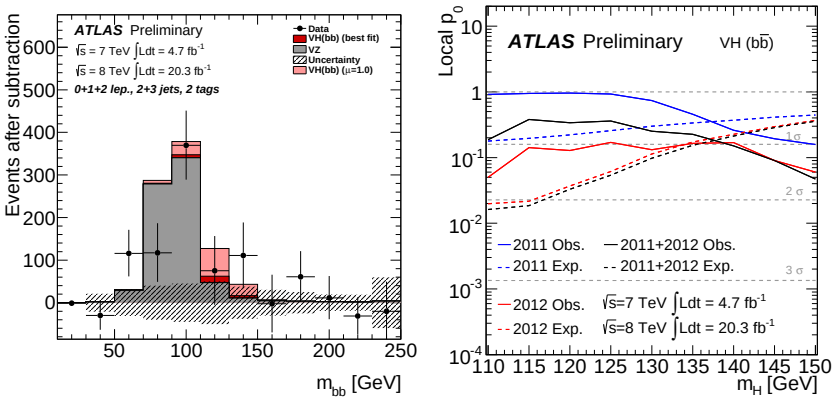

Figure 17: ATLAS results: (Left) The $m_{b\bar{b}}$ distribution in data after subtraction of all backgrounds except for the diboson processes and for the associated WH and ZH production of a SM Higgs boson with $m_H = 125$ GeV. (right) The observed local p-value as a function of m_H. The dashed curves show the expected local p-value under the hypothesis of a SM Higgs boson signal at that mass.

In 19 fb^{-1} of $\sqrt{s} = 8$ TeV data, CMS has searched for $H \to b\bar{b}$ in the VBF [117] production mode and placed a 95% CL limit on the signal strength of $\mu_{\text{VBF}} < 3.6$.

The most sensitive search for $t\bar{t}H$ production mode with $H \to b\bar{b}$ has been reported [119] by the CMS experiment using a partial data set of 5(5.1) fb^{-1} at $\sqrt{s} = 7$ (8) TeV respectively. Two $t\bar{t}$ final states are considered (a) the dilepton final state $t\bar{t} \to \ell^+\nu\ell^-\overline{\nu}b\bar{b}$ and (b) the lepton + jets final state $t\bar{t} \to \ell^+\nu q\overline{q}^{'}b\bar{b}$. The backgrounds in this search are low and dominated by $t\bar{t} + b\bar{b}$ production but the the small signal production cross-section reduces the search sensitivity. The 95% CL upper limit on the signal strength is $\mu_{\text{t}\bar{\text{t}}\text{H}} < 5.8$.

III.4.2. $H^0 \to \tau^+\tau^-$

In the $H \to \tau\tau$ search, τ lepton decaying to electrons (τ_e), muons (τ_μ) and hadrons (τ_{had}) are considered. $m_{\tau\tau}$ is reconstructed from the visible products from the two τ leptons and the missing energy observed in the event. Due to the presence of missing neutrinos, the $m_{\tau^+\tau^-}$ resolution is poor ($\approx$ 15%. As a result, a broad excess over the expected background in the $m_{\tau\tau}$ distribution is searched for. The major sources of background stem from Drell–Yan Z $\to \tau^+\tau^-$ and Z $\to e^+e^-$, W+jets, $t\bar{t}$ and multijet production. Events in all sub-channels are divided into categories based on the number and kinematic properties of additional energetic jets in the event. The sensitivity of the search is generally higher for categories with one or more additional jets. The VBF category consisting of a $\tau\tau$ pair with two energetic jets separated by a large pseudorapidity has the best signal-to-background and search sensitivity. Since the signal to background discrimination depends on $m_{\tau\tau}$ resolution which improves with the boost of the Higgs boson, the non-VBF categories are further subdivided according to the observed boost of the $\tau^+\tau^-$ system. The 0-jet category which has the poorest signal/background ratio is used to constrain the background yields, the reconstruction efficiencies, and the energy scales.

$H \to \tau^+\tau^-$ decays in the VH production mode are searched for in final states where the W or Z boson decays into leptons or into two jets (ATLAS only). While the decays to tau pairs are the dominant Higgs boson signal contribution, the final states used can additionally be produced by the decay of the Higgs boson into a pair of W bosons that both decay to leptons. The irreducible background in this search arises from non-resonant WZ and ZZ diboson production. The reducible backgrounds originate from W, Z and $t\bar{t}$ events that contain at least one fake lepton in the final state due to a misidentified jet. The shape and yield of the major backgrounds in each category is estimated from control samples in data. Contributions from non-resonant WZ and ZZ diboson production is estimated from simulations but corrected for reconstruction efficiency using control samples formed from data.

Fig. 18 (left) shows the CMS [121] $m_{\tau\tau}$ distributions combining all non-VH categories, weighting the distributions in each category of each sub-channel by the ratio between the expected signal and background yields for that category. The inset plot shows the difference between the observed data and expected background distributions, together with the expected distribution for a SM Higgs boson signal with $m_H = 125$ GeV. The p-value and significance of the observed excess are shown in Fig. 18(right). For $m_H = 125$ GeV, the significance of the observed excess at $m_H = 125$ GeV is 2.85 standard deviations and corresponds to a signal strength of $\mu = 1.1 \pm 0.4$.

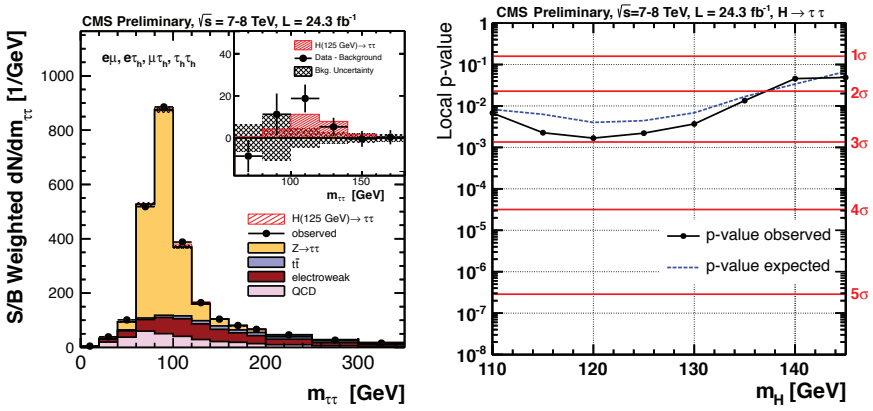

Figure 18: CMS results : (left) Combined observed and expected $m_{\tau\tau}$ distributions for $\tau_\mu\tau_{had}$, $\tau_e\tau_{had}$, $\tau_{had}\tau_{had}$ and $\tau_e\tau_\mu$ sub-channels. The insert shows the difference between the observed data and the expected background distributions, together with the expected signal distribution for a SM Higgs signal at $m_H = 125$ GeV. The integral of the distribution of signal events corresponds to the number of signal events observed in the 1-jet and VBF categories. (right) Observed and expected p-values, and the corresponding significance in number of standard deviations. These results include the results of the search in the VH mode.

Current ATLAS results [122] are based on a partial data sample of 4.7fb^{-1} at 7 TeV and 13.0fb^{-1} at 8 TeV. At $m_H = 125$ GeV, the observed (expected) deviation from the background-only hypothesis corresponds to a local significance of 1.1 (1.7)

standard deviations and the best fit value of ¯the signal strength $\mu = 0.7 \pm 0.7$. The 95 % CL upper limit on μ is 1.9 times the SM prediction.

III.5. Observed Signal Strengths

*****WE have to be careful with the refs for individual modes and point out that the combination is based on results available till Winter'13 *******

The μ value obtained by ATLAS [101] and CMS [100] in the five channels and the combined best fit value are displayed inFig. 19. The μ value for each channel and the combination is calculated for the best fit mass of 125.5 and 125.7 by ATLAS and CMS respectively. The ATLAS combination used only the $\gamma\gamma$, WW and ZZ channels for which the full 7 & 8 TeV data were analyzed. Table 12 summarizes the measurements from the Tevatron and the LHC (CHECK CONSISTENCY OF NUMBERS). All measurements are consistent with the expectation from the SM Higgs boson with a mass of 125 GeV.

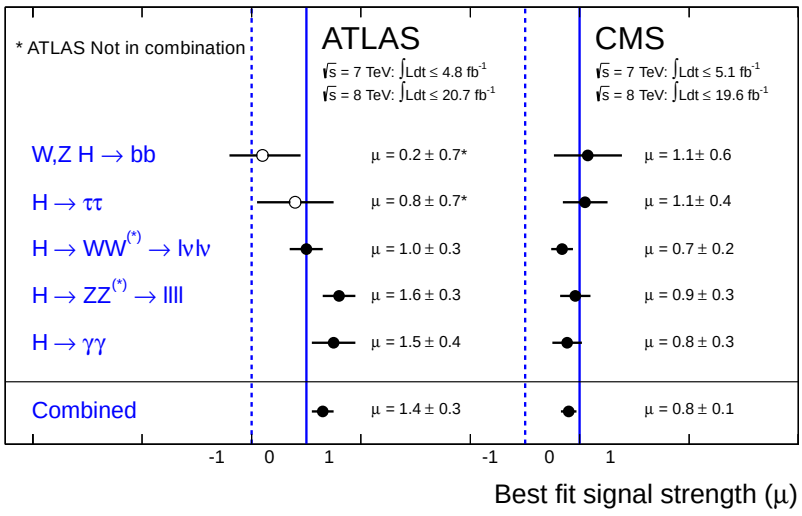

Figure 19: Signal strengths measured by the ATLAS [101,120], [122] and CMS [100] experiments in the five principal channels and their combination. ATLAS USES ONLY Gamgam, ZZ, WW , CMS uses only Hbb with partial dataset (HCP'12)

Table 4: Overall channel signal strengths, ****this plot has to be shrunk to show Hbb values****; check consistency of numbers with what is in the references; add correct references in table

	$\gamma\gamma$	ZZ (4ℓ)	WW ($\ell\nu\ell\nu$)	$\tau\tau$
ATLAS				
μ (at 125.5 GeV)	1.5±0.4	1.6±0.3	1.0±0.3	0.8±0.7
Z Exp.	4.1	4.4	3.8	1.6
Z Obs.	7.4	6.6	3.8	1.1
Mass (GeV)	126.8±0.2±0.7	124.3±0.5±0.5	-	-
Reference	[21]	[21]	[21]	[21]
CMS				
μ (at 125.5 GeV)	0.8±0.3	0.9±0.3	1.5±0.4	1.5±0.4
Z Exp.	3.9	7.1	5.3	2.6
Z Obs.	3.2	6.7	3.9	2.8
Mass (GeV)	125.6±0.2±0.7	125.6±0.2±0.7		125.6±0.2±0.7
Reference	[22]	[22]	[22]	[22]
Tevatron				
μ (at 125 GeV)	$6.0^{+3.4}_{-3.1}$	–	1.6±1.2	$1.7^{+2.3}_{-1.7}$
Reference	[24]	[24]	[24]	[24]

III.6. Searches for Rare Decays of the Higgs boson

This subsection will move away from Section 3

III.6.1. $H^0 \to Z\gamma$

The search for $H \to Z\gamma$ is performed in the final states where the Z boson decays into opposite sign and same flavor leptons ($\ell^+\ell^-$). ℓ here refers to $e$or μ. While the branching fraction for $H \to Z\gamma$ is comparable to $H \to \gamma\gamma$ (about 10^{-3}) at $m_H = 125$GeV, the observable signal yield is brought down by the small branching ratio of Z $\to (e^+e^- + \mu^+\mu^-) = 6.7 \times 10^{-2}$. In these channels, the $m_{\ell\ell\gamma}$ mass resolution is excellent (1-3%) so the analyses search for a narrow mass peak over a continuous background. The major backgrounds arise from the Z$+\gamma$, final state radiation in Drell–Yan decays and Z + jets process where a jet is misidentified as a photon.

Events are divided into mutually exclusive categories on basis of the expected $m_{Z\gamma}$ resolution and the signal-to-background

ratio. A VBF category is formed for $H \to Z\gamma$ candidates which are accompanied by two energetic jets separated by a large psuedorapidity. While this category contains only $\approx 2\%$ of the total event count, the signal-to-noise is about an order of magnitude higher. The search for a Higgs boson is conducted independently in each category and the results from all categories are then combined.

The CMS $m_{\ell^+\ell^-\gamma}$ spectrum with all search categories combined is shown in Fig. 20(left). The observed and expected 95% CL upper limit [123] on the signal strength μ are 9.5 and 10 respectively. The ATLAS expected and observed upper limits [124] on μ are 18.2 and 13.5 respectively.

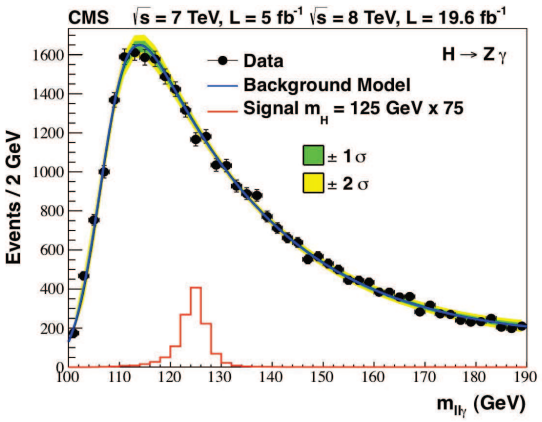

Figure 20: The $m_{\ell^+\ell^-\gamma}$ spectrum observed by CMS with all categories combined. Also shown is the expected signal due to a 125 GeV SM Higgs boson scaled by factor of 75 and the sum of the individual fits made to the data for each category.

III.6.2. $H^0 \to \mu^+\mu^-$

$H \to \mu^+\mu^-$ is the only channel where the Higgs coupling to second generation fermions can be measured at the LHC. The branching fraction in this channel for a 125 GeV SM Higgs boson is 2.2×10^{-4}, about ten times smaller than that for $H \to \gamma\gamma$. The dominant and irreducible background arises from the $Z/\gamma^* \to \mu^+\mu^-$ process which has a rate several orders of magnitude larger than that from the SM Higgs boson signal. Due to the precise muon momentum measurement achieved by

ATLAS and CMS, the $m_{\mu^+\mu^-}$ mass resolution is excellent ($\approx 2-3\%$) but rendered marginally asymmetric due to final state radiation from the muons. A search is performed for a narrow peak over a large but smoothly falling background. For optimal search sensitivity, events are divided into several categories. To take advantage of the superior muon momentum measurement in the central region, the two experiments subdivide events by the pseudorapidity of the muons. To suppress the Drell–Yan background, ATLAS requires $p_T^{\mu^+\mu^-} > 15$ GeV while CMS separates them into two $p_T^{\mu^+\mu^-}$ based categories. CMS further categorizes events by the number and the topology of additional energetic jets in the event.

The $m_{\mu^+\mu^-}$ distribution from ATLAS analysis of their 8 TeV data is shown in Fig. 21. No signal is observed for $m_H = 125$ GeV and an upper limit on the signal strength $\mu < 9.8$ is set. The CMS analysisCmsHmumuPAS13 of their 7 and 8 TeV data sets a limit of $\mu < 7.4$

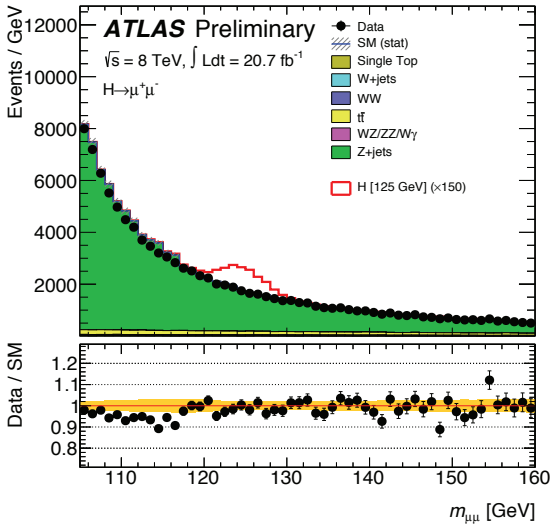

Figure 21: The $m_{\mu^+\mu^-}$ distribution for the events selected by ATLAS in their 8 TeV data sample . An expected signal for $m_H = 125$ GeV , scaled by a factor of 150, is shown atop the background dominated by Drell–Yan (Z + jets) process.

IV. Properties and Nature of of the New Bosonic Resonance

introduction here

A significant deviation in the measurement of the couplings or CP properties of the recently discovered Higgs boson could indirectly signal the presence of an extended Higgs sector.

IV.1. Main quantum numbers $\mathcal{J}^{\mathcal{PC}}$

The measurements of the signal event yields of the observed new state in all the channels discussed above and their compatiblility with the Standard Model Higgs boson predictions, gives qualitative, but nonetheless very compelling evidence of its nature.

This qualitative overall picture is further confirmed by the observation of the particle in the diphoton channel. According to the Landau-Yang theorem, in the diphoton channel excludes the spin-1 hypothesis and essentially restricts possibilities for the spin of the observed particle to 0 or 2 Technically higher spin values are not excluded and will be briefly discussed below. There are however several loopholes that have lead experiments not to discard *a priori* the spin-1 hypothesis.

The Landau-Yang theorem does not necessarily apply if the observed state is not decaying to a pair of photons but to a pair of scalars subsequently decaying to two very collimated pairs of photons (as for example in the case of $H \to a_1 a_1 \to \gamma\gamma$). This possibility has not been riguorously tested but it is not experimentally favored as tight selection criteria are applied on the electromagnetic shower shapes of the reconstructed clusters photons. Furthermore a data-driven estimate of the reducible background inclusive invariant mass distributino by the ATLAS experiment does not show any significant excess. A more systematic analysis of shower shapes and the fraction of conversions could be performed to further discriminate between the single prompt photon and the two overlapping photons hypotheses.

There are also various potential theoretical loopholes concerning the applicability of the Landau-Yang theorem, such as

off-shell vecor boson decays, Bose symmetry violation, or non commutative geometry theories.

Finally the tests of the custodial symmetry through the ratio λ_{WZ} also provide suppoting evidence against the spin-2 hypothesis due to the different acceptances

For the observed particle not to be of spin-0 and +1 parity would require an improbable conspiration of effects. It is nevertheless very important that this hypothesis be independently tested using as independent as possible analyses.

IV.1.b Charge conjugation $\mathcal{C}$

The charge conjugation quantum number is multiplicative, therefore given that the Higgs-like particle is observed in the $H \to \gamma\gamma$ channel, and given that photons are $\mathcal{C}-$ eigenstates, the observed neutral particle should be of charge $\mathcal{C}+$.

IV.1.d Spin ($\mathcal{J}$) and parity ($\mathcal{P}$) of the new observed state

To further assess the spin and parity quantum numbers of the discovered particle, a systematic analysis of its production and decay processes is done to measure its spin and parity properties. These analyses have been designed to be as independent as possible from the event yields measured in each exclusive categories, relying instead on the production and the decay angles, and on the threshold distributions, of the produced particle.

This leads to test hypotheses which are typically disfavored by the analysis of the rates, such as a pseudoscalar particle decaying to a pair of W or Z bosons which requires, decay through loops. The sizable interaction of the observed state with electroweak gauge bosons, if it were pseudoscalar, would imply low scale physics in the loops and therefore would be ruled out by the absence of direct observation of such states. Or to test spin-2 hypotheses for which no renormalizable model exist.

To further define, generate and test the newly observed state without theoretical prejudice, the most general tensor structure is used for the three possible spin hypotheses spin-0, spin-1 and spin-2. The spin-0 most general interactin amplitude with two gauge bosons can be written as follows [RefJHU]:

$$A^{(0)} = v^{-1}\left(g_1^{(0)} m_V^2 \varepsilon_1^* \varepsilon_2^* + g_2^{(0)} f_{\mu\nu}^{*(1)} f^{*(2),\mu\nu} + g_3^{(0)} f^{*(1),\mu\nu} f_{\mu\alpha}^{*(2)} \frac{q_\nu q_\alpha}{\Lambda^2} + g_4^{(0)} f_{\mu\nu}^{*(1)} \tilde{f}^{*(2),\mu\nu}\right)$$

Where the ε denotes the polarization vector of a spin-1 bosons, q the momentum of the a vector boson, $f^{(i),\mu\nu} = \varepsilon_i^\mu q_i^\nu - \varepsilon_i^\nu q_i^\mu$ is the field strength tensor of a gauge boson with momentum q_i and polarization ε_i, and Λ is the scale of new physics mass scale. The g_j^0 are dimensionless and momentum dependent complex form factors.

The first term corresponds to the Standard Model case 0^{++} where:

$$\mathcal{L} \supset g_1^{(0)} H Z_\mu Z^\mu$$

The second (CP conserving) and fourth (CP violating) terms correspond to 5 dimensional operator couplings through loops of the type:

$$\mathcal{L} \supset g_2^{(0)} H Z_{\mu\nu} Z^{\mu\nu} + g_2^{(0)} H Z_{\mu\nu} \tilde{Z}^{\mu\nu}$$

The third term corresponds to couplings through new physics at a scale Λ.

Similarly the most general spin-1 interaction amplitude with two gauge bosons can be expressed as follows:

$$A^{(2)} = g_1^{(1)}[(\varepsilon_1^* q)\,(\varepsilon_2^* \varepsilon_X)] + g_2^{(1)} \epsilon_{\alpha\beta\mu\nu} \varepsilon_X^\alpha \varepsilon_1^{*,\mu} \varepsilon_2^{*,\nu} \tilde{q}^\beta$$

Similarly to the general spin-0 case the $g_1^{(1),(2)}$ form factors are effective and dimensionless. Finally the general spin-2 case can be expressed as follows [RefJHU]:

$$
\begin{aligned}
A^{(2)} = \frac{1}{\Lambda}[&2g_1^{(2)} t_{\mu\nu} f^{*1,\mu\alpha} f^{*2,\nu\alpha} + 2g_2^{(2)} t_{\mu\nu} \frac{q_\alpha q_\beta}{\Lambda^2} f^{*1,\mu\alpha} f^{*2,\nu\beta} \\
&+ g_3^{(2)} \frac{\tilde{q}^\beta \tilde{q}^\alpha}{\Lambda^2} t_{\beta\nu} \left(f^{*1,\mu\nu} f^{*2}_{\nu\alpha} + f^{*2,\mu\nu} f^{*1}_{\nu\alpha} \right) \\
&+ g_4^{(2)} \frac{\tilde{q}^\mu \tilde{q}^\nu}{\Lambda^2} t_{\mu\nu} f^{*1,\alpha\beta} f^{*2}_{\alpha\beta} + 2g_5^{(2)} m_V^2 t_{\mu\nu} \varepsilon_1^{*\mu} \varepsilon_2^{*\nu} \\
&+ 2g_6^{(2)} m_V^2 \frac{\tilde{q}^\mu \tilde{q}^\nu}{\Lambda^2} t_{\mu\nu} \left(\varepsilon_1^{*\nu} \varepsilon_2^{*\alpha} - \varepsilon_1^{*\alpha} \varepsilon_2^{*\nu} \right) + g_7^{(2)} m_V^2 \frac{\tilde{q}^\mu \tilde{q}^\nu}{\Lambda^2} t_{\mu\nu} \varepsilon_1^* \varepsilon_2^* \\
&+ g_8^{(2)} \frac{\tilde{q}^\mu \tilde{q}^\nu}{\Lambda^2} t_{\mu\nu} f^{*1,\alpha\beta} \tilde{f}^{*2}_{\alpha\beta} + g_9^{(2)} t_{\mu\alpha} \tilde{q}^\alpha \epsilon_{\mu\nu\rho\sigma} \varepsilon_1^{*\nu} \varepsilon_2^{*\rho} q^\sigma \\
&+ g_{10}^{(2)} \frac{t_{\mu\alpha} \tilde{q}^\alpha}{\Lambda^2} \epsilon_{\mu\nu\rho\sigma} q^\rho \tilde{q}^\sigma \left(\varepsilon_1^{*\nu} \left(q \varepsilon_2^* \right) + \varepsilon_2^{*\nu} \left(q \varepsilon_1^* \right) \right)]
\end{aligned}
\tag{3}
$$

Where $t_{\mu\nu}$ is a symmetric traceless tensor, transverse to the momentum of the spin-2 state $t_{\mu\nu} q^\nu = 0$ [RefJHU]. Similar amplitudes are derived in the case of fermion couplings, as reported in Reference [YR3]. Studies of the spin and CP properties of the discovered state can either use an effective Lagrangian approach or generic scattering amplitudes. The two are fully equivalent. However typically the effective Lagrangian is used to generate specific hypotheses and the scattering amplitudes are used in in analyses.

The JHU generator [JHU1,JHU2] has been used to define benchmark scenarios for exotic hypoptheses for the nature of the observed state according to the general couplings of the observed new particle to gluons and quarks in production and to vector bosons in decay and includes all spin correlations and interferences of all contributing amplitudes. The defined models which have been investigated by experiments are reported in Table [**JHUtable**].

The $\gamma\gamma$ channel

The $\gamma\gamma$ channel in the WW^* channel through the production processes have also been discussed at length in the litterature, for the gluon fusion and vector boson fusion processes in Ref.

The threshold behavior of the cross section from associated production mechanisms such as the associated production with a gauge boson and the vector boson fusion processes can give additional sensitivity to the spin and parity of the observed

Table 5: benchmark scenarios for the analysis of the production and decay of the observed state with $J^{\mathcal{P}}$ quantum numbers. The subscripts refer to the specificities of the couplings of the observed state, where m denotes minimal couplings and h denotes couplings with higher dimension operators. For each scenarios only the non vanishing coupling constants are reported in this table.

Scenario	Production	Decay	Scenario
0^+_m	$gg \to X$	$g_1^{(0)} = 1$	SM Higgs bosons
0^+_h	$gg \to X$	$g_2^{(0)} \neq 0$	Pseudo-scalar
0^-	$gg \to X$	$g_4^{(0)} \neq 0$	SM Higgs bosons
1^+	$qq \to X$	$g_2^{(1)} \neq 0$	Pseudo vector
1^-	$qq \to X$	$g_a^{(1)} \neq 0$	Vector
2^+_m	$g_1^{(2)} \neq 0$	$g_1^{(2)} = g_5^{(2)} \neq 0$	Graviton tensor MC
2^+_m	$g_4^{(2)} \neq 0$	$g_4^{(2)} \neq 0$	Graviton tensor HD op.
2^+_h	$g_8^{(2)} \neq 0$	$g_8^{(2)} \neq 0$	Pseudo tensor

statethese analyses have not been performed yet. However, given the much larger expectation in the spin-2 case in the VH($b\bar{b}$) analysis, based on the observation made at the Fermilab tevatron in this channel,

The study of the spin and parity of the observed state is currently done only with the angular analysis of the Higgs decay products only. However ATLAS has produced first differential cross section measurements, in particular in the two-jets VBF-like channel which is sensitive to the spin and parity of the observed state. These measurements alone do not have sufficient sensitivity to be conclusive on the main quantum numbers of the observed state.

On the method

The consistency of the data in the various angular distributions can be measured by a goodness of fit test, but this alone does not give a measurement of the spin. In fact, how good a measurement is if the data is as consistent with another spin

hypothesis? Integer or fractional qunantities are usually measured by the rates to which they are related (*e.g.* the number of neutrino flavors using the Z-peak cross section, or the top quark charge using the $t\bar{t}\gamma$ cross-section). In this case, the spin is measured by excluding all other hypotheses, and accepting the main spin-0 hypothesis.

Excluding Spin 2 scenarios

The analysis of spin at LHC is mainly carried out in three different channels $H \to \gamma\gamma$, $H \to W^{(*)}W^{(*)} \to \ell\nu\ell\nu$ and $H \to Z^{(*)}Z^{(*)} \to 4\ell$.

In the case of the $H \to \gamma\gamma$ channel, the analysis is performed inclusively. The reasons being simplicity and that the categoriation in pseudo-rapidity of the photons is correlated to the production anlge $cos\theta^*_{CS}$. The definition chosen for the polar angle in the rest frame is the Collins-Soper frame, which is defined as the bisector axis of the mometa of the incoming protons in the diphoton rest frame. For the signal of course this has no impact as the distribution is fully uniform in the rest frame, it makes a slight difference for the background. Another change in the analysis which is the lower cut requirements on the transverse momentum of the photons. It is now done as a function of the reconstructed diphoton invariant mass similarly to the cuts performed in the main CMS analysis. The reason for this different choice for the spin is that fixed cuts introduce a large correlation between the invariant mass and the $cos\theta^*_{CS}$. With the new set of cuts the correlation is largely removed, at a level where a full decorrelation can be assumed. The background $cos\theta^*_{CS}$ distribution can then be derived simply from the sidebands in invariant mass. A large systematic uncertainty on the shape of the $cos\theta^*_{CS}$ distribution for the background is assumed to cover the potential error introduced from residual correlations between the mass and the production angle for the background. The results of the $H \to \gamma\gamma$ spin analysis are illustrated in Figure [**fig:qqscan**] a. The $H \to \gamma\gamma$ channel is mostly sensitive to the gluon-initiated production modes and very little to the quark-initiated ones. An angle that has not been used in this analysis, and which could potential add some sensitivity is the ϕ^* in the Collins-soper frame.

The $H \to W^{(*)}W^{(*)} \to \ell\nu\ell\nu$ analysis also had to be reappraised in order to perform an analysis of spin. Countrary to the spin analysis in the diphoton channel, the decay angle cannot be easily reconstructed due to the nuetrinos in the final state, instead an important feature is the V-A structure of the decay of the W bosons. If the observed state is a scalar, this gives a clear spin correlation pattern that implies that the leptons e or μ from the decays of the W bosons are produced close to one another in the transverse plane. In the main analysis this feature is used to gain sensitivity and the analysis largely relies on the use of the $\Delta Phi_{\ell\ell}$ and $M_{\ell\ell}$ distribution. For the spin the analysis cuts are relaxed and the main kinematic variables are used in two BDTs, one trained to discriminate the spin-0 signal from background and the second to discriminate the spin-2 signal from background. the discrimination between the two hypothesis is done from a 2D-fit in the plane of the two BDTs. The results of the $H \to W^{(*)}W^{(*)} \to \ell\nu\ell\nu$ analyses are illustrated in Figure [**fig:qqscan**] b, as a function of the fraction of quark versus gluon initiated processes. The $H \to W^{(*)}W^{(*)} \to \ell\nu\ell\nu$ channel is mostly sensitive to the quark-initiated production modes. It is therefore very complementary to the $H \to \gamma\gamma$ channel.

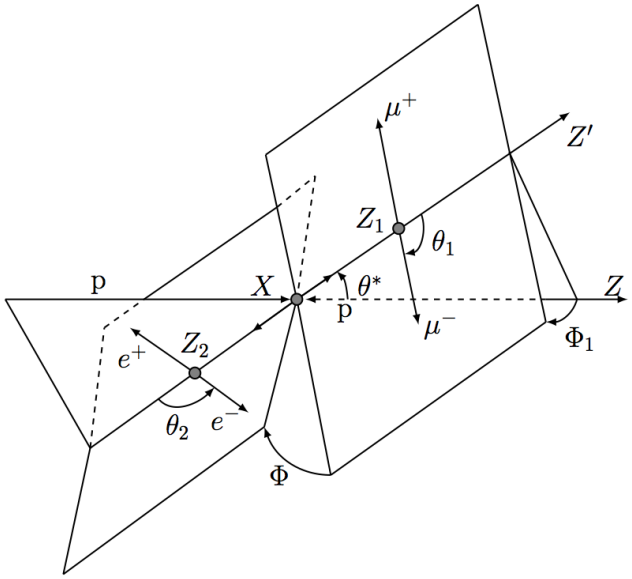

Figure 22: Angles defintions

The $H \to Z^{(*)}Z^{(*)} \to 4\ell$ channel has only recently performed an analysis in categories aiming at the VBF and VH associated production modes. Their impact is in fact still marginal as discussed in Section [**sec:couplings**]. The main inclusive selection is unchanged to perform the spin analysis. There are two approaches to this analysis. The first is based on a Matrix Element Likelihood (MELA) and the second is the combination of sensitive variables in a boosted decision tree. The observables sensitive to the spin and parity are the masses of the two Z bosons (due to the threshold dependence of the mass of the off-shell Z boson a production angle θ^*, and four decay angles, ϕ_1, ϕ, θ_1 andθ_2. The production and decay angles defined as:

- θ_1 and θ_2, the angles between the negative final state lepton and the direction of flight of Z1 (Z2) in the Z rest frame.

- ϕ, the angle between the decay planes of the four final state leptons expressed in the four lepton rest frame.

- ϕ_1, the angle defined between the decay plane of the leading lepton pair and a plane defined by the vector of the Z1 in the four lepton rest frame and the positive direction of the parton axis.

- θ^*, the production angle of the Z1 defined in the four lepton rest frame.

The results for this channel are illustrated in Figure [**fig:qqscan**] c, showing that this channel has a smaller sensitivity to the spin. Its sensitivity is approximately constant with respect to the fraction of the qq versus gg spin-2 initiated processes.

Given the complementarity of the $H \to \gamma\gamma$ and $H \to W^{(*)}W^{(*)} \to \ell\nu\ell\nu$ analyses the quantitative assessment of the exclusion of the scenarios investiated herein will profit from a combination of the results.

Excluding Spin 1

Assuming the non applicability of the Landau-Yang theorem, and to make sure that no stone are unturned, an analysis probing the spin-1 in the +1 and -1 parity hypotheses is carried out in the $H \to Z^{(*)}Z^{(*)} \to 4\ell$ channel. In both cases the observation is in fair agrement with the $J^P = 0^+$ hypothesis and the $J^P = 1^+$ hypothesis is excluded at 99.8% CL_s and the $J^P = 1^-$

hypothesis is excluded at 94% CL_s. A similar analysis is also being prepared using the $H \to W^{(*)}W^{(*)} \to \ell\nu\ell\nu$ channel.

Parity

The most senstive channel to the parity is the $H \to Z^{(*)}Z^{(*)} \to 4\ell$. When probing the $J^P = 0^-$, the data are fully consistent with the $J^P = 0^+$ and the $J^P = 0^-$ hypothesis is excluded at the 97.8% CL_s. It should be noted that as was the case in Section [**sec:SpinOne**], and although the overal distribution of the $J^P = 0^+$ hypothesis variables is unchanged, the quantitative assessment of the agreement of the data with it can vary when different hypotheses are tested due to differences in the regions of phase space where the two hypotheses can be separated.

Comments on the Statistical Procedure

In the definition of the ratio of profile likelihoods as test statistic used in the spin/Parity hypothesis testing, and in the spirit of being as independent as possible of the measured signal rate, the signal strength is considered as a nuisance parameter. There are two important issues arising from this apparently legitimate choice.

The first is that the ratio of the profile likelihood ratios test statistic and test statics in general that use the profiling of nuisance parameters, is that asymptotically their distribution should be independent of the true value of the nuisance parameters. If this is the case the resulting p-values are robust. This desirable feature is clearly not present in this case where the signal is yet extremely strong.

IV.2. Coupling properties measurements

Measuring the Higgs couplings without relying on the SM assumption requires a general framework that treats the deformations away from the SM coherently at the quantum level: Such a framework is needed to provide theoretical predictions for relevant observables to be confronted with experimental data. The effective Lagrangian approach offers such a coherent framework. It assumes that the new physics degrees of freedom are sufficiently heavy to be integrated out and simply give rise to effective interactions among the light SM particles. By construction these effective Lagrangians cannot account for deviations in Higgs physics induced by light degrees of freedom,

Table 6: Results in all benchmark scenarios for the analysis of the production and decay of the observed state with $J^{\mathcal{P}}$ quantum numbers. The subscripts refer to the specificities of the couplings of the observed state, where m denotes minimal couplings and h denotes couplings with higher dimension operators. For each scenarios only the non vanishing coupling constants are reported in this table. The combination for CMS combined only the ZZ and WW channels.

$\mathcal{J}^{\mathcal{PC}}$	ZZ	WW	$\gamma\gamma$	Combined
0^-	2.2% / 0.2%	-	-	-
0_h^-	- / 8.1%	-	-	-
1^+	6.0% / -	-	-	-
1^-	0.2% / -	-	-	-
$2^+_{q\overline{q}}$	16.9% / 1.5%	0.7% / 14%	5.0% / –	– / 0.5%
2^+_{gg}	<0.1% / <0.1%	2.0% / <0.1%	1.0%	<0.1% / –
2^-	<0.1% / <0.1%	-	-	-

unless they are added themselves as extra fields in the effective Lagrangians. In Section V, we will present several examples of models with light degrees of freedom affecting Higgs producton and decay rates.

IV.2.1. Effective Lagrangian formalism

The notation will have to be changed: $H \to \Phi$ to denote the Higgs doublet

The most general $SU(3)_C \times SU(2)_L \times U(1)_Y$-invariant Lagrangian for a weak doublet H at the level of dimension-6 operators was first classified in a systematic way in Refs. [127]. Subsequent analyses pointed out the presence of some redundant operators, and a minimal and complete list of operators was finally provided in Ref. [128]. Under the most conservative assumption about flavor, there are 59 independent ways to deform the SM. Of particular interest are the 18 CP-invariant and the 4 CP-breaking deformation-directions, in addition to 8 dipole operators, that affect, at tree-level, the Higgs production and decay rates [318,129,130].

A convenient basis of these operators relevant for Higgs physics, assuming that the Higgs is a CP-even weak doublet

and the baryon and lepton numbers are conserved, is the following:

$$\mathcal{L} = \mathcal{L}_{SM} + \sum_i \bar{c}_i O_i \,, \tag{4}$$

where the 18 operators are listed in Table 7, Table 8 and Table 9. When the operator $\mathcal{O}_i$ is not hermitian, like $\mathcal{O}_{u,d,l,Hud}$ and the dipole operators, it is understood that the hermitian-conjugated operator is added to the Lagrangian. The factor multiplying each operator in the effective Lagrangian has been conveniently defined such that the new physics dependence is fully encoded in the dimensionless coeffcients $\bar{c}_i$ which will all have to be smaller than 1 to ensure the consistency of the expansion in terms of higher dimensional operators. g', g, g_S are the SM gauge couplings, $y_{u,d,l}$ are the SM Yukawa couplings, λ is the SM Higgs quartic coupling and the v denotes the weak scale defined through the Fermi constant at tree-level $v \equiv 1/(\sqrt{2}G_F)^{1/2} \approx 246.2$ GeV. By $iH^\dagger \overleftrightarrow{D}^\mu H$ we denote the Hermitian derivative $iH^\dagger(D^\mu H) - i(D^\mu H)^\dagger H$, and $\sigma^{\mu\nu} \equiv i[\gamma^\mu, \gamma^\nu]/2$ and H^c is the Higgs charge-conjugate doublet: $H^c = i\sigma^2 H^*$. We have further assumed that each of the operators $O_{u,d,l}$ is flavor-aligned with the corresponding fermion mass term, as required in order to avoid large Flavor-Changing Neutral Currents (FCNC) mediated by the tree-level exchange of the Higgs boson. This implies one coefficient for the up-type quarks ($\bar{c}_u$), one for down-type quarks ($\bar{c}_d$), and one for the charged leptons ($\bar{c}_l$), i.e. the $\bar{c}_{u,d,l}$ are proportional to the identity matrix in flavor space. In principle, this assumption can be relaxed in favor of a less constraining Minimal Flavor Violation structure.

The choice of the basis of operators is not unique and using the equations of motion, i.e., performing field redefinitions, different dimension operators can be obtained as linear combinations of the operators in the previous tables and four-fermion operators. In particular, two other standard bases [131,128] involve the two extra bosonic operators

$$\mathcal{O}_{WW} \equiv \frac{g^2}{4m_W^2} H^\dagger H \, W^i_{\mu\nu} W^{i\,\mu\nu} = \mathcal{O}_W - \mathcal{O}_B + \mathcal{O}_{HB} - \mathcal{O}_{HW} + \frac{1}{4}\mathcal{O}_{BB}$$

$$\mathcal{O}_{WB} \equiv \frac{gg'}{4m_W^2} H^\dagger \sigma^i H \, W^i_{\mu\nu} B^{\mu\nu} = \mathcal{O}_B - \mathcal{O}_{HB} - \frac{1}{4}\mathcal{O}_\gamma \,.$$

Table 7: List of 9 CP-even and 4 CP-odd bosonic operators affecting Higgs production and decay rates. The 4 CP-odd operators involve the dual field strengths defined as $\tilde{F}_{\mu\nu} = {}^1\!/_2\,\epsilon_{\mu\nu\rho\sigma}F^{\rho\sigma}$ for $F = W, B, G$ (ϵ is the totally antisymmetric tensor normalized to $\epsilon_{0123} = 1$). See text for notations.

Operators involving bosons only
$\mathcal{O}_H = 1/(2v^2)\left(\partial^\mu\left(H^\dagger H\right)\right)^2$
$\mathcal{O}_T = 1/(2v^2)(H^\dagger \overset{\leftrightarrow}{D}^\mu H)^2$
$\mathcal{O}_6 = -\lambda/(v^2)\left(H^\dagger H\right)^3$
$\mathcal{O}_B = (ig')/(2m_W^2)(H^\dagger \overset{\leftrightarrow}{D}^\mu H)(\partial^\nu B_{\mu\nu})$
$\mathcal{O}_W = (ig)/(2m_W^2)(H^\dagger\sigma^i \overset{\leftrightarrow}{D}^\mu H)(D^\nu W_{\mu\nu})^i$
$\mathcal{O}_{HB} = (ig')/m_W^2\,(D^\mu H)^\dagger(D^\nu H)B_{\mu\nu}$
$\mathcal{O}_{HW} = (ig)/m_W^2\,(D^\mu H)^\dagger\sigma^i(D^\nu H)W^i_{\mu\nu}$
$\mathcal{O}_{BB} = g'^2/m_W^2\,H^\dagger H B_{\mu\nu}B^{\mu\nu}$
$\mathcal{O}_{GG} = g_S^2/m_W^2\,H^\dagger H G^A_{\mu\nu}G^{A\mu\nu}$
$\mathcal{O}_{H\tilde{B}} = (ig')/m_W^2\,(D^\mu H)^\dagger(D^\nu H)\tilde{B}_{\mu\nu}$
$\mathcal{O}_{H\tilde{W}} = (ig)/m_W^2\,(D^\mu H)^\dagger\sigma^i(D^\nu H)\tilde{W}^i_{\mu\nu}$
$\mathcal{O}_{B\tilde{B}} = g'^2/m_W^2\,H^\dagger H B_{\mu\nu}\tilde{B}^{\mu\nu}$
$\mathcal{O}_{G\tilde{G}} = g_S^2/m_W^2\,H^\dagger H G^A_{\mu\nu}\tilde{G}^{A\mu\nu}$

Table 8: List of 9 operators with bosons and fermions affecting Higgs production and decay rates. See text for notations.

Ops. involving bosons and fermions
$\mathcal{O}_u = y_u/v^2\,(H^\dagger H)\,\bar{q}_L H^c u_R$
$\mathcal{O}_d = y_d/v^2\,(H^\dagger H)\,\bar{q}_L H d_R$
$\mathcal{O}_l = y_l/v^2\,(H^\dagger H)\,\bar{L}_L H l_R$
$\mathcal{O}_{Hq} = i/v^2\,\left(\bar{q}_L\gamma^\mu q_L\right)\left(H^\dagger \overset{\leftrightarrow}{D}_\mu H\right)$
$\mathcal{O}^{(3)}_{Hq} = i/v^2\,\left(\bar{q}_L\gamma^\mu\sigma^i q_L\right)\left(H^\dagger\sigma^i \overset{\leftrightarrow}{D}_\mu H\right)$
$\mathcal{O}_{Hu} = i/v^2\,\left(\bar{u}_R\gamma^\mu u_R\right)\left(H^\dagger \overset{\leftrightarrow}{D}_\mu H\right)$
$\mathcal{O}_{Hd} = i/v^2\,\left(\bar{d}_R\gamma^\mu d_R\right)\left(H^\dagger \overset{\leftrightarrow}{D}_\mu H\right)$
$\mathcal{O}_{Hud} = i/v^2\,\left(\bar{u}_R\gamma^\mu d_R\right)\left(H^{c\,\dagger} \overset{\leftrightarrow}{D}_\mu H\right)$
$\mathcal{O}_{Hl} = i/v^2\,\left(\bar{l}_R\gamma^\mu l_R\right)\left(H^\dagger \overset{\leftrightarrow}{D}_\mu H\right)$

Table 9: List of 8 dipoles operators. See text for notations.

Ops. involving bosons and fermions
$\mathcal{O}_{uB} = (g'\, y_u)/m_W^2\, (\bar{q}_L H^c \sigma^{\mu\nu} u_R)\, B_{\mu\nu}$
$\mathcal{O}_{uW} = (g\, y_u)/m_W^2\, (\bar{q}_L \sigma^i H^c \sigma^{\mu\nu} u_R)\, W^i_{\mu\nu}$
$\mathcal{O}_{uG} = (g_S\, y_u)/m_W^2\, (\bar{q}_L H^c \sigma^{\mu\nu} t^A u_R)\, G^A_{\mu\nu} R$
$\mathcal{O}_{dB} = (g'\, y_d)/m_W^2\, (\bar{q}_L H \sigma^{\mu\nu} d_R)\, B_{\mu\nu}$
$\mathcal{O}_{dW} = (g\, y_d)/m_W^2\, (\bar{q}_L \sigma^i H \sigma^{\mu\nu} d_R)\, W^i_{\mu\nu}$
$\mathcal{O}_{dG} = (g_S\, y_d)/m_W^2\, (\bar{q}_L H \sigma^{\mu\nu} t^A d_R)\, G^A_{\mu\nu}$
$\mathcal{O}_{lB} = (g'\, y_l)/m_W^2\, (\bar{L}_L H \sigma^{\mu\nu} l_R)\, B_{\mu\nu}$
$\mathcal{O}_{lW} = (g\, y_l)/m_W^2\, (\bar{L}_L \sigma^i H \sigma^{\mu\nu} l_R)\, W^i_{\mu\nu}$

While the two operators $\mathcal{O}_B$ and $\mathcal{O}_W$ can be traded in favor of operators with operators (Y_f denotes the U(1) hypercharge of the fermion f, normalized to $Q = T_{3L} + Y/2$ and m^2 is the mass term of the SM Higgs potential Eq. (2))

$$\mathcal{O}_B = 2\tan^2\theta_W \left(-\mathcal{O}_T + \sum_{f=q,u,d,l,L} \frac{1}{2} Y_f\, \mathcal{O}_{Hf} \right)$$

$$\mathcal{O}_W = -6\,\mathcal{O}_H + 2\,((\mathcal{O}_u + \mathcal{O}_d + \mathcal{O}_l) + h.c.) + 4m^2|H^\dagger H|^2 - 8\,\mathcal{O}_6 + \mathcal{O}^{(3)}_{Hq} + \mathcal{O}^{(3)}_{HL}\,.$$

Things to add

• Discuss the constraints on the operators from non-Higgs physics and explain that only 8 operators are tested by Higgs physics only. → Section IV.2.b

• discuss custodail symmetry relations and the accidental cusotdial symmetry at the dim-6 level.

• Give the translation in terms of the κ used by the experimentalists → a table that will go in Section IV.1 → Section IV.2.c and Section IV.1

• Give expressions for the decay rate shifts induced by these operators. → Section IV.2.c

IV.2.2. Constraints on Wilson coefficients from precision EW and flavor measurements

IV.2.3. From the effective Lagrangians to Higgs observables

IV.3. Measurement of coupling properties

The analysis of the couplings of the Higgs boson consist in a simple reparametrization of the signal yields measured in all categories of all channels. There are two approaches to this analysis. The first which is closer to the observation aims at measuring the ratios of cross-sections for different production modes or ratios of decay branching ratios. It should be notes that this approach was not done using equivalent selection criteria in different channels, but reparameterizing the signal yields in all categories. The second, aims at measuring deviations from the Standard Model Higgs couplings. This approach uses coefficients κ which parametrize deviations from the Standard Model couplings, but is based on a similar principle of reparameterization of the signal yields in all categories. The difference of this approach to the previous one is that it needs to make futher assumptions on these coefficients or on the total width of the Higgs boson. The main assumptions in this analysis are the following.

- The signals observed in the different search channels originate from a single narrow resonance with a mass near 125.5 GeV. The case of several, possibly overlapping, resonances in this mass region is not considered.

- The width of the assumed Higgs boson near 125.5 GeV is neglected, both in the fitted signal model (for both approaches) and in the zero-width approximation (in the second case to allow the decomposition of signal yield).

- In the first case the main production modes are assumed to be those of the Standard Model and in the second, the tensor structure of the couplings is assumed to be the same as in the Standard Model. This means in particular that the observed state is assumed to be a CP-even scalar as in the SM.

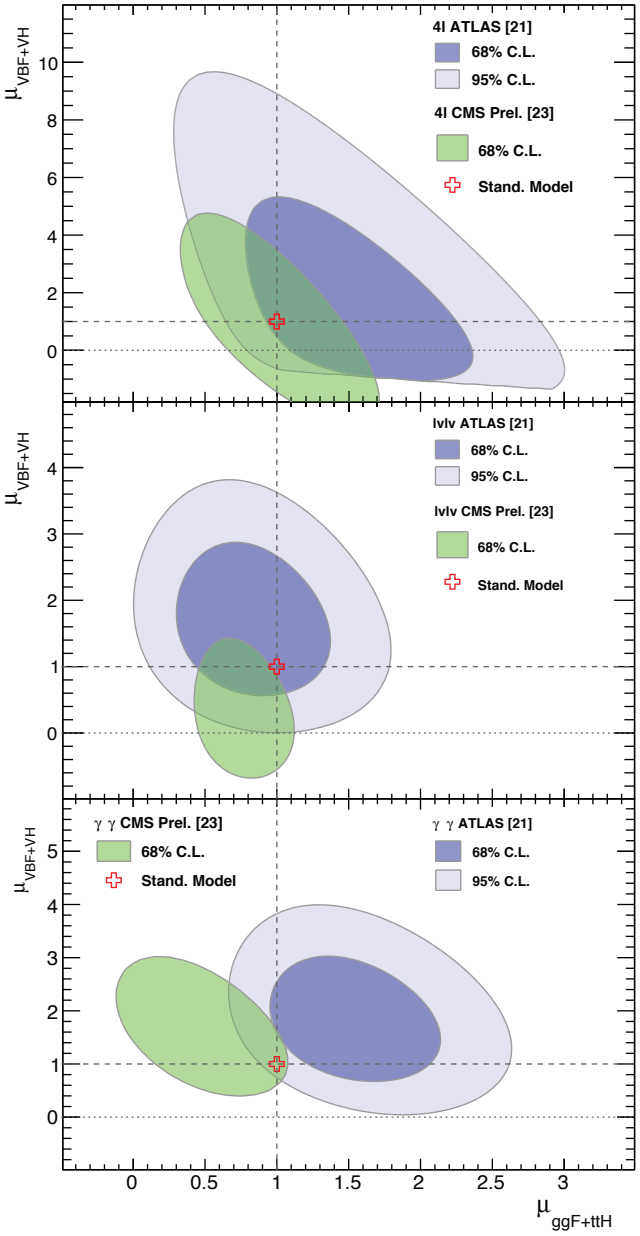

Figure 23:

IV.3.1. Modelling Signal Yields: the Empirical Approach

The overall statistical modelling of the data is described in detail in Refs.The likelihood function is a complex recipe using a large number of ingredients, including: probability density functions (pdf) for the signal and the background; normalization factors for the backgrounds and their direct measurements in

control regions; numerous signal modelling parameters affecting *e.g.* the acceptance, efficiency and the luminosity; all systematic uncertainties affecting both the normalizations and the pdfs; in particular the normalization of the expected signal. The latter is the critical part that is re-parametrized in the couplings analysis. It is nothing else than the number of fitted signal events which is re-interpreted in terms of factors modifying the expectation of the number of signal events in each category with respect ot the Standard Model Higgs boson signal. Only this part of the likelihood will be detailed here, the rest which is more complex and includes all the intricacies of the systematic uncertainties and their correlations is described in REF.

The number of signal events observed is parametrized in terms of scale factors for the cross section $\sigma_{i,SM}$ of each SM Higgs production mode, the branching ratios $B_{f,SM}$ of the SM Higgs boson decays, and the mass of the Higgs boson m_h. For each production mode i, a signal strength factor μ_i defined as $\mu_i = \sigma_i/\sigma_{i,SM}$ is introduced. Similarly, for each decay final state f, a factor $\mu_f = B_f/B_{f,SM}$ is introduced. For each analysis category (k) the number of signal events (n^k_{signal}) is parametrized as:

$$n^k_{signal} = \left(\sum_i \mu_i \sigma_{i,SM} \times A^k_{if} \times \varepsilon^k_{if} \right) \times \mu_f \times B_{f,SM} \times \mathcal{L}^{\parallel}$$

where A represents the detector acceptance, ε the reconstruction efficiency and $\mathcal{L}$ the integrated luminosity. The number of signal events expected from each combination of production and decay modes is scaled by the corresponding product $\mu_i\mu_f$, with no change to the distribution of kinematic or other properties. This parametrization generalizes the dependency of the signal yields on the production cross sections and decay branching fractions, allowing for a coherent variation across several channels. This approach is also general in the sense that it is not restricted by any relationship between production cross sections and branching ratios. For instance, it is possible to force the production cross section $\sigma_{WH} = 0$ while maintaining a non-zero branching ratio B_{WW}.

In Equation [eq:nsig], μ_i and μ_f are the main parameters of interest at which the combined likelihood can be estimated and for which it can be maximized. The simplest case with only one signal strength parameter is simply parametrized as $\mu = \mu_i = \mu_f$. In our combined model the production index $i \in \{ggH, VBF, VH, ttH\}$ and the decay index $f \in \{\gamma\gamma, WW, ZZ, bb, \tau\tau\}$.

A good way to comunicate our results in a form that could easily be used for subsequent fitting for model testng is to give contours or even values of the N-dimensional likelihood as a function of μ_i's for each individual channel, or alternatively the fitted value with the full correlation error matrix.

IV.3.2. Evidence for VBF production

The next to simplest parametrization is to fit the various production modes according to the couplings to vector bosons or fermions (mainly the top quark). in which case only two production parameters are used $\mu_{ggH+ttH} = \mu_{ggH} = \mu_{ttH}$ and $\mu_{VBF+VH} = \mu_{VBF} = \mu_{VH}$. These two parameters can be fitted in each channel individually where they implicitely include the μ_f factors of Equation [eq:nsig]. The result of these individual channels fits are shown in Figure [fig:ProdContourProf] a. These contours can be compared to the standard model value, but they cannot be combined as they implicitely include the branching fraction. The ratio of μ_{VBF+VH} and $\mu_{ggH+ttH}$ can instead be combined. This ratio shows not only the compatibility of the data with the Standard Model Higgs boson, but also the significance of the observation of the production of the Higgs boson in the VBF and VH modes. ATLAS has also performed a similar combination but relaxing the requirement that the ratio of VBF and VH is that of the Standard Model. In Figure [fig:ProdContourProf] b the VH production is instead profiled so that the results can give a measure of the presence of the VBF production mode and in which proportion with respect to the Standard Model. The result shown in Figure [fig:ProdContourProf] b show an evidence of the VBF production of the Higgs boson at the three standard deviations level. Given the overall compatibility of the individual channels with the Standard Model expectation, this does not come as

fundamental surprise. It is however a very nice measure of the compatibility of the results with the expectations from the Standard Model and a very nice corroboration of the projected sensitivities.

Another way to fit the results, is to perform ratios of ratios of branching ratios *i.e.* ratios of μ_f's. This approach is done only in ATLAS. In these ratios the individual production μ_i cancel when taking the ratio of $\mu_i \times BR$ within the same production modes. To simplify notations these ratios of ratios of branching ratios are denoted ρ. The results of the fits yield:

$$\rho_{\gamma\gamma/ZZ} = 1.1^{+0.4}_{-0.3}$$
$$\rho_{\gamma\gamma/WW} = 1.7^{+0.7}_{-0.5}$$
$$\rho_{ZZ/WW} = 1.6^{+0.8}_{-0.5}$$

where a value of 1 corresponds to the expectation from the Standard Model signal. The ratio $\rho_{ZZ/WW}$ gives already an idea of the ratio of the W and Z couplings from the decay modes only. This is not the case for the analysis based on couplings modifiers.

Modelling Signal Yields: the Couplings Modifiers Approach

Another way to parametrize and thereafter fit the data is to test modifications of the *Leading Order* couplings of the Standard Model higgs boson to the known Standard Model particles. This is very simply achieved by reparametrizing the μ_i and μ_f strength parameters. In terms of coupling modifiers κ which are LO motivated coupling scale factors defined in such a way that the cross sections σ_j and the partial decay widths Γ_j associated with the SM particle j scale with the factor κ_j^2 when compared to the corresponding SM prediction. Details can be found in Refs.This approach was initiated in Refs.

Taking the process $gg \to H \to \gamma\gamma$ as an example the number of signal events in a given category can be rescaled in the following way:

$$\sigma \times Br \to \mu_i \times \mu_f = \frac{\kappa_g^2.\kappa_\gamma^2}{\kappa_H^2}$$

where the values and uncertainties for both $\sigma_{SM}(gg \to \gamma\gamma)$ and $BR_{SM}(H \to \gamma\gamma)$ are taken from Refs.given Higgs boson mass hypothesis, meaning that the fit model does not change at all, only the signal yields are parametrized differently.

In each of these models the number of free parameters does not exceed four. The total number of relevant parameters in the model is

$$\mathcal{L} \supset \kappa_Z \frac{2m_Z^2}{v} Z_\mu Z^\mu H + \kappa_W \frac{2m_W^2}{v} W_\mu W^\mu H - \Sigma_f \kappa_f \frac{m_f}{v} f\overline{f} + \kappa_g \frac{\alpha_s}{12\pi v} G^a_{\mu\nu} G^{a,\mu\nu} H + \kappa_\gamma \frac{\alpha}{\pi v} A_{\mu\nu} A^{\mu\nu} H + \kappa_{Z\gamma} \frac{\alpha}{\pi v} A_{\mu\nu} Z^{\mu\nu} H$$

The main parameters in this effective Lagrangian which are relevant in our analyses are κ_t, κ_W, κ_Z, κ_b, κ_τ, κ_γ and κ_g. Other parameters such as κ_s, κ_c and κ_τ are fixed to κ_b, κ_t and κ_τ respectively for flavor symmetry considerations (the assumption on κ_μ could be relaxed when inclusing the dimuon channel search in the combination).

In this definition, where the most accurate estimates are simply rescaled, the SM predictions for all $\sigma \times Br$ are recovered when all $\kappa = 1$. Rigourously, this implies that for $\kappa \neq 1$ the higher-order accuracy is lost. In practice, NLO QCD corrections typically factorize with respect to coupling rescaling, and are accounted for.

Couplings occuring through loops can be treated in two ways. The first is to effectively scale them through κ_g and κ_g with respect to their Standard Model values and the second is to modify them according to the changes in the couplings of the Higgs boson to the Standard Model particles entering the loops. In hte latter case the processes $H \to \gamma\gamma$ and $gg \to H$, which are loop induced in the SM, are treated as a function of the more fundamental coupling scale factors κ_t, κ_b, κ_W, and similarly for all other particles that contribute to these SM loop processes. In these cases the scaled fundamental couplings are propagted through the loop calculations, including all interference effects, using the functional form derived from the SM REF.

Due to the limited strength and number of constrained, at this still early stage of the LHC program, only a limited

number of parameters can be simultaneously fit and restricting assumptions ned to be made on the parameters. Specific models are then designed to address specific question.

- The relative coupling of the Higgs boson to the W and Z bosons.

- The (mostly indirect) estimate of the relative coupling to fermions and to vector bosons.

- The effect of new particles beyond the standard model in the loops and in the decay (assuming that the couplings to the Standard Model particles are those of the Standard Model Higgs boson).

In these models the total width can either be scaled assuming that there no invisible or undetected widths or left effectively free in the fit (this is typically done by absorbing it in a more convenient parameter in terms with respect to the model considered).

Indirect Evidence for Couplings to Fermions

In this benchmark the assumptions are that only SM particles are assumed to contribute to the gluon fusion and the diphoton loops, all fermion couplings modifiers are required to scale simultaneously with a unique factor κ_F and all vector boson couplings modifiers must scale simultaneously with a unique factor κ_V, and that the there are no new physics contributions to the total width of the Higgs boson:

$$\kappa_V = \kappa_W = \kappa_Z$$
$$\kappa_F = \kappa_t = \kappa_b = \kappa_t = \kappa_g$$

It should be noted that in this model it is principally the gluon fusion process that measures directly the fermion scale factor κ_F^2. Instead the total width $(\kappa_H^2(\kappa_F, \kappa_V))$ scale factor can then be written as follows:

$$\kappa_H^2(\kappa_F, \kappa_V) = 0.75 \cdot \kappa_F^2 + 0.25 \cdot \kappa_V^2$$

and the diphoton scale factor $(\kappa_\gamma^2(\kappa_F, \kappa_V))$ will be expressed as follows:

$\kappa_\gamma^2(\kappa_F, \kappa_V) = 1.59.\kappa_V^2 - 0.66.\kappa_V\kappa_F + 0.07.\kappa_F^2$

The two photon decay is the only place where the relative sign of the fermion yukawa and the gauge boson couplings plays

a role. It is therefore through the diphoton channel that the sign degeneracy can be solved. The 2D fit result and the two 1D fits where one of the parameters is profiled are illustrated in Figure [**fig:spbm:CVCF**]. As expected the only contribution sensitive to the relative sign of the fermion yukawa and gauge boson couplings is the diphoton channel. All other channels are symmetric in κ_F. The 1D fits show the sensitivity to the resolve the sign degeneracy which is above two standard deviations. The fit to the data in this model prefers a positive relative sign. However the observed likelihood profile does not show such a difference in likelihood between the positive and negative solutions. Previous combinations even showed a preference for the negative sign solution. This ambiguity is largely due to the large measured signal in the diphoton channel while in average the measured yields in the $H \to W^{(*)}W^{(*)} \to \ell\nu\ell\nu$ and $H \to Z^{(*)}Z^{(*)} \to 4\ell$ channels are closer to the Standard Model expectations.

A model probing the relative couplings to fermions and bosons without any assumptions on the total width has also been implemented and give a result compatible with the Standard Model.

Digression on the Relative Sign of the Couplings

Although it is true that $\kappa_F \sim -1$ is not excluded a priori, it will imply the existence of another Higgs field with an unreasonably large coupling to top quarks.

Results in the 1D fits (as in Figure [**fig:spbm:CVCF**]) are therefore shown allowing κ_F to be negative, but the fit results corresponding to the positive κ_F branch only are also shown.

Probing the ratio of couplings to the W and Z bosons

Two general models designed to probe the ratio of the W to Z couplings are designed without assumptions on the total width. The first requires that all fermion couplings scale with a single coupling modifier and the total width is absorbed in a factor κ_{ZZ}.

In this model the $H \to \gamma\gamma$ and the gluon fusion process loops are fixed. The $H \to \gamma\gamma$ loop is however dominated by the coupling to the W boson. Another model, where the $H \to \gamma\gamma$ coupling is assumed to be effective to avoid the inlfuence of

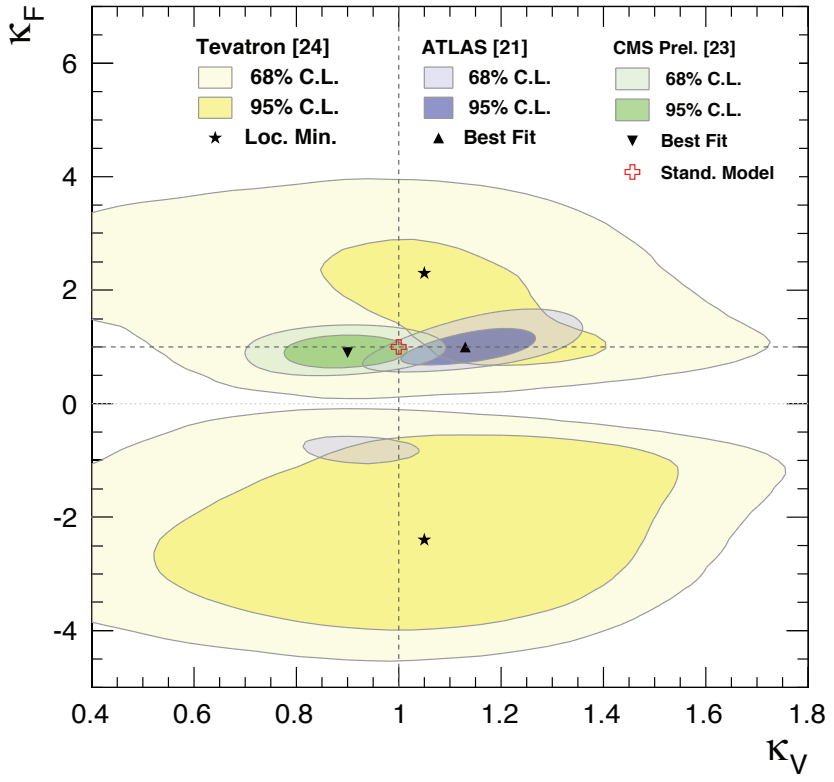

Figure 24:

contributions beyond the Standard Model potentially affecting the $H \to \gamma\gamma$ yield, is also implemented to probe the ratio of W and Z bosons couplings:

The 1D fit results for these two models are shown in Figure [**fig:bm:CW/CZ,Cgam/CZ,CF/CZ,CZ2/CH**] where the in both cases the parameter of interest is ρ_{WZ}. In both cases the ratio of these couplings is compatible with the Standard Model. The 1D fits of the other parameters are also shown to illustrate the overall compatibility of the models with the Standard Model.

The compatibility of ρ_{WZ} does not really come as a surprise given the observed ratio of ratios of branching ratios. In this case however the information from the production processes is also present, as for instance in the VBF production which is parametrized as follows as a function of the W and Z-fusion processes (σ_{WWH} and σ_{ZZH}):

where the very small interference term is ignored.

These models are often referred to as probing the custodial symmetry which protects the ρ parameter from potentially large radiative corrections. It is of fundamental interest to probe the ratio of the couplings of the observed state to W and Z bosons, it should however be noted that precision eletroweak measurements have measured the ρ parameter to a much better precision.

Probing New Physics in Loops and in the Decay

The models described above implemented modifications to the couplings to Fermions and vector bosons, with and without assumptions on the total width. Another approach, taking advantage of the opportunities of the recently discovered state to reveal the presence of new physics in the loops or in its decay, is to assume that all couplings to fermions and bosons are those of the Standard Model Higgs boson $\kappa_F = \kappa_V = 1$ and allow effective $H \to \gamma\gamma$ and the gluon couplings to float, either assuming the total width to be fixed or not.

Assuming the total width to be fixed allows to probe new physics beyond the standard model in the loops only. The total width is then defined as follows as a function of the two effective coupling modifiers:

where κ_g and κ_γ are the two main parameters of interest. The results of the fit of this model to the data are shown in Figure [**fig:bm:Cg,Cgamma,BRinv**] a. The slight tension observed in this case (with a probability of compatibility of approximately 5%) reflects the large yield observed in the $H \to \gamma\gamma$ channel. This tension and large value of the κ_γ has drawn a lot of attention. Such a large value however has not been confirmed by CMS's latest results.

In the approach where new physics is allowed in the decay, instead of parametrizing the rates using the total width an invisible and undetected branching fraction is introduced. The results of this model are shown in Figure [**fig:bm:Cg,Cgamma,BRinv**] b.

A limit on the invisible or undetected branching fraction of $Br_{inv} < 0.6$ at the 95% CL is observed.

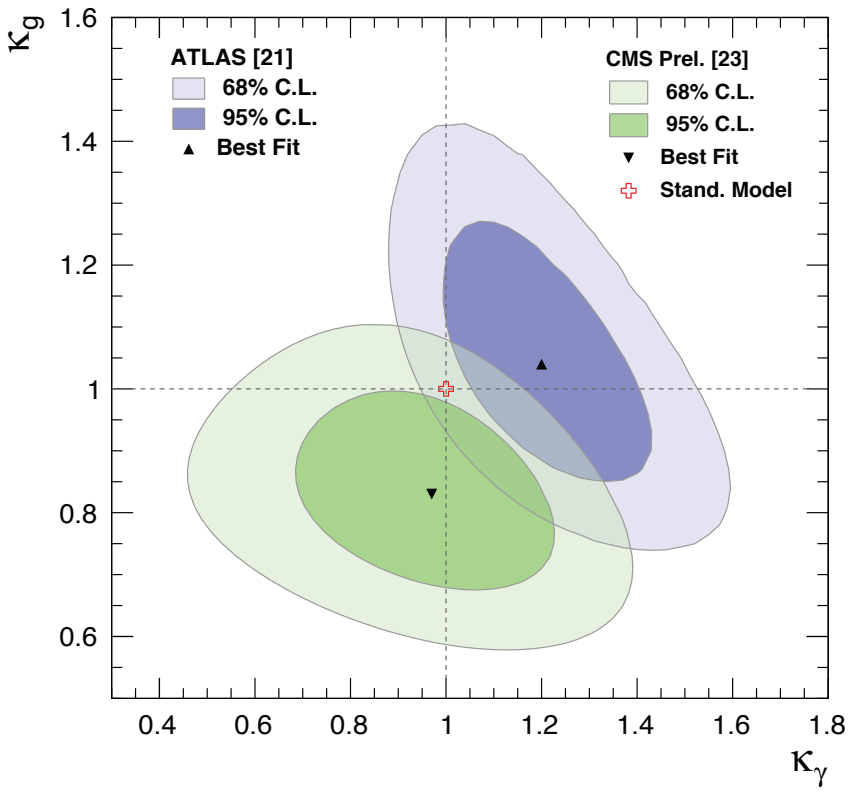

Figure 25:

IV.4. Production properties

- Fiducial Cross sections.
- Differential cross sections.

Here we need also some TH input especially on the TH input.

V. New Physics Models of EWSB compatible with a SM-like Higgs Signal at LHC

The main theoretical motivation to add a Higgs boson to the Standard Model was that, without it, the longitudinal components of the massive EW gauge bosons would form a strongly coupled system as their scattering amplitude would have grown with their energy, destroying all the predictive power of the model above $4\pi v \sim 3$ TeV. On the contrary, the discovery of a light scalar with couplings not deviating by more than 15% from the SM predictions makes it is possible

Table 10: Overall channel signal strengths

	$\gamma\gamma$	ZZ (4ℓ)	WW ($\ell\nu\ell\nu$)	$\tau\tau$
ATLAS				
μ (at 125.5 GeV)	1.5±0.4	1.6±0.3	1.0±0.3	0.8±0.7
Z Exp.	4.1	4.4	3.8	1.6
Z Obs.	7.4	6.6	3.8	1.1
Mass (GeV)	126.8±0.2±0.7	124.3±0.5±0.5	-	-
Reference	[21]	[21]	[21]	[21]
CMS				
μ (at 125.5 GeV)	0.8±0.3	0.9±0.3	1.5±0.4	1.5±0.4
Z Exp.	3.9	7.1	5.3	2.6
Z Obs.	3.2	6.7	3.9	2.8
Mass (GeV)	125.6±0.2±0.7	125.6±0.2±0.7		125.6±0.2±0.7
Reference	[22]	[22]	[22]	[22]
Tevatron				
μ (at 125 GeV)	$6.0^{+3.4}_{-3.1}$	–	1.6±1.2	$1.7^{+2.3}_{-1.7}$
Reference	[24]	[24]	[24]	[24]

Table 11: Overall channel signal strengths

	$\gamma\gamma$	ZZ (4ℓ)	WW ($\ell\nu\ell\nu$)	$\tau^+\tau^-$	$b\overline{b}$
ATLAS					
ggF	√	√	√	√	–
VBF	√	√	√	√	–
VH	√	√	√*	√	√
ttH	√*	–	–	–	√*
CMS		–	–	–	–
ggF	√	√	√	√	–
VBF	√	√	√	√	√*
VH	√	√	√*	√	√
ttH	√*	–	√*	√*	√*
Tevatron					
ggF	√	√	√	√	–
VH	–	–	√*	√	√
ttH	–	–	–	–	√

to keep the SM interactions perturbative all the way to the

Table 12: Invisible and rare decay channels

	$\mu\mu$	Zγ	Invisible
ATLAS			
ggF	$\surd^{*}$	$\surd^{*}$	$\surd^{**}$
VBF	–	–	–
VH	–	–	$\surd^{*}$
CMS			
ggF	$\surd$	$\surd$	$\surd^{**}$
VBF	$\surd$	$\surd$	$\surd$
VH	–	$\surd$	$\surd^{*}$

Planck scale. This picture is admittedly very attractive and it is in remarkable agreement with data but it posits that the Higgs boson is an elementary scalar field, which comes with an intrinsic instability of its mass under radiative as we already explained. Either this instability is perceived as accidental and is dismissed, or it is taken as a serious problem and calls for new physics around the TeV scale. Supersymmetric models are the best solution to maintain the perturbativity of the SM while alleviating the instability issue. Another possibility is that the Higgs boson itself has a finite size and composite and thus never feels the UV degrees of freedom that would drag its mass to higher scales. Both classes of models predict specific modifications from the SM Higgs properties. In this Section, we will discuss these possible deviations in detail, and, when pertinent, we will also review the searches at colliders for additional states in the EWSB sector, for instance additional Higgs bosons.

The realization of Supersymmetry at low energies has many good qualities that render it attractive as a model of new physics. First of all since for every fermion there is a boson of equal mass and effective coupling to the SM-like Higgs, in the case of exact supersymmetry it yields an automatic cancellation of loop corrections to the Higgs mass parameter: (analogous to Eq. (1)) $\delta_{m_H^2} = 0$ [8,10]. In practice we know that SUSY must

be broken in nature since no superpartners of the SM particles have been observed so far, hence:

$$\delta_{m_H^2} = \frac{3\lambda_F^2}{8\pi^2}\left[m_F^2 - m_B^2\right]\ln\left(\mu^2/Q^2\right) \tag{5}$$

where the difference $(m_F^2 - m_B^2)$ is directly related to the squared of the supersymmetry breaking scale, M_{SUSY}. Hence, as far as the third generation bosonic superpartners, that couple most significantly to the Higgs boson, are not many orders of magnitude above their SM top, bottom and tau partners, i.e. $M_{SUSY} \simeq \mathcal{O}$(1- few TeV), there is no naturalness problem [9,133]. Another interesting feature of SUSY theories is related to the dynamical generation of EWSB [132]. In the SM we need to put by hand a negative Higgs mass parameter squared, m^2, to induce EWSB. In SUSY, instead, even if the relevant Higgs mass parameter is positive in the ultraviolet, it may become negative and induce electroweak symmetry breaking radiatively through the strong effect of the top quark-Higgs coupling in its renormalization group evolution. Moreover, supersymmetry with a supersymmetry breaking scale of order 1 TeV allows for grand unification of the electromagnetic, weak and strong gauge interactions in a consistent way, strongly supported by the prediction of the electroweak mixing angle at low energy scales, with an accuracy at the percent level [135,136]. In addition, supersymmetry theories can provide a suitable dark matter candidate and even a low energy physics explanation of baryogenesis, all of this compatible with existing precision data.

In the following we will explore the Higgs sector in specific SUSY models. In all of them there is one neutral Higgs boson with properties that resemble those of the SM Higgs boson whereas additional neutral and charged Higgs bosons are also predicted and are intensively being sought for at the LHC (see Section VI). In the simplest SUSY model the lightest Higgs boson mass, that usually plays the role of the SM-like Higgs, is predicted to be less than 135 GeV for stops in the TeV to few TeV range [137,138,139,140,141,142,143,144,145,146,147,148]. whereas, larger values of the SM-like Higgs boson mass - up to about 250 GeV- can be obtained in non-minimal SUSY extensions of the SM. [150,151,152,153,154,155,156]. In general,

to accommodate a SM-like Higgs boson with mass of 125 GeV results in constraints on the supersymmetric parameter space of specific SUSY models, as we will discuss below.

In the context of weakly coupled models of EWSB we will also briefly discussed generic 2HDM's without the need for low energy supersymmetry. These models, although do not address the hierarchy problem in any specific way, provide an excellent ground for exploring deviations from SM Higgs properties and possible novel search channels for other Higgs bosons particles in a more model independent way.

The SUSY direct searches performed at the LHC together with the remarkable agreement of Higgs couplings with the SM prediction , and to some extent also the EW precision data and the flavor constraints, question low energy supersymmetric models as a natural solution of the hierarchy problem. At the same time, in part as a result of the new insights on strongly-interacting theories obtained from an holographic perspective, the idea that the Higgs boson itself could be a composite bound state emerging from a new strongly-coupled sector has regained some interest. The composite Higgs idea is an interesting incarnation of EWSB via strong dynamics that smoothly interpolates between the standard Technicolor approach and the true SM limit. To avoid the usual conflict with EW data, it is sufficient if not necessary that a mass gap separates the Higgs resonance from the other resonances of the strong sector. Such a mass gap can naturally follows from dynamics if the strongly-interacting sector exhibits a global symmetry, G, broken dynamically to a subgroup H at the scale f , such that the coset G/H contains a fourth Nambu–Goldstone bosons that can be identified with the Higgs boson. Simple examples of such coset are $SU(3)/SU(2)$ or $SO(5)/SO(4)$, the latter being favored since it is invariant under the custodial symmetry (it is also possible to have non-minimal custodial cosets with extra Goldstone bosons, see for instance [391]) . Attempts to construct composite Higgs models in 4D have been made by Georgi and Kaplan (see for instance [390]) and modern incarnations have been recently investigated in the framework of 5D warped models where, according to the principles of the AdS/CFT correspondence,

the holographic composite Higgs boson then originates from a component of a gauge field along the 5th dimension with appropriate boundary conditions. A last crucial ingredient in the construction of viable composite Higgs models is the concept of partial compositeness [392], i.e., the idea that there are only linear mass mixings between elementary fields and composite states. After diagonalization of the mass matrices, the SM particles, fermions and gauge bosons, are admixtures of elementary and composite states and thus they interact with the strong sector, and in particular with he Higgs boson, through their composite component. This setup has important consequences on the flavor properties, chiefly the suppression of large flavor changing neutral currents involving light fermions. It also plays an important role in dynamically generating a potential for the would-be Goldstone bosons. Partial compositeness also links the properties of the Higgs boson to the spectrum of the fermionic resonances as the partners of the top quark which, as in MSSM, at really the agents that trigger the EWSB and raise the mass of the Higgs boson to 125 GeV.

V.1. Higgs Bosons in the Minimal Supersymmetric Standard Model (MSSM)

The particle masses and interactions in a supersymmetric theory are uniquely defined as a function of the Superpotential and the Kähler potential [**SUSY-pdg**]. A fundamental theory of supersymmetry breaking, however, is unknown at this time. Nevertheless, one can parameterize the low-energy theory in terms of the most general set of soft supersymmetry-breaking renormalizable operators [134]. The simplest realistic model of low-energy supersymmetry is the Minimal Supersymmetric extension of the Standard Model (MSSM) [10,133], that associates a supersymmetric partner to each gauge boson and chiral fermion of the SM, and provides a realistic model of physics at the weak scale. However, even in this minimal model with the most general set of soft supersymmetry-breaking terms, more than 100 new parameters are introduced [157]. Fortunately, only a subset of these parameters impact the Higgs phenomenology through tree-level and quantum effects. Reviews of the properties and phenomenology of the Higgs bosons

of the MSSM can be found for example in Refs. [17], [158] and [133].

The MSSM contains the particle spectrum of a two-Higgs-doublet model (2HDM) extension of the SM and the corresponding supersymmetric partners. Two Higgs doublets,

$$\Phi_1 = \frac{1}{\sqrt{2}} \begin{pmatrix} \phi_1^0 + i a_1^0 \\ \phi_1^- \end{pmatrix}, \tag{6}$$

$$\Phi_2 = \frac{1}{\sqrt{2}} \begin{pmatrix} \phi_2^+ \\ \phi_2^0 + i a_2^0 \end{pmatrix}, \tag{7}$$

with Y=-1 and Y=1, respectively, are required to ensure an anomaly-free SUSY extension of the SM and to generate mass for both "up"-type and "down"-type quarks and charged leptons [11]. In our notation $\Phi_{1(2)}$ gives mass to the down(up) type fermions. The Higgs potential reads

$$\begin{aligned} V = {} & m_1^2 \Phi_1^\dagger \Phi_1 + m_2^2 \Phi_2^\dagger \Phi_2 - m_3^2 \left(\Phi_1^T i\sigma_2 \Phi_2 + \text{h.c.} \right) + \frac{1}{2}\lambda_1 \left(\Phi_1^\dagger \Phi_1 \right)^2 \\ & + \frac{1}{2}\lambda_2 \left(\Phi_2^\dagger \Phi_2 \right)^2 + \lambda_3 \left(\Phi_1^\dagger \Phi_1 \right) \left(\Phi_2^\dagger \Phi_2 \right) + \lambda_4 |\Phi_1^T i\sigma_2 \Phi_2|^2 \\ & + \left[\frac{1}{2}\lambda_5 \left[\left(\Phi_1^T i\sigma_2 \Phi_2 \right)^2 + h.c. \right] + \left[\lambda_6 \left(\Phi_1^\dagger \Phi_1 \right) + \lambda_7 \left(\Phi_2^\dagger \Phi_2 \right) \right] \Phi_1^T i\sigma_2 \Phi_2 + \text{h.c.} \right] \end{aligned} \tag{8}$$

where $m_i^2 = \mu^2 + m_{H_i}^2$, with μ the supersymmetric Higgsino mass parameter and m_{H_i} (for i=1,2) the Higgs doublet soft supersymmetric breaking mass parameters; $m_3^2 \equiv B\mu$ is associated to the B-term soft SUSY breaking parameter; and λ_i, for i=1-7, all the Higgs quartic couplings. After the spontaneous breaking of the electroweak symmetry, five physical Higgs particles are left in the spectrum: one charged Higgs pair, $H^\pm$, one CP-odd scalar, A, and two CP-even states, H and h.

$$H^\pm = \sin\beta \phi_1^\pm + \cos\beta \phi_2^\pm, \qquad A = \sin\beta \, \text{Im}\phi_1^0 + \cos\beta \, \text{Im}\phi_2^0;$$

$$\begin{aligned} h &= -\sin\alpha \left(\text{Re}\left(\phi_1^0\right) - v_1 \right) + \cos\alpha \left(\text{Re}\left(\phi_2^0\right) - v_2 \right) \\ H &= \cos\alpha \left(\text{Re}\left(\phi_1^0\right) - v_1 \right) + \sin\alpha \left(\text{Re}\left(\phi_2^0\right) - v_2 \right). \end{aligned}$$

with $< \phi_i^0 >= v_i$ for i=1,2 and $v_1^2 + v_2^2 \approx (246 \text{ GeV})^2$. The angle α diagonalizes the CP-even Higgs squared-mass matrix, while β diagonalizes both the CP-odd and charged Higgs sectors, and

h and H are defined as the lightest and heaviest CP-even Higgs boson, respectively.

V.1.1. The MSSM Higgs Boson Masses

Quite generally for any two Higgs doublet model, including the MSSM, the phenomenology depends strongly on the size of the mixing angle α and therefore on the quartic couplings,

$$\sin\alpha = \frac{\mathcal{M}_{12}^2}{\sqrt{\left(\mathcal{M}_{12}^2\right)^2 + \left(\mathcal{M}_{11}^2 - m_h^2\right)^2}}$$

where

$$\mathcal{M}_{12}^2 = -\left(m_A^2 - (\lambda_3+\lambda_4)\,v^2\right)\sin\beta\cos\beta + \lambda_7 v^2\sin^2\beta + \lambda_6 v^2\cos^2\beta$$

$$\mathcal{M}_{11}^2 = \left(m_A^2 + \lambda_5 v^2\right)\sin^2\beta + \lambda_1 v^2\cos^2\beta + 2\lambda_6 v^2\cos\beta\sin\beta$$

The spectrum is given by

$$m_{h,H}^2 = \frac{\mathcal{M}_{11}^2 + \mathcal{M}_{22}^2 \pm \sqrt{\left(\mathcal{M}_{11}^2 - \mathcal{M}_{22}^2\right)^2 + 4\left(\mathcal{M}_{12}^2\right)^2}}{2}$$

with

$$\mathcal{M}_{22}^2 = \left(m_A^2 + \lambda_5 v^2\right)\cos^2\beta + \lambda_2 v^2\sin^2\beta + 2\lambda_7 v^2\cos\beta\sin\beta\ .$$

The charged Higgs boson mass is given by

$$m_{H^\pm}^2 = m_A^2 + (\lambda_5 - \lambda_4)\,\frac{v^2}{2}.$$

The supersymmetric structure of the theory imposes constraints on the Higgs sector of the model. In particular, at tree level, the parameters of the Higgs self-interaction, λ_{1-4}, are defined in terms of the electroweak gauge coupling constants,

$$\lambda_1 = \lambda_2 = g_2^2/4,\ \ \lambda_3 = -\left(g_1^2 - g_2^2\right)/4\ \ \lambda_4 = -g_2^2/2,$$

and $\lambda_{5,6,7} = 0$. As a result, all Higgs sector parameters at tree level are determined by only two free parameters: the ratio of the Φ_1 and Φ_2 vacuum expectation values, $\tan\beta = v_2/v_1$, and one Higgs boson mass, conventionally chosen to be the CP-odd Higgs boson mass, m_A. The other tree-level Higgs boson masses are then given in terms of these parameters. In the large $m_A \gg M_Z$ limit, also called the decoupling limit [159],

$\sin\alpha \to -\cos\beta$, $\cos\alpha \to \sin\beta$, $\cos(\beta-\alpha) \to 0$, and the lightest CP-even Higgs h behaves as the SM Higgs. The same behavior is obtained if the quartic couplings are such that $\mathcal{M}_{12}^2 \sin\beta = -(\mathcal{M}_{11}^2 - m_h^2)\cos\beta$ [178]. The latter condition represents a situation in which the coupling of h to fermions and weak gauge bosons become the same as in the SM, without decoupling the rest of the non-standard scalars and it is of particular interest due to the fact that the recently discovered Higgs boson has SM-like properties. In the MSSM this condition, denote as alignment [177] can only occur once quantum corrections to the quartic couplings have been included.

The tree level value of m_h is maximized for not only for large $m_A \gg M_Z$ but also for $\tan\beta \gg 1$. In the large m_A limit, one finds $m_h^2 \simeq (M_Z \cos 2\beta)^2$ and $m_A \simeq m_H \simeq m_{H^\pm}$, up to corrections of $\mathcal{O}({M_Z}^2/m_A)$. Below the scale m_A, the Higgs sector of the effective low-energy theory consists only of h, which behaves as the SM Higgs boson. This scenario would have been excluded already by LEP and would not accommodate the recently discovered Higgs boson. However, radiative corrections have a significant impact on the values of Higgs boson masses and couplings in the MSSM. In particular, m_h can be lifted to agree with present LHC measurements.

The dominant radiative effects to the SM-like Higgs mass arise from the incomplete cancellation between top and scalar-top (stop) loops and at large $\tan\beta$ also from sbottom and stau loops. The loop contributions to the tree level quartic couplings depend on the SUSY spectrum, and render $\lambda_{5,6,7}$ non zero. The stop, sbottom and stau masses and mixing angles depend on the supersymmetric Higgsino mass parameter μ and on the soft-supersymmetry-breaking parameters [10,133]: M_Q, M_U, M_D, M_L, M_E, and A_t, A_b A_τ. The first three of these are the left-chiral and the two right-chiral top and bottom scalar quark mass parameters. The next two are the left-chiral stau/sneutrino and the right-chiral stau mass parameters, and the last three are the trilinear parameters that enter in the off-diagonal squark/slepton mixing elements: $X_t \equiv A_t - \mu\cot\beta$ and $X_{b,\tau} \equiv A_{b,\tau} - \mu\tan\beta$. The corrections affecting the Higgs boson masses, production, and decay properties depend on all

of these parameters in various ways. At the two-loop level, also the masses of the gluino and the electroweak guagino enter in the calculations. For simplicity, we shall initially assume that A_t, A_b, A_τ, μ, and the gluino and electroweak guagino masses are real parameters. The impact of complex phases on MSSM parameters, which will induce CP-violation in the Higgs sector, is addressed below.

Radiative corrections to the Higgs boson masses have been computed using a number of techniques, with a variety of approximations; see Refs. [137,138,139,140,141,142,143,144,145,146,147,148,149]. The radiative corrections to the m_h depend strongly on the top quark mass ($\sim m_{\rm t}^4$) and the stop mixing parameter ($\sim X_t^2$ and $\sim X_t^4$), and there is also a logarithmic dependence on the stop masses. For large $\tan\beta$, the stau/sbottom mixing parameters and masses are also relevant. In the large m_A (decoupling) limit and for $\tan\beta \gg 1$, that maximizes m_h at tree level, the m_h value can be maximized at loop level for $X_t \simeq \sqrt{6} M_{\rm SUSY}$, where $M_{\rm SUSY} \simeq M_Q \simeq M_U \simeq M_D$ is an assumed common value of the soft SUSY-breaking squark mass parameters. This choice of X_t is called the "maximal-mixing scenario". For fixed X_t, the value of m_h can varied by a few to several GeV by varying $M_{\rm SUSY}$ a few TeV or m_t within its experimental error, as well as varying SUSY particle parameters entering only beyond the one- loop order. Moreover, in the large $\tan\beta$ regime light staus and/or sbottoms with sizable mixing, governed by the μ parameter, yield negative radiative corrections to the mass of the lightest Higgs boson, and can lower it by several GeV [145,167]. Allowing for experimental and theoretical uncertainties, one finds for $M_{\rm SUSY} \lesssim 2$ TeV, large m_A, $\tan\beta \gg 1$ and for $X_t \simeq \sqrt{6} M_{\rm SUSY}$, that the maximal value for the lightest Higgs mass is $m_h^{\rm max} = 135$ GeV [164,165,166]. Interestingly, the upper bound on the lightest neutral scalar boson is a prediction for both the CP-conserving (CPC) and CP-violating (CPV) [195] MSSM scenarios.

The newly discovered SM-like Higgs boson, if interpreted as the lightest MSSM Higgs with a mass of about 125 GeV, provides information on the possible MSSM parameter space. In particular a sizable mixing in the stop sector is required

($X_t \geq 1.5 M_{\rm SUSY}$) for values of $M_{\rm SUSY} \simeq M_Q \simeq M_U \simeq M_D \simeq$ 1 to a few TeV [167,169,168,170,171,172,173,174]. See for example Fig. 26. In a bottom up approach, considering the third generation soft SUSY breaking parameters as input and deriving constraints from the requirement of $m_h \simeq$125 GeV, one observes that one can have a light stop as low as experimentally allowed [175] and the other one of order of the mixing parameter, or both stops below a TeV with $X_t \geq 1.5$ TeV, see for example Fig. 27. It is also possible to consider both stops significantly above a few TeV by varying/lowering the values of X_t and $\tan\beta$, in that case the impact of higher loops in the computation of the Higgs mass becomes relevant, see Fig. 28 [149].

For a given CP odd Higgs mas m_A, the masses of the other two Higgs bosons, H and $H^{\pm}$, also receive radiative corrections, but in the absence of additional CP violating phases, and for m_A larger than $m_h \simeq 125$ GeV, they are all similar, and at most about a few tens of GeV apart. For m_A smaller instead, the heavy Higgs is the SM one, $m_H \simeq 125$ GeV and $m_h \simeq m_A$, but this scenario is strongly challenged by present data, and we will not concentrate on it in this review [163]. For a more detailed discussion of the effect of radiative corrections on the heavy Higgs masses see for example Refs. [17] and [158]. .

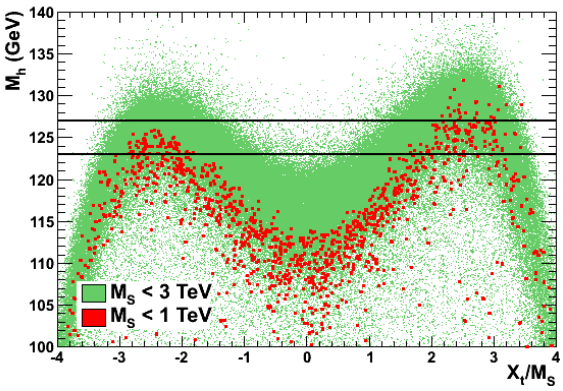

Figure 26: Ref. 169. See full-color version on color pages at end of book.

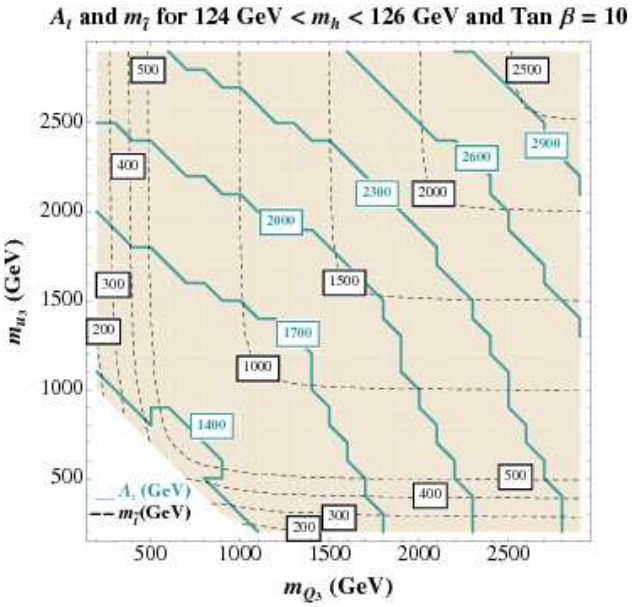

Figure 27: Ref. 167. See full-color version on color pages at end of book.

Figure 28: Ref. 149. See full-color version on color pages at end of book.

V.1.2. MSSM Higgs Boson Couplings

The phenomenology of the Higgs sector depends on the couplings of the Higgs bosons to gauge bosons, and fermions. The couplings of the two CP-even Higgs bosons to $W^{\pm}$ and Z bosons are given in terms of the angles α and β

$$g_{hVV} = g_V m_V \sin(\beta - \alpha) \qquad g_{HVV} = g_V m_V \cos(\beta - \alpha) \quad (9)$$

where $g_V \equiv 2m_V/v$, for $V = W^{\pm}$ or Z. There are no tree-level couplings of A or $H^{\pm}$ to VV. The couplings of the Z boson to two neutral Higgs bosons, which must have opposite CP-quantum numbers, are given by

$$g_{hAZ} = g_Z \cos(\beta - \alpha)/2 \qquad g_{HAZ} = -g_Z \sin(\beta - \alpha)/2\,. \quad (10)$$

Charged Higgs-W boson couplings to neutral Higgs bosons and four-point couplings of vector bosons and Higgs bosons can be found in Ref. 11.

The tree-level Higgs couplings to fermions obey the following property: the neutral components of one Higgs doublets, Φ_1, couple exclusively to down-type fermion pairs while the neutral components of the other doublet, Φ_2, couple exclusively to up-type fermion pairs [11,160]. This Higgs-fermion coupling structure defines the Type-II 2HDM [161]. In the MSSM, fermion masses are generated when both neutral Higgs components acquire vacuum expectation values, and the relations between Yukawa couplings and fermion masses are (in third-generation notation)

$$h_b = \sqrt{2}\, m_b/\left(v\cos\beta\right) \qquad h_t = \sqrt{2}\, m_t/\left(v\sin\beta\right). \tag{11}$$

Similarly, one can define the Yukawa coupling of the Higgs boson to τ-leptons (the latter is a down-type fermion).

The couplings of the neutral Higgs bosons to $f\bar{f}$ relative to the SM value, $gm_f/2M_W$, are given by

$$\begin{aligned}
h b\bar{b}: &\qquad -\sin\alpha/\cos\beta = \sin\left(\beta-\alpha\right) - \tan\beta\cos\left(\beta-\alpha\right)\,,\\
h t\bar{t}: &\qquad \cos\alpha/\sin\beta = \sin\left(\beta-\alpha\right) + \cot\beta\cos\left(\beta-\alpha\right)\,,\\
H b\bar{b}: &\qquad \cos\alpha/\cos\beta = \cos\left(\beta-\alpha\right) + \tan\beta\sin\left(\beta-\alpha\right)\,,\\
H t\bar{t}: &\qquad \sin\alpha/\sin\beta = \cos\left(\beta-\alpha\right) - \cot\beta\sin\left(\beta-\alpha\right)\,,\\
A b\bar{b}: &\quad \gamma_5\tan\beta\,, \qquad A t\bar{t}: \quad \gamma_5\cot\beta\,,
\end{aligned} \tag{12}$$

where the γ_5 indicates a pseudoscalar coupling. In each relation above, the factor listed for $b\overline{b}$ also pertains to $\tau^+\tau^-$. The charged Higgs boson couplings to fermion pairs are given by

$$\begin{aligned}
g_{H^-t\bar{b}} &= \frac{g}{\sqrt{2}M_W}\left[m_t\cot\beta\frac{1+\gamma_5}{2} + m_b\tan\beta\frac{1-\gamma_5}{2}\right]\,,\\
g_{H^-\tau^+\nu} &= \frac{g}{\sqrt{2}M_W}\left[m_\tau\tan\beta\frac{1-\gamma_5}{2}\right]\,,
\end{aligned} \tag{13}$$

The non-standard neutral Higgs bosons have significantly enhanced couplings to down-type fermions at sizeable $\tan\beta$. From the above equations it is clear that this occurs whenever we are close to the alignment limit: $\cos(\beta-\alpha) \ll 1$, where in the mass eigenbasis only one Higgs acquires a vev. [177,178]. In this case the lightest Higgs boson behaves like the SM one

and H and A have $\tan\beta$ enhanced couplings to down type fermions, and analogous enhanced couplings are in place for the charged Higgs. The alignment limit is usually identified with decoupling, $m_A \gg M_Z$. However, alignment can occur without decoupling, both in the MSSM, once radiative corrections are taken into account, and most generically in 2HDM's. This possibility is intriguing, since it implies that a 125 GeV Higgs with SM couplings (or less than a few percent away) can occur irrespective of the rest of the Higgs sector being at the electroweak scale or much heavier [177]. For the most updated and detailed study on alignment without decoupling in 2HDM's with or without supersymmetry see [178].

Quite in general, radiative corrections can modify significantly the values of the Higgs boson couplings to fermion pairs and to vector boson pairs. In a first approximation, when radiative corrections to the quartic couplings are computed, the diagonalizing angle α is shifted from its tree-level value, and hence one may compute a "radiatively-corrected" value for $\cos(\beta-\alpha)$. This shift provides an important source of the radiative corrections to the Higgs couplings [147], [167]. The radiative corrections to the angle α can enable the alignment without decoupling for sizeable values of the Higgs mass parameter $\mu \geq M_{\rm SUSY}$ and sizeable $\tan\beta$. Additional contributions from the one-loop vertex corrections to tree-level Higgs couplings must also be considered [142,196,197,198,199,200,201,202]. These contributions alter significantly the Higgs-fermion Yukawa couplings at large $\tan\beta$, both in the neutral and charged Higgs sector. Moreover, these radiative corrections can modify the basic relationship $g_{h,H,A b\bar{b}}/g_{h,H,A\tau^+\tau^-} \propto m_b/m_\tau$, and change the main features of MSSM Higgs phenomenology.

V.1.3. Decay Properties and Production Mechanisms of MSSM Higgs Bosons

In the MSSM, neglecting CP-violating effects, one must consider the decay properties of three neutral Higgs bosons and one charged Higgs pair. One needs to secure that the mass, CP nature and decay and production properties of one of the neutral Higgs bosons is in agreement with Higgs data. This

implies that some degree of alignment is necessary so that the lightest MSSM Higgs couplings to gauge bosons and fermions do not depart from SM predictions more than what is allowed by present Higgs precision measurements.

In the alignment region $\cos(\beta - \alpha) \to 0$, and for heavy SUSY particles, the decay rates of h into SM particles are nearly indistinguishable from those of the SM Higgs boson. If the additional Higgs bosons are sufficiently heavy the alignment is triggered by decoupling and departures would be minimal. If m_A is below a few hundred GeV then departures from alignment depend on the radiative corrections to the mixing angle α that are proportional to ratios of mass parameters associated to the SUSY particles, and hence do not decouple for a heavy SUSY spectra. The main effects occur in departures from the $h \to b\bar{b}$ decay rate, hence in its total width and, indirectly, in all branching ratios. As mentioned before additional effects may be induced through SUSY-QCD radiative corrections to the $hb\bar{b}$ coupling that may be relevant even in the presence of heavy SUSY particles.

The SM-like branching ratios of h can be modified if decays into supersymmetric particles are kinematically allowed [203]. Most interesting, if light superpartners exist that couple to photons and/or gluons, the h loop-induced coupling to gg and $\gamma\gamma$ could deviate sizeably from the corresponding SM predictions [205,167,204] MORE REFS HERE?. In particular, light staus, close to a 100 GeV with large mixing can enhance the Higgs decay rate into di-photons by up to 40% with respect to the SM, without being in conflict with stability of the Higgs potential [179]. Light charginos, close to the LEP limit, can also vary the Higgs to diphoton decay rate for small values of $\tan\beta \simeq 2$, but limits on the chargino mass preclude them to be larger than a 10% [180]. Given the smallness of the Higgs to dipohoton rate, and hence its negligible contribution to the total Higgs decay width, both light staus and charginos have the possibility of altering $BR(h \to \gamma\gamma)$ without altering any other decay rates. Light stops and light sbottoms could contribute to the Higgs-diphoton rate, but in practice they are strongly constrained by the fact that they would at the same time yield a

much larger contribution to gluon fusion Higgs production. The Higgs-digluon decay rate and gluon fusion Higgs production can be suppressed due to sbottom effects at large $\tan\beta$ and large μ, but in practice such effect is very small for masses above 500 GeV as presently preferred by LHC searches [**sbottoms-LHC**]. Light stops, instead, can give relevant contributions to the Higgs-di-gluon rate and gluon fusion Higgs production. Depending on the value of the stop mixing and the stop masses both suppression or enhancement with respect to the SM value are possible. In practice, due to the requirement from m_h, light stops can only moderately vary the effective gluon-Higgs coupling and correspondingly the gluon fusion-Higgs production rate [181].

Given that some degree of alignment is necessary to agree with data, for the heavier Higgs states there are two possibilities to be considered, and in both cases the heavier Higgs states, H, A and $H^{\pm}$, are roughly mass degenerate (with masses $\pm$ 20 GeV or less apart) i) Alignment triggered by decoupling, hence $m_A \geq$ several hundred GeV: The AWW and AZZ couplings vanish, and the HWW and HZZ couplings are very small. The dominant decay branching ratios strongly depend on $\tan\beta$. After incorporating the leading radiative corrections to Higgs couplings from both QCD and supersymmetry, the following decay features are relevant in the MSSM. The decay modes $H, A \to b\overline{b}$, $\tau^+\tau^-$ dominate when $\tan\beta$ is large (this holds even away from decoupling). For small $\tan\beta$, the $t\overline{t}$ decay mode dominates above its kinematic threshold. In contrast to the lightest SM-like Higgs boson, the vector boson decay modes of H are strongly suppressed due to the suppressed HVV couplings in the decoupling limit. For the charged Higgs boson, $H^+ \to t\bar{b}$ dominates. ii) Alignment without decoupling, hence $m_A \leq$ a few hundred GeV. The main difference with the previous case is that in the low $\tan\beta$ regime ($\tan\beta \leq$ 5) additional decay channels may be allowed which involve decays into the lightest SM-like Higgs. For A and H, besides the $H, A \to b\overline{b}$, $\tau^+\tau^-$ decay modes, also *e.g.,* $A \to Zh$, $H \to hh$ as well as $H \to WW/ZZ$ decay modes are available. For the

charged Higgs boson, $H^+ \to \tau^+\nu_\tau$ dominates below the $t\bar{b}$ threshold, and also $H^\pm \to W^\pm h$ may be searched for.

In the case of sufficiently light SUSY particles, the heavy Higgs boson decays into charginos, neutralinos and third-generation squarks and sleptons can be important if they are kinematically allowed [207]. Once again one interesting possibility is a significant branching ratio for the decay of a neutral Higgs boson to the invisible mode $\tilde{\chi}_1^0\tilde{\chi}_1^0$ (where the lightest neutralino $\tilde{\chi}_1^0$ is the lightest supersymmetric particle) [208], which poses a challenge at hadron colliders.

The production mechanisms for the SM Higgs boson at e^+e^- and hadron colliders can also be relevant for the production of the MSSM neutral Higgs bosons. However, one must take into account the possibility of enhanced or suppressed couplings with respect to those of the Standard Model, as previously discussed. The supersymmetric-QCD corrections due to the exchange of virtual squarks and gluinos may modify the cross sections depending on the values of these supersymmetric particle masses. At both lepton and hadron colliders there are new mechanisms that produce two neutral Higgs bosons, as well as processes that produce charged Higgs bosons singly or in pairs. In the following we summarize the main processes for MSSM Higgs boson production. For more detailed discussions see Refs. [17,158], and for the state-of-the-art calculations of higher order QCD, electroweak and SUSY corrections and combined effects as well as estimates of uncertainties at hadron colliders see [19,20,21] and references therein.

The main production mechanisms for the neutral MSSM Higgs bosons at e^+e^- colliders are Higgs-strahlung ($e^+e^- \to Zh, ZH$), vector boson fusion ($e^+e^- \to \nu\bar{\nu}h, \nu\bar{\nu}H$)—with W^+W^- fusion about an order of magnitude larger than ZZ fusion—and s-channel Z boson exchange ($e^+e^- \to Ah, AH$) [209]. For the Higgs-strahlung process, it is possible to reconstruct the mass and momentum of the Higgs boson recoiling against the particles from the Z boson decay, and hence sensitive searches for Higgs bosons decaying even to invisible final states can be applied.

The main charged Higgs boson production process at e^+e^- colliders is via s-channel γ or Z boson exchange ($e^+e^- \to H^+H^-$). Charged Higgs bosons can also be produced in top quark decays via $t \to b + H^+$ if $m_H^\pm < m_t - m_b$ or via the one-loop process $e^+e^- \to W^\pm H^\mp$ [210,211], which allows the production of a charged Higgs boson with $m_H^\pm > \sqrt{s}/2$, even when H^+H^- production is kinematically forbidden. Other single charged Higgs production mechanisms include $t\bar{b}H^-/\,\bar{t}bH^+$ production [34], $\tau^+\nu H^-/\,\tau^-\bar{\nu}H^+$ production [212], and a variety of processes in which $H^\pm$ is produced in association with a one or two other gauge and/or Higgs bosons [213].

At hadron colliders, the dominant neutral Higgs production mechanism over the majority of the MSSM parameter space is gluon-gluon fusion, mediated by triangle loops containing heavy top and bottom quarks and the corresponding supersymmetric partners [214]. As previously discussed, the effect of light stops that may contribute to the the gluon fusion production will be partially cancelled, by the fact that they need to have sizeable mixing, while light sbottoms that could suppress gluon fusion through mixing effects are disfavored by data. Higgs boson radiation off bottom quarks becomes important for large $\tan\beta$, where at least two of the three neutral Higgs bosons have enhanced couplings to bottom-type fermions [215,216]. In the search for non-standard neutral Higgs bosons, A and H, the production can be via either of the above channels in the final inclusive di-tau mode and via radiation off bottom quarks in the 4b's final mode. It turns out that the $b\bar{b}\phi, \phi \to b\bar{b}$ channel depends strongly on the radiative corrections affecting the relation between the bottom quark mass and the bottom Yukawa coupling [142,147,200,201], while in the channels with $\tau^+\tau^-$ final states, compensations occur between large corrections in the Higgs boson production and decay. As a result, the $b\bar{b}A$ channel is more sensitive to the specific SUSY scenario, while the the inclusive $\tau^+\tau^-$ channel is rather robust under variations of the SUSY spectra. At high $\tan\beta$ the production and decay rates of H are similar to those of A, and given that A and H are nearly degenerate in mass, the signal cross section is increased by roughly a factor of two. Detailed discussions of the impact

of radiative corrections in these search modes are presented in Refs. [238] and [246].

The vector boson fusion and Higgs-strahlung production of the CP-even Higgs bosons as well as the associated production of neutral Higgs bosons with top quark pairs have lower production cross sections by least an order of magnitude with respect to the dominant ones, depending on the precise region of MSSM parameter space.

Charged Higgs bosons can be produced in several different modes at hadron colliders. If $m_{H^\pm} < m_t - m_b$, the charged Higgs boson can be produced in decays of the top quark via the decay $t \to bH^+$, which would compete with the SM process $t \to bW^+$. Relevant QCD and SUSY-QCD corrections to BR($t \to H^+b$) have been computed [217,218,219,220]. For values of $m_{H^\pm}$ near m_t, width effects are important. In addition, the full $2 \to 3$ processes $pp/p\bar{p} \to H^+\bar{t}b + X$ and $pp/p\bar{p} \to H^-t\bar{b} + X$ must be considered. If $m_{H^\pm} > m_t - m_b$, then charged Higgs boson production occurs mainly through radiation from a third generation quark. Charged Higgs bosons may also be produced singly in association with a top quark via the $2 \to 3$ partonic processes gg, $q\bar{q} \to t\bar{b}H^-$ (and the charge conjugate final states). For charged Higgs boson production cross section predictions for the Tevatron and the LHC, see Refs. [10,221,222,223,224,225,226,227]. Charged Higgs bosons can also be produced via associated production with $W^\pm$ bosons through $b\overline{b}$ annihilation and gg-fusion [228]. They can also be produced in pairs via $q\overline{q}$ annihilation [229]. The inclusive H^+H^- cross section is less than the cross section for single charged Higgs associated production [229–231].

V.1.4. Benchmark Scenarios in the MSSM for a 125 GeV light Higgs

The experimental uncertainties on the measurements of the production cross sections times branching ratios are at present rather large, and a Higgs sector that differs significantly from the SM case can still fit the data. Hence it is important to explore scenarios were the lightest Higgs agrees with present data but still allows for novel new physics features, and to consider the implications of such scenarios in the search for the

remaining MSSM Higgs bosons. The additional Higgs boson are sought for mainly via the channels

$$
\begin{aligned}
&pp \to A/H \to \tau^+\tau^- \;\; (inclusive)\,, \quad b\bar{b}A/H, A/H \to \tau^+\tau^- \;\; (with \;\; b{-}tag)\,, \\
&b\bar{b}\phi, \phi \to b\bar{b} \;\; (with \;\; b{-}tag)\,, \\
&pp \to t\bar{t} \to H^{\pm}W^{\mp}\, b\bar{b}, \;\; H^{\pm} \to \tau\nu_{\tau} \;\; , \\
&gb \to H^{-}t \quad or \quad g\bar{b} \to H^{+}\bar{t}, \;\; H^{\pm} \to \tau\nu_{\tau} \;\; .
\end{aligned}
\tag{14}
$$

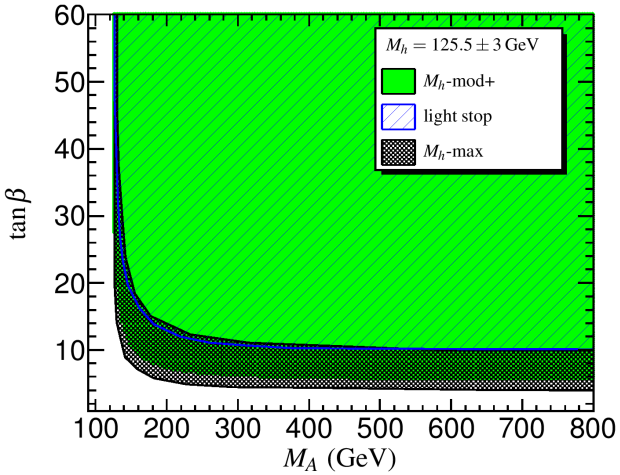

Figure 29: Allowed regions in the $m_A \tan\beta$ plane, compatible with the lightest Higgs boson mass, $m_h = 125.5 \pm 3$ GeV, for the maximal mixing scenario (hatched black region), the moderate stop mixing benchmark scenario (green shaded region) and the light stop scenario (blue hatched region), as defined in Ref. 163. See full-color version on color pages at end of book.

The non-observation of any additional state in these production and decay modes puts by now stringent constraints on the MSSM parameter space, in particular on the values of the tree level parameters m_A and $\tan\beta$. Similarly, the non-observation of supersymmetric particles puts constraints on masses of stops and sbottoms as well as gluinos and electroweak gauginos that are relevant for the Higgs sector. It is possible to do an scan of the MSSM parameters assuming a simplified structure of the Higgs radiative corrections [**maiani**], or varying a restricted number of the most relevant parameters [**pMSSM7**] and obtain

a best fit to the various, measured rates of cross sections and branching ratios, assuming the lightest Higgs boson is the one recently discovered at the LHC. However, due to the large number of free parameters that are relevant for the Higgs sector, a complete scan of the MSSM parameter space is impractical in experimental analyses and phenomenological studies. In the past, for LEP and also for the Tevatron and the LHC it has been useful to define a set of benchmark scenarios to highlight interesting conditions for MSSM Higgs searches. Now taking into account the recent discovery of a Higgs-like state of 125.5 GeV, it is most useful to define updated MSSM benchmarks scenarios that over a wide range of their parameter space are compatible with both the mass and the detected production and decay rates of the observed signal [163]. They include i) an updated version of the maximal mixing scenario with a larger value of the gluino mass compatible with LHC bounds. This scenario was originally defined to consider values of the stop mixing to maximize the m_h value and, as a result, only a small region of parameter space is compatible with $m_h = 125.5 GeV$ ii) a moderate mixing scenario in which the light CP-even Higgs boson can be interpreted as the newly discovered state within almost the whole parameter space of the $m_A - \tan\beta$ plane that is unexcluded by limits from Higgs searches at LEP and the LHC, iii) a light stop scenario with stop masses in the few to several hundred GeV range that can give contributions to gluon fusion Higgs production iv) a light stau scenario where the light stau can enhance the SM branching ratio into diphotons for large $\tan\beta$ v) a tau-phobic scenario that exhibits variations of $BR(h \to b\bar{b})$ and $BR(h \to \tau^+\tau^-)$ with respect to their SM values.

The above benchmarks are just examples that interpret the LHC signal as the lightest CP-even MSSM Higgs boson. In Fig. 29 we show the regions in the $m_A - \tan\beta$ plane that are compatible with a light CP even Higgs mass, $m_h = (125.5 \pm 3)$ GeV, for the above benchmarks scenarios. The parameter space allowed by cases ii, iv and v are overlapping, hence only the moderate mixings scenario is shown in the figure. The defined scenarios exemplify cases where deviations from the SM

properties would be in place in all of the allowed parameter space due to loop effects and irrespective of the precise value of m_A (cases iii and iv above), where h tends to behave as a SM-like Higgs as the theory approaches the decoupling limit (cases i and ii above) and where h behaves SM-like due to alignment for specific regions of $\tan\beta$ and large μ irrespective of the value of m_A (case v). The above benchmarks have also different behavior for the properties of the heavy Higgs bosons. In particular, the light stau scenario the decay of $A/H \to \tilde{\tau}_1^+\tilde{\tau}_1^-$ becomes relevant. It the above benchmarks it is also possible to have decays of $H \to hh$ in regions of moderate m_A and moderate $\tan\beta$ as far as one is away from alignment. Also for the previous benchmarks, considering the traditional $A/H \to \tau^+\tau^-$ search channel, one would observe variations in the LHC reach depending on the values of μ and M_2. If both parameters are small, as in the maximal and moderate mixing scenarios, then the decays of heavy neutral Higgs bosons into gauginos become competitive for small to moderate $\tan\beta$ and m_A. On the contrary, if at least one of the two parameters becomes larger as in the rest of the benchmark scenarios, then the decay of heavy neutral Higgs bosons into gauginos closes up and the reach in $A/H \to \tau^+\tau^-$ is significantly enhanced for the same regions of $\tan\beta$ and m_A. Lastly varying the parameter μ in both sign and magnitude within the previous benchmarks, the radiative corrections to the bottom Yukawa coupling can vary significantly, and alters significantly the 4b's channel and to a lesser extent the inclusive di-tau channel reach. Future precision measurements of the Higgs boson couplings to fermions and gauge bosons together with information on heavy Higgs searches will provide powerful information on the SUSY parameter space [178]. Initial studies can be found in Refs. [**maiani**], [**pMSSM7**].

V.2. Indirect constraints on additional states

Indirect bounds from a global fit to precision measurements of electroweak observables can be derived in terms of MSSM parameters [269] in a way similar to what was done in the SM. prediction of the MSSM. Given the MSSM and SM predictions for M_W as a function of m_t, and varying the Higgs boson mass

and the SUSY spectrum, one finds that the MSSM overlaps with the SM when SUSY masses are large, of $\mathcal{O}(2$ TeV), and the light SM-like Higgs boson has a mass in the experimentally preferred mass range: m_h $\tilde{1}$14–129 GeV. The MSSM Higgs boson mass expectations are compatible with the constraints provided by the measurements of m_t and M_W [270]. A global fit for m_h in the Constrained MSSM, for example, yields $m_h = 119.1^{+3.4}_{-2.9}$ GeV after including the constraints from LHC data, instead of the pre-LHC value of $m_h = 111.5^{+3.5}_{-1.2}$ GeV, improving the consistency of the model predictions with the LEP exclusion [271] [4]. These global fit studies show that a SM-like Higgs with mass 125 GeV or larger would start to build up some tension with $g_\mu - 2$ that may ultimately lead to exclude the CMSSM or other types of constrained SUSY scenarios for which similar results can be obtained.

Improvements in our understanding of B-physics observables put indirect constraints on MSSM scenarios in regions in which Higgs boson searches at the Tevatron and the LHC are sensitive. In particular, BR($B_s \to \mu^+\mu^-$), BR($b \to s\gamma$), and BR($B_u \to \tau\nu$) play an important role within minimal flavor-violating (MFV) models [272], in which flavor effects proportional to the CKM matrix elements are induced, as in the SM. For example, see Refs. [273–276]. The supersymmetric contributions to these observables come both at the tree- and loop-level, and have a different parametric dependence, but share the property that they become significant for large values of $\tan\beta$, which is also the regime in which searches for non-standard MSSM Higgs bosons at hadron colliders are the most powerful.

In the SM, the relevant contributions to the rare decay $B_s \to \mu^+\mu^-$ come through the Z-penguin and the $W^\pm$-box diagrams [277]. In supersymmetry with large $\tan\beta$, there are also significant contributions from Higgs-mediated neutral currents [278–281], which depend on the SUSY spectra, and grow with the sixth power of $\tan\beta$ and decrease with the fourth power of the CP-odd Higgs boson mass m_A. Therefore, the

[4] This fit does not include the direct limits on the Higgs boson mass from any collider.

upper limits from the Tevatron and the LHC [282] put strong restrictions on possible flavor-changing neutral currents (FCNC) in the MSSM at large $\tan\beta$ [283].

Further constraints are obtained from the rare decay $b \to s\gamma$. The SM rate is known up to NNLO corrections [284,285] and is in good agreement with measurements [286]. In the Type-II 2HDM and in the absence of other sources of new physics at the electroweak scale, a bound $m_{H^\pm} > 295$ GeV has been derived [284]. Although this indirect bound appears much stronger than the results from direct charged Higgs searches, it can be invalidated by new physics contributions, such as those which can be present in the MSSM. In the minimal flavor-violating MSSM, there are new contributions from charged Higgs as well as chargino-stop and gluino-sbottom diagrams. The charged Higgs boson's contribution is enhanced for small values of its mass and can be partially canceled by the chargino and gluino contributions or by higher-order $\tan\beta$-enhanced loop effects.

The branching ratio $B_u \to \tau\nu$, measured by the Belle [287,288] and BaBar [289,290] collaborations, also constrains the MSSM. The SM expectation is in slight tension with the latest experimental results [291]. In the MSSM, there is an extra tree-level contribution from the charged Higgs which interferes destructively with the SM contribution, and which increases for small values of the charged Higgs boson mass and large values of $\tan\beta$ [292]. Charged Higgs effects on $B \to D\tau\nu$ decays [293], constrain in an important way the parameter space for small values of the charged Higgs boson mass and large values of $\tan\beta$, and exclude a region that is otherwise allowed by values of $B_u \to \tau\nu$ [291,294,295]. These two observables are only mildly dependent on the SUSY spectra.

Charged Higgs bosons can play a role in explaining the evidence for CP violation in $D^0 \to \pi^+\pi^-$, K^+K^- decays recently presented by LHCb [296] and CDF [297]. In a particular minimal flavor violating 2HDM, tree-level charged Higgs insertions can give large contributions to CP violation in D^0 decays while also being consistent with stringent bounds

from $D^0 - \bar{D}^0$ mixing, BR($b \to s\gamma$), and BR($B_u \to \tau\nu$), as well as direct searches such as $H \to \tau^+\tau^-$ [298].

Several studies [273–276,299,300] have shown that, in extended regions of parameter space, the combined B-physics measurements impose strong constraints on the MSSM models to which Higgs boson searches at the Tevatron and the LHC are sensitive. Consequently, the observation of a non-SM Higgs boson at the Tevatron or the LHC would point to a rather narrow, well-defined region of MSSM parameter space [273,301] or to something beyond the minimal flavor violation framework.

Another indirect constraint on the Higgs sector comes from the search for dark matter. If dark matter particles are weakly interacting and massive, then particle physics can provide models which predict the correct relic density of the universe. In particular, the lightest supersymmetric particle, typically the lightest neutralino, is an excellent dark matter particle candidate [302]. Within the MSSM, the measured relic density places constraints in the parameter space, which in turn - for specific SUSY low energy spectra- have implications for Higgs searches at colliders, and also for experiments looking for direct evidence of dark matter particles in elastic scattering with atomic nuclei. Large values of $\tan\beta$ and small m_A are relevant for the $b\overline{b}A/H$ and $A/H \to \tau^+\tau^-$ searches at the Tevatron and the LHC, and also provide a significant contribution from the CP-even Higgs H exchange to the spin-independent cross sections for direct detection experiments such as CDMS or Xenon, for example. Consequently, a signal at colliders would raise prospects for a signal in indirect detection experiments and vice-versa [299,301,303–305]. theoretical uncertainties in the calculation of dark matter scattering cross sections, and in the precise value of the local dark matter density and velocity distributions, which may dilute these model-dependent correlations.

V.3. Higgs Bosons in Singlet extensions of the MSSM

In the Minimal Supersymmetric Standard Model, the Higgs mass parameter μ sets the scale of electroweak symmetry breaking. However, μ is the only supersymmetric mass parameter in the theory, that is present when SUSY is unbroken, and hence

there is a priori no reason why it should be of order of the electroweak scale, or the supersymmetry breaking scale, but rather it would naturally be of order M_{GUT} or M_{Planck}. The fact that phenomenologically it is required that μ is at the electroweak/TeV scale is known as the μ problem. Supersymmetric models with additional singlets can provide a solution to the μ problem [**muproblem**], by promoting the μ parameter to a dynamical singlet superfield S that only interacts with the MSSM Higgs doublets through a coupling λ_S at the level of the superpotential. An effective μ is generated when the real scalar component of S acquires a vacuum expectation value $< S >$

$$\mu_{eff.} = \lambda_S < S > . \tag{15}$$

After the minimization of the Higgs potential the vacuum state relates the vacuum expectation values of the three neutral scalars, ϕ_1^0, ϕ_2^0 and S, to their soft supersymmetry breaking masses, hence, one expects that these vevs should all be of order M_{SUSY} and therefore the μ problem is solved.

The solution of the μ problem through the addition of a singlet superfield to the MSSM comes along with the existence of an extra global U(1) symmetry, known as the Peccei-Quinn (PQ) symmetry. Once the PQ symmetry is spontaneously broken by the Higgs vevs a pseudo-Nambu-Goldstone boson, the PQ axion appears in the theory. For values of λ_S of order one the lack of detection of such an axion rules out the theory. Making λ_S very small ($\leq 10^{-6}$) would decouple the axion and render things compatible with experimental results, but then one would be trading the μ problem by a λ_S problem, since there is no explanation to why λ_S should be so small. Promoting the PQ symmetry to a local symmetry involving additional gauge bosons and matter fields could be a viable option that has been explored in the literature. Alternatively there is the possibility to break the PQ symmetry explicitly by introducing a discrete Z_3 symmetry that allows the existence of a PQ odd S^3 term in the superpotential. This model extension has been called the Next-to- Minimal Supersymmetric SM (NMSSM) [309]. It is known however that discrete symmetries may came along with the existence of domain wall structures that imply that our

universe would consist of disconnected domains with different ground states, creating unacceptably large anisotropies in the cosmic microwave background [**domainwalls**]. To avoid the problem of domain walls one can consider the existence of non-renormalizable operators that would lead to the preferred vacuum state. However the same operators in turn may originate quadratically divergent tadpole contributions that could shift the vev of S to be much larger, order M_{GUT}, and ruin the singlet solution to the μ problem. To cure the problem of destabilizing tadpoles, discrete R-symmetries have been proposed that secure that tadpoles would only appear at very high order loops and be safely suppressed. Depending on the symmetries imposed on the theory, different models with singlet extensions of the MSSM (xMSSM) have been proposed. In Table **@Tb.xmssm-model@** we show the most studied examples: the NMSSM, the Nearly-Minimal Supersymmetric SM (nMSSM) [310], and the U(1)'-extended MSSM (UMSSM) [**UMSSM**], specifying the new parameters appearing in the superpotential and the respective symmetries. A Secluded U(1)'-extended MSSM (sMSSM) [**sMSSM**] contains three singlets in addition to the standard UMSSM Higgs singlet; this model is equivalent to the nMSSM in the limit that the additional singlet vev's are large, and the trilinear singlet coupling, λ_S, is small [**limitsMSSM**].

Based on the extended models defined in Table **@Tb.xmssm-model@**, we write the most generic supersymmetric and soft supersymmetry breaking scalar potentials for the three scalar fields: Φ_1, ϕ_2 and S:

$$\begin{aligned} V_{xMSSM} = & |\lambda_S \Phi_2 \cdot \Phi_1 + t_F + \kappa S^2|^2 + |\lambda_S S|^2 \left(|\Phi_1|^2 + |\Phi_2|^2\right) \\ & \frac{g'^2 + g^2}{8} \left(|\Phi_1|^2 - |\Phi_2|^2\right)^2 + \frac{g^2}{2} \left(|\Phi_1|^2 |\Phi_2|^2 - |\Phi_2 \cdot \Phi_1|^2\right) \\ & \frac{g_1'^2}{2} \left(Q_{\Phi_1} |\Phi_1|^2 + Q_{\Phi_2} |\Phi_2|^2 + Q_S |S|^2\right)^2 \end{aligned} \tag{16}$$

$$\begin{aligned} V_{\rm soft} = & m_{H_1}^2 |\Phi_1|^2 + m_{H_2}^2 |\Phi_2|^2 + m_s^2 |S|^2 \\ & + \left(A_s \lambda_S S H_u \cdot H_d + \frac{\kappa}{3} A_\kappa S^3 + t_S S + h.c.\right). \end{aligned} \tag{17}$$

where $\Phi_2 \cdot \Phi_1 = \epsilon_{ij} \Phi_2^i \Phi_1^j$ and the couplings g', g, and g_1' are associated to the $U(1)_Y$, $SU(2)_L$, and $U(1)'$ gauge symmetries,

Table 13: Symmetries associated to the different Singlet extension Models and terms in the superpotential that only involve Higgs and Singlet fields. Also the number of neutral states in the Higgs sector are given in the CP conserving case.

Model	MSSM	NMSSM	nMSSM	UMSSM
Symmetry	-	Z_3	Z_5^R, Z_7^R	$U(1)'$
Superpotential	$\mu\Phi_2\cdot\Phi_1$	$\lambda_S S\Phi_2\cdot\Phi_1+\frac{\kappa}{3}S^3$	$\lambda_S S\Phi_2\cdot\Phi_1+t_F S$	$\lambda_S S\Phi_2\cdot\Phi_1$
H_i^0	2	3	3	3
A_i^0	1	2	2	1

respectively. t_F and t_S are supersymmetric and SUSY breaking tadpole terms, respectively, m_s is a SUSY breaking mass term for the scalar component of the field S, and A_s and A_κ are the trilinear soft SUSY breaking mass parameters associated to the new terms $\lambda_S S\Phi_2\cdot\Phi_1$ and $\frac{\kappa}{3}S^3$ in the superpotential, with the B-term of the MSSM expressed as $B\mu\equiv A_s\mu_{eff}$. In particular, κ and A_κ are the parameters for the NMSSM model, while t_F and t_S are those of the nMSSM. The UMSSM depends on the new coupling g_1' as well as on the $U(1)'$ charges of the Higgs fields, Q_{Φ_1}, Q_{Φ_2} and Q_S, that are free parameters with the restriction that they have to add to zero to preserve gauge invariance. In a given $U(1)'$ construction the charges are specified. The addition of the singlet scalar field/s imply that additional CP-even and CP-odd Higgs bosons will appear in the spectra, whereas the charged Higgs sector remains the same as in the MSSM given that the number of Higgs doublets remains unchanged. The mixing with the extra scalar S alters the masses and properties of the physical Higgs bosons, that in general can differ significantly from the SM or the MSSM. A detailed discussions of typical mass spectra and decay properties in these models can be found for example in [**CPNSH**,**xmssm-Langacker**]. Moreover, these models have extra neutralinos and in some cases extra neutral gauge bosons, Z'. The extra gauge boson sector is constrained by experimental data through direct Z' searches as well as the Z-Z' mixing angle $\alpha_{ZZ'}$ constrained to be less that $\mathcal{O}(10^{-3})$ by precision electroweak data .

V.3.1. The xMSSM Higgs Boson Masses and Phenomenology

In singlet extensions of the MSSM the lightest Higgs mass at tree level, $m_{H_1}^{tree}$ receives a contribution from the singlet scalar that renders it larger that the MSSM value, in particular for small values of $\tan\beta$. The tree level upper bound reads

$$m_{H_1}^{tree} \leq M_Z^2 \cos^2 2\beta + \frac{1}{2}\lambda_S^2 v^2 \sin^2 2\beta \tag{18}$$

At the one-loop level, the top and stop loops are the dominant contributions. Gauge couplings in the UMSSM are small compared to the top quark Yukawa coupling so the one-loop gauge contributions are negligible. Corrections exclusive to the NMSSM and the nMSSM enter only at the two loop level. Therefore, thre is no significant model-dependent contributions at one loop order and the MSSM one-loop corrections, governed by the SUSY top and stop loops, and with sbottom and stau loops for large $\tan\beta$, are universal in these models. As a result for large $\tan\beta$, the lightest Higgs mass does not differ in any significant way for the MSSM one. In Fig. 30 from Ref. **@Ref.xmssm-Langacker@**, the mass ranges for the lightest CP-even Higgs boson in the MSSM, NMSSM, nMSSM and UMSSM are shown scanning over parameters as shown in Table **@Tb.xmssm-scan@**. The value of M_{SUSY} is fixed to 1 TeV and the radiative corrections are computed only at one loop level, The upper bounds in Fig. 30 are indicative, since two loop corrections, as has been shown for the MSSM, can be rather relevant and have not been included.

Figure 30: Mass ranges for the lightest CP-even Higgs boson in each extended MSSM scenarios discussed in the text, and in the MSSM, for comparison. The range of scan parameters is shown in Table **@Tb.xmssm-scan@**. The value of M_{SUSY} is fixed to 1 TeV and the radiative corrections are computed only at one loop level. Ref. **@Ref.xmssm-Langacker@**. See full-color version on color pages at end of book.

V.4. Supersymmetry with Extended Gauge Sectors

In the MSSM, the tree-level value of the lightest CP-even Higgs mass originates from the D-term dependence of the scalar potential that comes from the Supersymmetric Kinetic terms in the Kähler potential. The D-terms lead to tree-level quartic couplings which are governed by the squares of the gauge couplings of the weak interactions, under which the Higgs has non-trivial charges and hence the lightest Higgs mass is bounded to be smaller than M_Z If new gauge interactions were present at the TeV scale, and the Higgs bosons would have non-trivial charges under them, there would be new D-term contributions that would lead to an enhancement of the tree-level Higgs mass value. Since the low energy gauge interactions reduce to the known $SU(3)_c \times SU(2)_L \times U(1)_Y$ ones, in order for this mechanism to work, the extended gauge and Higgs sector should be integrated out in a non-supersymmetric way. This means that there must be supersymmetry breaking terms that are of the order or larger than the new gauge boson masses. The enhancement of the tree-level quartic couplings would then depend on the square of the gauge couplings of the extended Higgs sector but will be suppressed when the heavy gauge boson masses are larger than the supersymmetry breaking scale and will acquire its full potential only for large values of this scale.

One of the simplest possibilities is to extend the weak interactions to an $SU(2)_1 \times SU(2)_2$ sector, such that the known weak interactions are obtained after the spontaneous breakdown of these group to $SU(2)_L$ [182]. This may be achieved by introducing a bi-doublet Σ under the two $SU(2)$ gauge groups, which acquire a non-trivial vacuum expectation u in the diagonal direction. The heavy gauge boson masses are therefore given by $M^2_{W'} = (g_1^2 + g_2^2)u^2/2$, and the weak coupling $g^2 = g_1^2 g_2^2/(g_1^2 + g_2^2)$.

In order to obtain a new tree-level contribution to the Higgs potential, the Higgs bosons must be charged under the new interactions. One possibility is to assume that the third generation quarks and leptons as well as the Higgs doublets have charges under the $SU(2)_1$ group, while the second and third generations have charges under $SU(2)_2$. This provides a

natural explanation of the largeness of the third generation couplings compared to the first and second generation ones.

Under these conditions, the D-term contributions to the neutral Higgs effective potential are given by

$$V_D = \frac{g^2\Delta + g_Y^2}{8}\left(|H_2^0|^2 - |H_1^0|^2\right)^2$$

with

$$\Delta = \frac{1 + \dfrac{4m_\Sigma^2}{g_2^2 u^2}}{1 + \dfrac{4m_\Sigma^2}{\left(g_1^2 + g_2^2\right)u^2}},$$

and where m_Σ is the supersymmetry breaking term associated with the bidoublet Σ. It is easy to see that while the MSSM D-term is recovered when $m_\Sigma \to 0$, it is replaced by the $SU(2)_1 \times U(1)_Y$ D-term when m_Σ becomes much larger than $M_{W'}$. The tree-level mass now reads

$$\left(m_h^2\right)_{\text{tree}|} = \frac{g^2\Delta + g_Y^2}{4} v^2 \cos^2 2\beta,$$

and reduces to the MSSM value, $M_Z^2 \cos^2 2\beta$, for $\Delta = 1$.

Assuming $g_1 \simeq g_2$, values of $g_{1,2}$ of order one are necessary to obtain the proper value of the weak gauge coupling. In addition, if values of m_Σ of order $M_{W'}$ are assumed, enhancements of order 50 percent of the MSSM D-term contribution to the Higgs mass may be obtained. Such enhancements are sufficient to allow the obtention of the measured Higgs mass value without the need of very heavy stops or large stop mixing parameters.

The gauge extension described above leads to new, heavy gauge and Higgs bosons, as well as new neutralinos and charginos. Constraints from precision measurements put bounds of the order of a few TeV on the mass of these gauge bosons, which may be probed at the higher energy run of the LHC collider. If the new guagino supersymmetry breaking masses are smaller then the gauge boson masses, the new electro-weakinos will have masses of the order of the few TeV and therefore the weak scale phenomenology reduces to the MSSM one.

Although we have concentrated on a particular gauge extension of the MSSM, the results are quite general. Provided the MSSM Higgs bosons are charged under the extended gauge group and the supersymmetry breaking parameters associated with the new spontaneously broken gauge sector are large compared to the new gauge boson masses, non-decoupled D-terms for the Higgs fields will be generated, leading to a modification of the tree-level Higgs mass prediction. Similar gauge extensions, including also new abelian gauge groups have been considered, for instance, in Refs. [183]- [190]

Gauge extensions of the MSSM can also lead to an enhancement of the Higgs mass value by modifying the renormalization group evolution of the Higgs quartic coupling to low energies. In the MSSM, the evolution of the quartic coupling is governed by the top-quark Yukawa interactions and depends on the fourth power of the top-quark mass. The neutralino and chargino contributions, which depend on the fourth power of the weak gauge couplings, are small due to the smallness of these couplings.

Depending on the values of the soft supersymmetry breaking parameters in the gaugino and Higgsino sectors, the $SU(2)_1$ gauginos may become light, with masses of the order of the weak scale. Since the $SU(2)_1$ coupling may be significantly larger than the $SU(2)_L$ one, for small values of the Higgsino mass parameter μ, the associated charginos and neutralinos may modify the evolution of the quartic coupling in a significant way [191]. This may lead to a significant increase of the lightest CP-even Higgs mass, even for small values of $\tan\beta \simeq 1$ for which the D-term contributions become small. In addition, under these conditions, light charginos may lead to a significant modification of the Higgs diphoton decay rate, which may be as large as 50% of the SM value.

V.5. Effects of CP violation and R-parity violation

In the Standard Model, CP-violation (CPV) is induced by phases in the Yukawa couplings of the quarks to the Higgs field, which results in one non-trivial phase in the CKM mixing matrix. SUSY scenarios with new CPV phases are theoretically appealing, since additional CPV beyond that observed in the K, D, and B meson systems is required to explain the observed

cosmic matter-antimatter asymmetry [258,259]. In the MSSM CP violation effects in the Higgs sector appear at the quantum level and are mostly determined by CP phases active in the third generation squark soft SUSY breaking trilinear mass parameters as well as in the guagino/gluino masses. In extensions of the MSSM such as singlet extensions CP violation effects can be effective already at tree level and due to the larger number of new parameters there are many more sources of CP violation. In general CP violation effects in the Higgs sector are importantly constrained from Electric Dipole Momemts (EDM's) data.

V.5.1. Effects of CP Violation on the MSSM Higgs Spectrum

In the MSSM, there are additional sources of CPV from phases in the various mass parameters. In particular, the gaugino mass parameters (M_i, $i = 1, 2, 3$), the Higgsino mass parameter, μ, the bilinear Higgs squared-mass parameter, m_{12}^2, and the trilinear couplings of the squark and slepton fields to the Higgs fields, A_f, may carry non-trivial phases. The two parameter combinations $\arg[\mu A_f (m_{12}^2)^*]$ and $\arg[\mu M_i (m_{12}^2)^*]$ are invariant under phase redefinitions of the MSSM fields [260,261]. Therefore, if one of these quantities is non-zero, there would be new sources of CP-violation, which affects the MSSM Higgs sector through radiative corrections [195,261–266]. The mixing of the neutral CP-odd and CP-even Higgs boson states is no longer forbidden. Hence, m_A is no longer a physical parameter. However, the charged Higgs boson mass $m_{H^\pm}$ is still physical and can be used as an input for the computation of the neutral Higgs spectrum of the theory.

For large values of $m_{H^\pm}$, corresponding to the decoupling limit, the properties of the lightest neutral Higgs boson state approach those of the SM Higgs boson. That is, for $m_{H^\pm} \gg M_W$, the lightest neutral Higgs boson is approximately a CP-even state, with CPV couplings that are suppressed by terms of $\mathcal{O}(m_W^2/m_{H^\pm}^2)$. In particular, the upper bound on the lightest neutral Higgs boson mass, takes the same value as in the CP-conserving case [261]. Nevertheless, there still can be significant mixing between the two heavier neutral mass eigenstates. For a detailed study of the Higgs boson mass spectrum and

parametric dependence of the associated radiative corrections, see Refs. [262,265].

Major variations to the MSSM Higgs phenomenology occur in the presence of explicit CPV phases. In the CPV case, vector boson pairs couple to all three neutral Higgs boson mass eigenstates, H_i $(i = 1, 2, 3)$, with couplings

$$g_{H_iVV} = \cos\beta\mathcal{O}_{1i} + \sin\beta\mathcal{O}_{2i}$$

$$g_{H_iH_jZ} = \mathcal{O}_{3i}\left(\cos\beta\mathcal{O}_{2j} - \sin\beta\mathcal{O}_{1j}\right) - \mathcal{O}_{3j}\left(\cos\beta\mathcal{O}_{2i} - \sin\beta\mathcal{O}_{1i}\right)$$

where the g_{H_iVV} couplings are normalized to the analogous SM coupling and the $g_{H_iH_jZ}$ have been normalized to $g_Z^{\rm SM}/2$. $\mathcal{O}_{ij}$ is the orthogonal matrix relating the weak eigenstates to the mass eigenstates. It has non-zero off-diagonal entries mixing the CP-even and CP-odd components of the weak eigenstates. The above couplings obey the relations

$$\sum_{i=1}^{3} g_{H_iZZ}^2 = 1 \quad \text{and} \quad g_{H_kZZ} = \varepsilon_{ijk}\, g_{H_iH_jZ}$$

where ε_{ijk} is the Levi-Civita symbol.

Another consequence of CPV effects in the scalar sector is that all neutral Higgs bosons can couple to both scalar and pseudoscalar fermion bilinear densities. The couplings of the mass eigenstates H_i to fermions depend on the loop-corrected fermion Yukawa couplings (similarly to the CPC case), on $\tan\beta$ and on the $\mathcal{O}_{ji}$. The resulting expressions for the scalar and pseudoscalar components of the neutral Higgs boson mass eigenstates to fermions and the charged Higgs boson to fermions are given in Refs. [262,267].

The production processes of neutral MSSM Higgs bosons in the CPV scenario are similar to those in the CPC scenario, except for the fact that in any process, the CP eigenstates h, H, and A can be replaced by any of the three neutral Higgs mass eigenstates H_i. This is the case, since, in the presence of CP violation, the H_i's do not have well-defined CP quantum numbers. Regarding the decay properties, the lightest mass eigenstate, H_1, predominantly decays to $b\overline{b}$ if kinematically allowed, with a smaller fraction decaying to $\tau^+\tau^-$, similar

to the CPC case. If kinematically allowed, a SM-like neutral Higgs boson, H_2 or H_3 can decay predominantly to H_1H_1 leading to many new interesting signals both at lepton and hadron colliders; otherwise it will decay preferentially to $b\overline{b}$.

V.5.2. Searches for Neutral Higgs Bosons in CPV Scenarios

At LEP, all three neutral Higgs eigenstates could have been produced by Higgs-strahlung, $e^+e^- \to H_i\mathrm{Z}$, and in pairs, $e^+e^- \to Z^* \to H_iH_j$, with $i \neq j$. The production rates depend on the details of the CPV scenario. Possible cascade decays such as H_2 or $H_3 \to H_1H_1$ can lead to interesting experimental signatures in the Higgs-strahlung processes, $e^+e^- \to H_2\mathrm{Z}$ or $H_3\mathrm{Z}$, however, the searches in the CPV MSSM scenario are experimentally more difficult. The cross sections for the Higgs-strahlung and pair production processes are given in Refs [195,261,262,266].

The Higgs boson searches at LEP were interpreted [**mssm-2006**] in a CPV benchmark scenario [195] for which the parameters were chosen so as to maximize the phenomenological differences with respect to the CPC scenario. Using the most conservative theoretical calculations available at each point in the $(m_{H_1}, \tan\beta)$ plane, parts of the region $m_{H_1} < 60$ GeV and $\tan\beta < 40$ were excluded, and values of $\tan\beta$ lower than 3 were excluded for all values of $m_{H_1} < 114$ GeV. The Tevatron CP-conserving results and projections for MSSM Higgs searches, as well as the existing projections for LHC MSSM CP-conserving searches have been reinterpreted in the framework of CP-violating MSSM Higgs in Ref. 268.

V.6. Non-Supersymmetric two Higgs Doublet Models

Supersymmetry demands the existence of two Higgs doublets such that one doublet couples to up-type quarks and the other to down-type quarks and charged leptons. This Higgs-fermion coupling structure is the one identifyed as Type II 2HDM and assures that masses for both up and down-type quarks can be generated in a supersymmetric and gauge invariant way. Two Higgs doublet models, however, can have a more diverse Higgs-fermion coupling structure and can be viewed as

a simple extension of the SM to realize the spontaneous breakdown of $SU(2)_L \times U(1)_Y$ to $U(1)_{\rm em}$. Quite generally, if the two Higgs doublets contain opposite hypercharges, the scalar potential will contain mixing mass parameters of the kind $m_{12}^2 \Phi_1^T i\sigma_2 \Phi_2 + h.c.$. In the presence of such terms, both Higgs doublets will acquire vacuum expectation values, $v_1/\sqrt{2}$ and $v_2/\sqrt{2}$, respectively, and the gauge boson masses will keep their SM expressions with the Higgs vacuum expectation value v replaced by $v = \sqrt{v_1^2 + v_2^2}$. Moreover, a new parameter appears in the theory defined as $\tan\beta = v_2/v_1$. Apart from the mass terms, the most generic renormalizable and gauge invariant scalar potential contains seven quartic couplings, which are defined in Eq. (8).

Considering two doublets with hypercharges, with $Y_{\Phi_1} = -1$ and $Y_{H_2} = 1$ as in Eqs. (6) and (7), and the most general, renormalizable Higgs potential will be given by Eq. (8). The same as in the MSSM case, after electroweak symmetry breaking and in the absence of CP-violation, the physical spectrum contains a pair of charged Higgs bosons $H^{\pm}$, a CP-odd Higgs boson A and two neutral CP-even Higgs bosons, h and H. The angles α and β diagonalized the

The complete 2HDM is defined only after considering the interactions of the Higgs fields to fermions. Yukawa couplings of the generic from

$$-h_{ij}^a \bar{\Psi}_L H_a \Psi_R + h.c.$$

may be added to the renormalizable Lagrangian of the theory. Contrary to the SM, the two Higgs doublet structure does not ensure the alignment of the fermion mass terms $m_{ij} = h_{ij}^a v_a/\sqrt{2}$ with the Yukawa couplings h_{ij}^a. This implies that quite generally, the neutral Higgs boson will mediate flavor changing interactions between the different mass eigenstates of the fermion fields. Such flavor changing interactions should be suppressed in order to describe properly the Kaon, D and B meson phenomenology. The Glashow-Weinberg theorem [308] states that, in the presence of multiple Higgs doublets the tree-level FCNC's mediated by neutral Higgs bosons will be absent if all fermions of a given electric charge couple to no more

than one Higgs doublet. Hence, the simplest way of avoiding such transitions is to assume the existence of a symmetry that ensures the couplings of the fermions of each given quantum number (up and down quarks, charged and neutral leptons) to only one of the two Higgs doublets. Different models may be defined depending on which of these fermion fields couple to a given Higgs boson. Models of type I are those in which all SM fermions couple to a single Higgs field. In type II models down quarks and charged leptons couple to a common Higgs field, while the up-quarks and neutral leptons couple to the other. In models of type III quarks couple to one of the Higgs bosons, while leptons couple to the other. Finally, in models of type IV, up-quarks and charged leptons couple to one of the Higgs fields while down-quarks and neutral leptons couple to the other.

Beyond the constraints coming from FCNC effects, in electroweak models based on the SM gauge group, the tree-level value of ρ is determined by the Higgs multiplet structure. By suitable choices for the hypercharges, and in some cases the mass splitting between the charged and neutral Higgs sector or the vacuum expectation values of the Higgs fields, it is possible to obtain a richer combination of doublets, as well as singlets, triplets and higher multiplets compatible with precision measurements [307].

The two Higgs doublet model phenomenology depends strongly on the size of the mixing angle α and therefore on the quartic couplings, see Eqs. For large values of m_A, $\sin\alpha \to -\cos\beta$, $\cos\alpha \to \sin\beta$, $\cos(\beta-\alpha) \to 0$, and the lightest CP-even Higgs h behaves as the SM Higgs. The same behavior is obtained if the quartic couplings are such that $\mathcal{M}_{12}^2 \sin\beta = -(\mathcal{M}_{11}^2 - m_h^2)\cos\beta$. The latter condition represents a situation in which the coupling of h to fermions and weak gauge bosons become the same as in the SM, without decoupling the rest of the non-standard scalars and it is of particular interest due to the fact that the recently discovered Higgs boson has SM-like properties. We will denote this situation as alignment.

In type II Higgs doublet models, at large values of $\tan\beta$ and moderate values of m_A, the non-standard Higgs bosons H, A

and $H^\pm$ couple strongly to bottom-quarks and τ-leptons. Hence the decay modes of the non-standard Higgs bosons tend to be dominated by b-quarks and tau-leptons modes, including top quarks or neutrinos in the case of the charged Higgs. However, for large and negative values of λ_4, the charged Higgs boson mass may be sufficiently heavy to allow on-shell decays

$$H^\pm \to W^\pm + (H, A)\,, \qquad\qquad g_{H^\pm W^\mp H,A} \simeq \frac{M_W}{v} \sin(\beta-\alpha)\,(p+k)^\mu$$

where p^μ and k^μ are the scalar field momenta. On the other hand, for large and positive values of λ_5, the above charged Higgs decay into a $W^\pm$ and the CP-odd Higgs boson may be allowed, but the heavy Higgs H may be sufficiently heavy to decay into a CP-odd Higgs boson and an on-shell Z.

$$H \to Z + A, \qquad\qquad g_{HZA} \simeq \frac{M_Z}{v} \sin(\beta-\alpha)\,(p+k)^\mu$$

The decay $H^\pm \to W^\pm + H$, on the other hand may be allowed only if $\lambda_4 < -\lambda_5$. The couplings controlling all the above decay modes are proportional to $\sin(\beta-\alpha)$ and therefore they are unsuppressed in the alignment limit. Moreover, these could still be the dominant decay modes at moderate values of $\tan\beta$, invalidating the current bounds on these particles, obtained assuming a dominant decay into bottom-quarks or τ-leptons.

The quartic couplings are restricted by the condition of stability of the effective potential as well as by the restriction of obtaining the proper value of the lightest CP-even Higgs mass. Close to the alignment limit, the lightest CP-even Higgs mass becomes, approximately independent of m_A and is given by

$$\begin{aligned} m_h^2 \simeq\; & v^2 \left(\lambda_1 \cos^4\beta + \lambda_2 \sin^4\beta + 2\tilde{\lambda}_3 v^2 \cos^2\beta \sin^2\beta\right) \\ & + v^2 \left(4\lambda_6 \cos^3\beta \sin\beta + 4\lambda_7 \sin^3\beta \cos\beta\right) \end{aligned} \tag{19}$$

where $\lambda_3 = \lambda_3 + \lambda_4 + \lambda_5$.

The stability conditions imply the positiveness of all masses, as well as the avoidance of run-away solutions to large negative values of the fields in the scalar potential. These conditions imply

$$\lambda_1 \geq 0, \qquad\qquad \lambda_2 \geq 0, \qquad\qquad \lambda_3 + \lambda_4 - |\lambda_5| \geq -\sqrt{\lambda_1 \lambda_2},$$

$$\lambda_3 \geq -\sqrt{\lambda_1\lambda_2}, \qquad\qquad 2|\lambda_6+\lambda_7| < \frac{\lambda_1+\lambda_2}{2} + \tilde{\lambda}_3$$

where the first four are necessary and sufficient conditions in the case of $\lambda_6 = \lambda_7 = 0$, while the last one is a necessary condition in the case all couplings are non-zero. Therefore, to obtain the conditions that allow the decays $H^\pm \to W^\pm H, A$ and $H \to ZA$, λ_3 should take large positive values in order to compensate the effects of λ_4 and λ_5.

V.7. Composite Higgs models

Within the SM, EWSB is posited but has no dynamical original. Furthermore, the Higgs boson appears unnaturally light. A scenario that remidies these two catches is to consider the Higgs boson as a bound state of new dynamics becoming strong around the weak scale. The Higgs boson can be made significantly lighter than the other resonances of the strong sector if it appears as a pseudo-Nambu–Goldstone bosons.

V.7.1. Little Higgs

The idea behind the Little Higgs models [393,394] is to identify the Higgs doublet as a (pseudo) Nambu–Goldstone boson while keeping some sizable non-derivative interactions. By analogy with QCD where the pions $\pi^{\pm,0}$ appear as Nambu–Godstone bosons associated to the breaking of the chiral symmetry $\mathrm{SU}(2)_\mathrm{L} \times \mathrm{SU}(2)_\mathrm{R}/\mathrm{SU}(2)$, switching on some interactions that break explicitly the global symmetry will generate a mass to the would-be massless Nambu–Goldstone bosons of the order of $g\Lambda_{G/H}/(4\pi)$, where g is the coupling of the symmetry breaking interaction and $\Lambda_{G/H} = 4\pi f_{G/H}$ is the dynamical scale of the global symmetry breaking G/H. In the case of the Higgs boson, the top Yukawa interaction or the gauge interactions themselves will certainly break explicitly (part of) the global symmetry since they act non-linearly on the Higgs boson. Therefore, obtaining a Higgs mass around 100 GeV would demand a dynamical scale $\Lambda_{G/H}$ of the order of 1 TeV, which is known to lead to too large oblique corrections. Raising the strong dynamical scale by at least one order of magnitude requires an additional selection rule to ensure that a Higgs mass

is generated at the 2-loop level only

$$m_h^2 = \frac{g^2}{16\pi^2}\Lambda_{G/H}^2 \to m_h^2 = \frac{g_1^2 g_2^2}{(16\pi^2)^2}\Lambda_{G/H}^2$$

The way to enforce this selection rule is through a "collective breaking" of the global symmetry:

$$\mathcal{L} = \mathcal{L}_{G/H} + g_1\mathcal{L}_1 + g_2\mathcal{L}_2.$$

Each interaction $\mathcal{L}_1$ or $\mathcal{L}_2$ individually preserves a subset of the global symmetry such that the Higgs remains an exact Nambu–Goldstone boson whenever either g_1 or g_2 is vanishing. A mass term for the Higgs boson can be generated by diagrams involving simultaneously both interactions only. At one-loop, there is no such diagram that would be quadratically divergent. Explicitly, the cancellation of the SM quadratic divergences is achieved by a set of new particles around the Fermi scale: gauge bosons, vector-like quarks, and extra massive scalars, which are related, by the original global symmetry, to the SM particles with the same spin. Contrary to supersymmetry, the cancellation of the quadratic divergences is achieved by same-spin particles. These new particles, with definite couplings to SM particles as dictated by the global symmetries of the theory, are perfect goals for the LHC.

The simplest incarnation of the collective breaking idea, the so-called littlest Higgs model, is based on a non-linear σ-model describing the spontaneous breaking SU(5) down to SO(5). A subgroup $\mathrm{SU}(2)_1 \times \mathrm{U}(1)_1 \times \mathrm{SU}(2)_2 \times \mathrm{U}(1)_2$ is weakly gauged. This model contains a weak doublet, that is identified with the Higgs doublet, and a complex weak triplet whose mass is not protected by collective breaking. Other popular little Higgs models are the minimal moose, the simplest little Higgs, the bestest little Higgs.... For comprehensive reviews, see [395], [396].

Generically, oblique corrections in Little Higgs models are reduced either by increasing the coupling of one of the gauge group (in the case of product group models) or by increasing the mass of the W and Z partners, leading ultimately to a fine-tuning of the order of a few percents, i.e., improving only

marginally the situation of the MSSM (see for instance [397] and references therein). The compatibility of Little Higgs models with experimental data is significantly improved when the global symmetry involves a custodial symmetry as well as a T-parity [398] under which, in analogy with R-parity in SUSY models, the SM particles are even and their partners are odd. Such Little Higgs models would therefore appear in colliders as jet(s) with missing transverse energy [399] and the ATLAS and CMS searches for squarks and gluinos [400] can be recasted to obtain limits on the masses of the heavy vector-like quarks. The T-even top partner, with an expected mass below 1 TeV to cancel the top loop quadratic divergence without too much fine-tuning, would decay dominantly into a $t + Z$ pair or into a $b + W$ pair or even into $t + H$. The latest CMS and ATLAS direct searches [401] for vector-like top partner puts a lower bound around 700 GeV on their mas, excluding the most natural region of the parameter space of these models.

The motivation for Little Higgs models is to solve the little hierarchy problem, i.e., to push the need for new physics (responsible for the stability of the weak scale) up to around 10 TeV. Per se, Little Higgs models are effective theories valid up to their cutoff scale $\Lambda_{G/H}$. Their UV completions could either be weakly coupled or strongly coupled.

V.7.2. Models of partial compositeness

The Higgs boson is a special object. Even in composite models, it cannot appear as a regular resonance of the strong strong without endangering the viability of the setup when confronting to data. The way out is that the Higgs appears as a pseudo Nambu–Goldstone boson: the new strongly sector is supposed to be invariant under a global symmetry G spontaneously broken to a subgroup H at the scale f. To avoid conflict with EW precision measurements, it is better to avoid the strong interactions themselves to break the EW symmetry, hence the SM gauge symmetry itself should be contained in H, seeTable 14 for a few examples of coset spaces.

Table 14: Global symmetry breaking patterns and the corresponding Goldstone boson contents of the SM, the minimal composite Higgs model, the next to minimal composite Higgs model, the minimal composite two Higgs doublet model. Note that the SU(3) model does not have a custodial invariance. a denotes a CP-odd scalar while h and H are CP-even scalars.

Model	Symmetry Pattern	Goldstones
SM	SO(4)/SO(3)	W_L, Z_L
—	SU(3)/SU(2)×U(1)	W_L, Z_L, h
MCHM	SO(5)/SO(4)×U(1)	W_L, Z_L, h
NMCHM	SO(6)/SO(5)×U(1)	W_L, Z_L, h, a
MC2HM	SO(6)/SO(4)×SO(2) ×U(1)	$W_L, Z_L, h, H, H^{\pm}, a$

The SM (light) fermions and gauge bosons cannot be part of the strong sector itself since LEP data have already put stringent bounds on the compositeness scale of these particules far above the TeV scale. The gauge bosons couple to the strong sector by a weak gauging of an SU(2)×U(1) subgroup of the global symmetry G. Inspiration for the construction of such models comes from the AdS/CFT correspondence: the components of a gauge field along extra warped space dimension being interpretated as the Goldstone boson resulting from the breaking of global symmetry of the strong sector, seeFig. 31. The couplings of the SM fermions to the strong sector could a priori take two different forms: (i) a bilinear coupling of two SM fermions to a composite scalar operator of the form $\mathcal{L} = y\,\bar{q}_L u_R \mathcal{O} + \text{hc}$ in simple analogy with the SM Yukawa interactions. This is the way fermion masses were introduced in Technicolor theories and it generically comes with severe flavor problems and calls for extended model building gymnastic [402] to circumvent them; (ii) a linear mass mixing with fermionic vector-like operators: $\mathcal{L} = \lambda_L\,\bar{q}_L \mathcal{Q}_R + \lambda_R \bar{\mathcal{U}}_L u_R$. $\mathcal{Q}$ and $\mathcal{U}$ are two fermionic composite operators of mass M_Q and M_U. Being part of the compsite sector, they can have a direct coupling of generic order Y_* to the Higgs boson. In analogy with the photon-rho mixing in QCD, once the linear mixings are diagonalized, the physical states are a linear combination of elementary and

composite fields. Effective Yukawa couplings are generated and read for instance for the up-type quark

$$y = Y_* \sin\theta_L \sin\theta_R \tag{20}$$

where $\sin\theta_i = \lambda_i/\sqrt{M_U^2 + \lambda_i^2}$, $i = L, R$, measure the amount of compositeness of the SM left- and right-handed up-quark. If the strong sector is flavor-anarchic, i.e., if the couplings of the Higgs to the composite fermions does not exhibit any particular flavor structure, the relation Eq. (20) implies that the light fermions are mostly elementary states ($\sin\theta_i \ll 1$), while the third generation quarks need to have a sizable degree of compositeness. The partial compositeness mechanism offers an appealing dynamical explanation of the hierarchies in the fermion masses. In fact, assuming the strong sector to be almost conformal above the confinement scale, the low-energy values of the mass-mixing parameters $\lambda_{L,R}$ are determined by the (constant) anomalous dimension of the composite operator they mix with. If the UV scale at which the linear mixings are generated is large, then $\mathcal{O}(1)$ differences in the anomalous dimensions can generate naturally large hierarchies in the fermion masses via RG running [403]. While the introduction of partial compositeness greatly ameliorated the flavor problem of the original composite Higgs models, nevertheless it did not solve the issue completely, at least in the case where the strong sector is assumed to be flavor-anarchic [404].

Another nice aspect of the partial compositeness sctuture is the dynamical generation of the Higgs potential. The Higgs being a pseudo-Nambu–Goldstone boson, its mass does not receive any contribution from the strong sector itself but it is generated at the one-loop level via the couplings of the SM particles to the strong sector since these interactions are breaking the global symmetries under which the Higgs doublet transforms non-linearly. The leading contribution to the potential arises from top loops and it take the form:

$$V(H) = m_\rho^4 \frac{\sin\theta_{tL}\sin\theta_{tR}}{16\pi^2}\left(\alpha\cos(H/f) + \beta\sin^2(H/f) + \gamma\sin^4(H/f)\right), \tag{21}$$

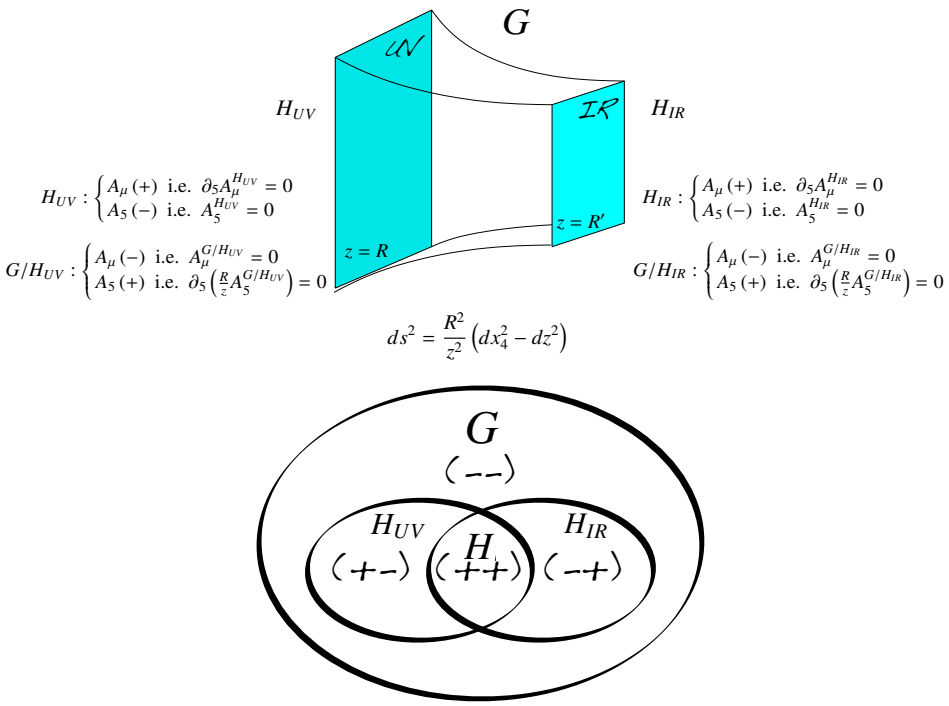

Figure 31: Composite models built in five dimensional Anti-de-Sitter space-time and their symmetry breaking pattern interpretation. In 5D, the gauge symmetry in the bulk, G, is broken by suitable boundary conditions to H_{UV} on the UV brane and to H_{IR} on the IR brane. The low energy theory mimics in 4D a strongly interacting sector invariant under a global symmetry G spontaneously broken to H_{IR} at the IR scale with a subgroup H_{UV} which is weakly gauged. The number of Goldstone bosons is equal to $\dim(G/H_{IR})$, $\dim(H_{UV}/H)$ being eaten to give a mass to some gauge bosons ($H = H_{UV} \cap H_{IR}$). The remaining $\dim(G/H_{IR}) - \dim(H_{UV}/H)$ massless Goldstones are described on the 5D side by the massless A_5^H modes.

where α, β, γ are numbers of order 1 subject to selection rules following the transformation properties of the top quark under the global symmetries of the strong sector[1], and $m_\rho \approx g_\rho f$ is the typical mass scale of the strong sector resonances. The

[1] For instance in the SO(5)/SO(4) composite models, when the top quark is embedded into a spinorial representation of SO(5), then $\gamma = 0$ and when it is part of a **5**, **10** or **14** representation, $\alpha = 0$ as it can be inferred by looking at the structure of the H-dependent invariants built out of these

gauge contribution to the potential takes the form (g denotes the SU(2) gauge coupling)

$$m_\rho^4 \frac{g^2/g_\rho^2}{16\pi^2} \sin^2 (H/f) \,,$$

which is parametrically suppressed with respect to the top contribution by $g^2/(g_\rho y_t)$. The gauge term is always positive, and cannot trigger EWSB by itself. When $\alpha = 0$ as in the models favored by current data, the minimization condition of the potential simply reads

$$\sin^2 \frac{\langle H \rangle}{f} = -\frac{\beta}{2\gamma}$$

which implies that the natural expectation is the scale f is generically of the order of the weak scale. Obtaining $v \ll f$, as required phenomenologically, requires some degree of tuning, which scales like $\xi \equiv v^2/f^2$. A mild tuning of the order of 10% ($\xi \approx 0.1$) is typically enough to comply with electroweak precision constraints. This is an important point: in the partial compositeness models , the entire Higgs potential is generated at one loop, therefore the separation between v and f can only be obtained at a price of a tuning. This marks a difference with respect to the Little Higgses models, which realize a parametric hierarchy between the quartic and mass through the collective symmetry breaking mechanism. In fact in Little Higgs models, the quartic is a tree-level effect, leading to a potential

$$V(H) \approx \frac{g_{\rm SM}^2}{16\pi^2} m_\rho^2 H^2 + g_{\rm SM}^2 H^4$$

where $g_{\rm SM}$ generically denotes the SM couplings. The minimization condition now reads $v^2/f^2 \sim g_\rho^2/(16\pi^2)$, therefore v is formally loop suppressed with respect to f. This is the major achievement of the Little Higgs constructions, which however comes at the price of the presence of sub-TeV vectors carrying EW quantum numbers and therefore giving rise generically to large oblique corrections to the propagators of the W and the Z gauge bosons.

representations [412]. The coefficient γ also generically comes with extra power of the top compositeness fractions.

After minimization, the potential Eq. (21) leads to an estimate of the Higgs mass as

$$m_H^2 \approx g_\rho^3\, y_t 2\pi^2 v^2.$$

It follows that the limit $f \to \infty$, i.e. $\xi \to 0$, is a true decoupling limit: all the resonances of the strong sector become heavy but the Higgs whose mass is protected by the symmetries of the coset G/H. When compared to the experimentally measured Higgs mass, this estimate puts an upper bound on the strength of the strong interactions: $1 \lesssim g_\rho \lesssim 2$. In this limit of not so large coupling, the Higgs potential receives additional contributions. In particular, the fermionic resonances in the top sector which follow from the global symmetry structure of the new physics sector can help raising the Higgs mass. For instance in the minmal SO(5)/SO(4) model, using some dispersion relation technics, one obtains [406]

$$m_H^2 \approx \frac{6}{\pi^2}\frac{m_t^2}{f^2}\frac{m_{Q_4}^2 m_{Q_1}^2}{m_{Q_1}^2 - m_{Q_4}^2}\log\left(\frac{m_{Q_1}}{m_{Q_4}}\right)$$

where Q_4 and Q_1 are fermionic color resonances transforming as a weak bidoublet of hypercharge $Y = 1/6$ and $Y = 7/6$ and a weak signlet with hyperchare $Y = -1/3$. Therefore a 125 GeV mass is obtained if at least one of the fermionic resonance is light than $\sim 1.4f$ GeV. As in supserymmetric scenarios, the top sector is playing a crucial role in the dynamics of EWSB and can provide the first direct signs of new physics. The direct searches for these top partners, in particular the ones with exotic electric charges 5/3, are already exploring the natural parameter spaces of these models [407,408,401].

The main physics properties of a pseudo Nambu–Goldstone Higgs boson can be captured in a model-independent way by a few number of higher-dimensional operators. Indeed, the strong dynamics at the origin of the composite Higgs singles out a few operators among the complete list presented ealier in Section IV: these are the operators that involve extra powers of the Higgs doublets and they are therefore generically suppressed by a factor $1/f^2$ as opposed to the operators that involve extra derivatives or gauge bosons and are suppressed by a

factor $1/(g_\rho^2 f^2)$. The relevant effective Lagrangian describing a strongly interactint light Higgs is:

$$\mathcal{L}_{\rm SILH} = \frac{c_H}{2f^2}\left(\partial_\mu\left(H^\dagger H\right)\right)^2 + \frac{c_T}{2f^2}\left(H^\dagger\left(D_\mu H\right) - \left(D_\mu H\right)^\dagger H\right)^2 - \frac{c_6\lambda}{f^2}\left(H^\dagger H\right)^3 + \left(\sum_f \frac{c_f\, y_f}{f^2} H^\dagger H \bar{f}_L H f_R + \text{h.c.}\right) . \tag{22}$$

Typically, these new interactions induce devitations in the Higgs couplings that scale like $\mathcal{O}(v^2/f^2)$, hence the measurements of the Higgs couplings can be translated into some constraints on the compositeness scale, $4\pi f$, of the Higgs boson. The peculiarity of these composite models is that, due to the Goldstone nature of the Higgs boson, the direct couplings to photons and gluons are futher suppressed and generically the coupling modifiers defined in Section IV scale like

$$\kappa_{W,Z,f} \sim 1 + \mathcal{O}\left(\frac{v^2}{f^2}\right) ,$$
$$\kappa_{Z\gamma} \sim \mathcal{O}\left(\frac{v^2}{f^2}\right) ,$$
$$\kappa_{\gamma,g} \sim \mathcal{O}\left(\frac{v^2}{f^2}\times\frac{y_t^2}{g_*^2}\right) ,$$

where we denoted by g_* the typical coupling strength among the states of the strongly coupled sector and y_t is the top Yukawa coupling, the largest interaction that breaks the Goldstone symmetry. The coupling modifiers also receive additional contributions from the other resonances of the strong sector, in particular the fermionic resonances of the top sector that are required to be light to generate a 125 GeV Higgs mass. Some indirect information on the resonance spectrum could thus be inferred by a precise measurement of the Higgs coupling deviations. However, it was realized [409] that the task is actually complicated by the fact that these top partners give a contribution to both κ_t (resulting from a modification of the top Yukawa coupling) and κ_γ and κ_g (resulting from new heavy particles running into the loops) and the structure of interactions are such that the net effect vanishes for inclusive quantities like $\sigma(gg \to h)$ or $\Gamma(h \to \gamma\gamma)$ as a consequence of

the Higgs low energy theorem. So one would need to rely on differential distribution, like the Higgs p_T distribution, to *see* the top partner effects in Higgs data [410].

V.7.3. Minimal composite Higgs models

The minimal composite Higgs models (MCHM) are concrete examples of the partial compositeness paradigm. The Higgs doublet is described by the coset space SO(5)/SO(4) where a subgroup $\mathrm{SU}(2)_L\times\ \mathrm{U}(1)_Y$ is weakly gauged under which the four Goldstone bosons transform as a doublet of hypercharge 1. There is some freedom on how the global symmetry is acting on the SM fermions: in MCHM4 [412] the quarks and leptons are embedeed into spinorial representations of SO(5), while in MHCM5 [411] they are part of fundamental representations (it might also be interesting phenomenologically to consider larger representations like MCHM14 [413] with SM inside a representation of dimension 14). The non-linearly realized symmetry acting on the Goldstone bosons leads to general predictions of the coupling of the Higgs boson to the EW gauge bosons. For instance, it can be shown that the quadratic terms in the W and W bosons read

$$m_W^2\,(h)\left(W_\mu W^\mu+\frac{1}{2\cos^2\theta_W}Z_\mu Z^\mu\right)$$

with $m_W(h)=\dfrac{gf}{2}\sin\dfrac{h}{f}$. Expanding around the EW vacuum, we obtain the expression of the weak scale

$$v=f\sin\left(\langle h\rangle/f\right),$$

and the values of the modified Higgs couplings to the W and Z:

$$g_{HVV}=\frac{2m_V^2}{v}\sqrt{1-v^2/f^2}\,,\quad g_{HHVV}=\frac{2m_V^2}{v^2}\left(1-2v^2/f^2\right)\,.$$

The Higgs couplings to the fermions depend on the representation in which the SM fermions are embedded into. For the most commonly used embeddings, they take the following forms

$$\begin{aligned}\text{MCHM4}:\ g_{Hff}&=\frac{m_f}{v}\sqrt{1-v^2/f^2}\,,\\ \text{MCHM5}:\ g_{Hff}&=\frac{m_f}{v}\frac{1-2v^2/f^2}{\sqrt{1-v^2/f^2}}\,,\\ \text{MCHM14}:\ g_{Hff}&=\frac{m_f}{v}\sqrt{1-v^2/f^2}\,.\end{aligned}$$

The (κ_V, κ_f) experimental fit of the Higgs couplings can thus be used to derive a lower bound on the Higgs compositeness $4\pi f \gtrsim 9$ TeV, which is less stringent than the indirect bound obtained from EW precision data, $4\pi f \gtrsim 15$ TeV [414], which is however subject to various assumptions [415].

V.8. Searches for signatures of extended Higgs sectors

The couplings of H^0 to vector bosons are compatible with those of the Standard Model Higgs boson to within approximately ∼20%. The couplings of the newly observed state to fermions have been established only indirectly under the assumption of the gluon fusion production mode (with dominant contribution from the top quark loop) and have been only possibly seen in the $H \to \tau^+\tau^-$ channel at the LHC and $H \to b\overline{b}$ channels at the Tevatron and the LHC. These measurements described in Sections references have established the existence of one state of the electroweak symmetry breaking sector, but not that it is the only one.

Various classes of models beyond the Standard Model discussed in Sections reference require extended Higgs sectors. These models, and in particular the MSSM and the NMSSM serve as guiding principle of the experimental searches for additional scalar states beyond the Standard Model. However these searches are made as model independent as possible and can be summarized in the following classes: (i) the search for an additionnal CP-even state motly in the high mass domain decaying to vector bosons, which would correspond to the heavy CP-even state in a generic 2HDM where the light state would be the discovered H^0 or a generic additional singlet; (ii) the search for a CP-odd state in the high mass domain decaying to pairs of fermions, which would correspond to the CP-odd state A in a generic 2HDM; (iii) the search for charged Higgs bosons, which also appear in generic 2HDMs; (iv) the search for a CP-odd state a in the low mass region which appears in the NMSSM; and (v) doubly charged Higgs which are motivated in extensions of the Higgs sector with triplets.

(i) Searches for an additional CP-even state

(a) Exclusion limits from LEP

The negative result of LEP searches for the SM Higgs boson and the absolute lower limit on its mass of 114 GeV strongly disfavors the existence of a lower mass CP-even state, but does not exclude it if its couplings are reduced enough with respect to those of the SM Higgs boson. Among the MSSM new benchmarks, the low-m_H is one example which is disfavored by current direct constraints. The light CP-even Higgs boson of the NMSSM with a strong singlet component is antother example. Additional motivation for these scenarions is given by the slight excess observed at LEP [LEP excess] at a Higgs boson mass hypothesis of approximately 100 GeV. The light CP-even Higgs boson h was also searched for in association with the CP-odd A, these searches are described in Section reference.

(b) Searches at Tevatron and at the LHC

The searches for the Standard Model Higgs boson before the discovery were covering a wide range of mass hypotheses, at LHC until recently the range of investigation was from 100 GeV and 600 GeV. It has been extended to mass of up to 1 TeV. At the Tevatron this mass range was limited to up to 200 GeV. Masses lower than 114 GeV are strongly excluded by LEP limits. Since the discovery the SM HIggs boson searches are reappraised to search for a heavy CP-even state. This state could be the heavy CP-even Higgs boson of a 2HDM, or a generic additional singlet. In both cases the natural width of the additional H state can be very different from that of the SM Higgs boson. To preserve unitarity of the longitudinal vector boson scattering and the longitudinal vector boson scattering into fermion pairs, the couplings of the additionnal CP-even Higgs boson to gauge bosons and fermions should not be too large and should constrain the natural width to be smaller than that of the unique SM Higgs boson at high mass (provided that trilinear and quartic couplings are reasonable and that no new state affects the heavy state total width). It is therefore reasonable to consider total widths for the high mass CP-even state smaller than the equivalent SM width. For the sake of generality these searches should be done as a function of Higgs boson mass and total width. Until recently only two cases have

been investigated: (i) the SM width using the complex pole scheme (CPS), and (ii) the narrow width approximation.

One example of searches for high mass CP-even Higgs bosons decaying to a pair of gauge bosons in the narrow width approximation in the $H \to W^{(*)}W^{(*)} \to \ell\nu\ell\nu$ inclusive search channel by the ATLAS collaboration is given in Figure [**HighMassCPeven**]. The searches for the Higgs boson in the $H \to \gamma\gamma$ and $H \to W^{(*)}W^{(*)}$ in the $\ell\nu\ell\nu$ and $\ell\nu q\overline{q}$ channels and the $H \to Z^{(*)}Z^{(*)}$ searches in the 4ℓ, $\ell\ell q\overline{q}$ and $\ell\ell\nu\nu$ channels have also been done, but in most cases are simple reinterpretations of the SM Higgs search in the CPS scheme. Recent references are summarized in Table [**BSMsummary**].

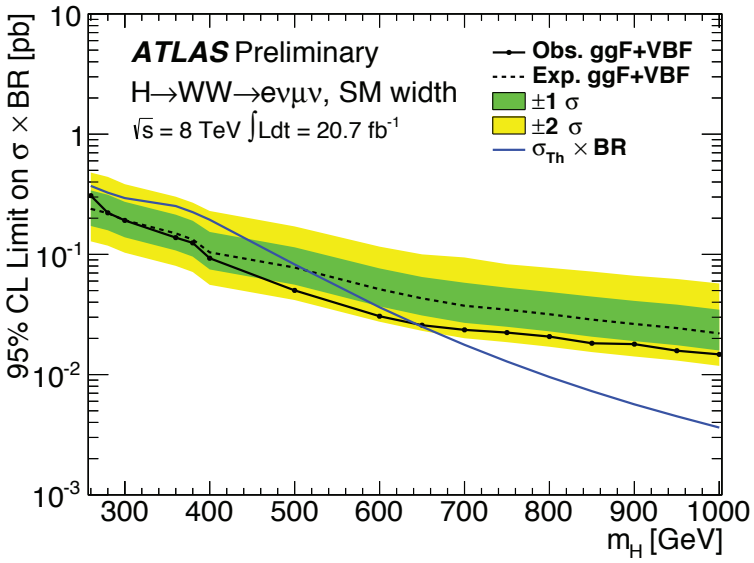

Figure 32: The 95% C.L.exclusion contours for. See full-color version on color pages at end of book.

(c) Searches for an additional state with the presence of H^0

In the post discovery era, analyses in general need to take into account the presence of the newly discovered state. For searches with sufficently high resolution of additionnal states non degenerate in mass, the strength of the observed state and limits on the signal strength of a potential additional state can

be set independetly as discussed in the next section. However in some cases, such as when a channel does not have a sufficiently high mass resolution or when the states are nearly degenerate in mass, specifc analyses need to be designed. There are two examples of such analyses: (i) the search for an additionnal state in the $H \to W^{(*)}W^{(*)} \to \ell\nu\ell\nu$ channel in ATLAS and (ii) the search for nearly degenerate states in the $H \to \gamma\gamma$ channel with the CMS detector.

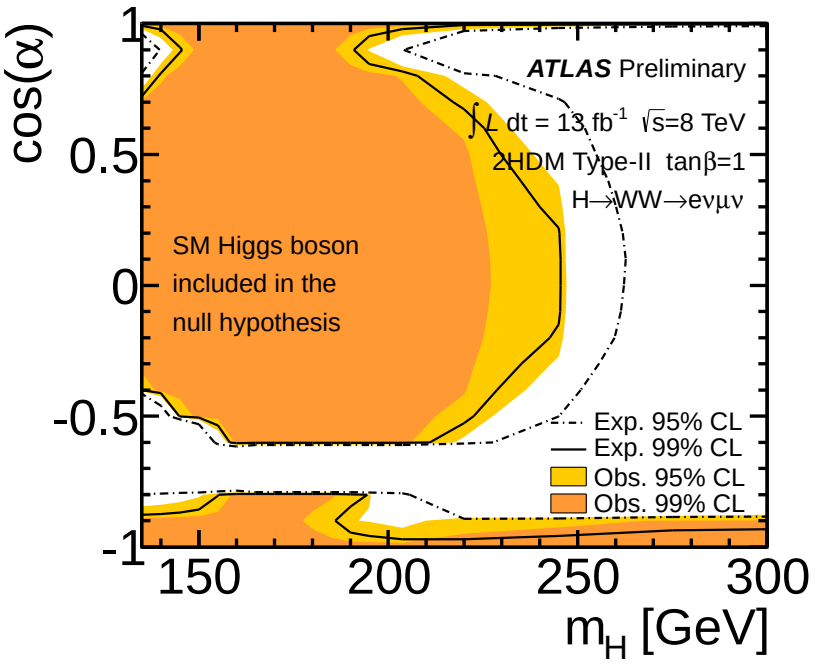

Figure 33: The 95% C.L.exclusion contours for. See full-color version on color pages at end of book.

The search for an additionnal state in the $H \to W^{(*)}W^{(*)} \to \ell\nu\ell\nu$ is done using boosted decision tree combining several discriminating kinematic characteristics to optimally separate the signal from the background and a high mass signal H from the lower mass state h [**2HDM-ATLAS-Ref**]. A simultaneous fit of the two states h and H is then made to test the presence of an

additionnal state. In this case the usual null hypothesis of background, is generated including a SM signal. The results of this search are shown in Figure [**2HDM-ATLAS**].

The CMS search for nearly degenerate mass states decaying to a pair of photons [**CMS-gamgam-degenerate**] is more generic and could for instance apply to CP-odd Higgs bosons as well. It consists in a fit to the diphoton mass spectrum using two nearly degenerate mass templates.

(d) Interpretation benchmarks in the light of the discovered Higgs boson

Two specific benchmark scenarios driven by unitarity relations are proposed in Ref. YR3. Assuming the existence of an aditionnal state h' with coupling scale factors (as deviations from the SM Higgs boson couplings) denoted κ'_V and κ'_F for the couplings of h' to vector bosons and fermions respectively. The gauge boson scattering unitarity then yields the following sum rule:

$$\kappa_V^2 + \kappa_V'^2 = 1$$

and the unitarization of the gauge boson scattering to fermions yields:

$$\kappa_V \kappa_F + \kappa'_V * \kappa'_F = 1$$

The two benchmark scenarios are then defined as follows: (i) a single couplings scale factor is assumed for the gauge bosons and the fermions, with an additionnal parameter to take into account decays to new states; (ii) two parameters are used to describe independently the couplings to fermions and the couplings to vector bosons. A direct application of the latter is CP-even sector of the type-I 2HDM.

(ii) Searches for an additional high mass CP-odd state

(a) Exclusion limits from LEP

In e^+e^- collisions at LEP centre-of-mass energies, the main production mechanisms of the neutral MSSM Higgs bosons are the Higgs-strahlung processes $e^+e^- \to h\mathrm{Z}$, $H\mathrm{Z}$ and the pair production processes $e^+e^- \to hA$, HA, while the fusion

processes play a marginal role. Higgs boson decays to $b\bar{b}$ and $\tau^+\tau^-$ are used in these searches.

The searches and limits from the four LEP experiments are described in Refs. [232–235]. The combined LEP data did not contain any excess of events which would imply the production of a Higgs boson, and combined limits were derived [**mssm-2006**]. For $m_A \gg M_Z$ the limit on m_h is nearly that of the SM searches, as $\sin^2(\beta-\alpha) \approx 1$. For high values of $\tan\beta$ and low m_A ($m_A \leq m_h^{max}$) the $e^+e^- \to hA$ searches become the most important, and the lightest Higgs h is non SM-like. In this region, the 95% C.L. mass bounds are $m_h > 92.8$ GeV and $m_A > 93.4$ GeV. In the m_h-max. scenario, values of $\tan\beta$ from 0.7 to 2.0 are excluded taking $m_t = 174.3$ GeV, while a much larger $\tan\beta$ region is excluded for other benchmark scenarios such as the no-mixing one.

Neutral Higgs bosons may also be produced by Yukawa processes $e^+e^- \to f\overline{f}\phi$, where the Higgs particle $\phi \equiv h$, H, A, is radiated off a massive fermion ($f \equiv b$ or $\tau^\pm$). These processes can be dominant at low masses, and whenever the $e^+e^- \to h$Z and hA processes are suppressed. The corresponding ratios of the $f\overline{f}h$ and $f\overline{f}A$ couplings to the SM coupling are $\sin\alpha/\cos\beta$ and $\tan\beta$, respectively. The LEP data have been used to search for $b\overline{b}\,b\overline{b}$, $b\overline{b}\tau^+\tau^-$, and $\tau^+\tau^-\,\tau^+\tau^-$ final states [236,237]. Regions of low mass and high enhancement factors are excluded by these searches.

Searches at the TeVatron and LHC

The best sensitivity is in the regime with low to moderate m_A and with large $\tan\beta$ which enhances the couplings of the Higgs bosons to down-type fermions. The corresponding limits on the Higgs boson production cross section times the branching ratio of the Higgs boson into down-type fermions can be interpreted in MSSM benchmark scenarios [238]. If $\phi = A, H$ for $m_A > m_h^{\max}$, and $\phi = A, h$ for $m_A < m_h^{\max}$, the most promising channels at the Tevatron are $b\bar{b}\phi, \phi \to b\overline{b}$ or $\phi \to \tau^+\tau^-$, with three tagged b-jets or $b\tau\tau$ in the final state, respectively, and the inclusive $p\overline{p} \to \phi \to \tau^+\tau^-$ process, with contributions from both $gg \to \phi$ and $b\bar{b}\phi$ production. Although

Higgs boson production via gluon fusion has a higher cross section than via associated production, it cannot be used to study the $\phi \to b\overline{b}$ decay mode since the signal is overwhelmed by QCD background.

The CDF and DØ collaborations have searched for neutral Higgs bosons produced in association with bottom quarks and which decay into $b\overline{b}$ [239,240], or into $\tau^+\tau^-$ [241,242]. The most recent searches in the $b\overline{b}\phi$ channel with $\phi \to b\overline{b}$ analyze approximately 2.6 fb^{-1} of data (CDF) and 5.2 fb^{-1} (DØ), seeking events with at least three b-tagged jets. The cross section is defined such that at least one b quark not from ϕ decay is required to have $p_T > 20$ GeV and $|\eta| < 5$. The decay widths of the Higgs bosons are assumed to be much smaller than the experimental resolution. The invariant mass of the two leading jets as well as b-tagging variables are used to discriminate the signal from the backgrounds. The QCD background rates and shapes are inferred from data control samples, in particular, the sample with two b tagged jets and a third, untagged jet. Separate signal hypotheses are tested and limits are placed on $\sigma(p\overline{p} \to b\overline{b}\phi) \times \mathrm{BR}(\phi \to b\bar{b})$. a local excess of approximately 2.5σ significance in the mass range of 130-160 GeV, but DØ's search is more sensitive and sets stronger limits. The DØ result shown in Fig. **@Fg.tevmssmxsbr@** displays a ≈ 2 sigma local upward fluctuation in the 110 to 125 GeV mass range.

CDF and DØ have also performed searches for inclusive production of Higgs bosons with subsequent decays to $\tau^+\tau^-$ [243,244,245], although these limits have been superseded by the LHC searches.

The bounds from the $b\overline{b}\phi, \phi \to b\overline{b}$ channel depend strongly on the radiative corrections affecting the relation between the bottom quark mass and the bottom Yukawa coupling. In the channels with $\tau^+\tau^-$ final states, however, compensations occur between large corrections in the Higgs boson production and decay. The total production rates of bottom quarks and τ pairs mediated by the production of a CP-odd Higgs boson in the

large $\tan\beta$ regime are approximately given by

$$\sigma_{b\bar{b}A} \times \mathrm{BR}\left(A \to b\bar{b}\right) \simeq \sigma^{\mathrm{SM}}_{b\bar{b}A} \;\; \frac{\tan^2\beta}{(1+\Delta_b)^2} \frac{9}{(1+\Delta_b)^2+9}\,,$$

and

$$\sigma_{gg\to A,b\bar{b}A} \times \mathrm{BR}\left(A \to \tau^+\tau^-\right) \simeq \sigma^{\mathrm{SM}}_{gg\to A,b\bar{b}A} \;\; \frac{\tan^2\beta}{(1+\Delta_b)^2+9}\,,$$

where $\sigma^{\mathrm{SM}}_{b\bar{b}A}$ and $\sigma^{\mathrm{SM}}_{gg\to A,b\bar{b}A}$ denote the values of the corresponding SM Higgs boson cross sections for a SM Higgs boson mass equal to m_A. The function Δ_b includes the dominant effects of SUSY radiative corrections for large $\tan\beta$ [142,147,200,201], and it depends strongly on $\tan\beta$ and on the SUSY mass parameters. The $b\bar{b}A$ channel is more sensitive to the value of Δ_b through the factor $1/(1+\Delta_b)^2$ than the inclusive $\tau^+\tau^-$ channel, for which this leading dependence on Δ_b cancels out. As a consequence, the limits derived from the inclusive $\tau^+\tau^-$ channel depend less on the precise MSSM scenario chosen than those of the $b\bar{b}A$ channel.

The production and decay rates of the CP-even Higgs bosons with $\tan\beta$-enhanced couplings to down-type fermions—H (or h) for m_A larger (or smaller) than m_h^{max}, respectively—are governed by formulas similar to the ones presented above. At high $\tan\beta$, one of the CP-even Higgs bosons and the CP-odd Higgs boson are nearly degenerate in mass, enhancing the signal cross section by roughly a factor of two, without complicating the experimental signature except in a small mass region in which the three neutral MSSM Higgs boson masses are close together and each boson contributes to the total production rate. Detailed discussions of the impact of radiative corrections in these search modes are presented in Refs. [238] and [246].

ATLAS and CMS also search for $\phi \to \tau^+\tau^-$ in pp collisions at $\sqrt{s} = 7$ TeV. ATLAS seeks tau pairs in 1.06 fb^{-1} of data [247,248], and CMS's search uses 4.6 fb^{-1} of data [**cms-tautau-pub**,**cms-taumutaumu-prel**]. The searches are performed in categories of the decays of the two tau leptons: $e\tau_{\mathrm{had}}$, $\mu\tau_{\mathrm{had}}$, $e\mu$, and $\mu\mu$, where τ_{had} denotes a tau lepton which decays to one or more hadrons plus a tau neutrino, e denotes $\tau \to e\nu\nu$,

and μ denotes $\tau \to \mu\nu\nu$. The dominant background comes from $Z \to \tau^+\tau^-$ decays, although $t\bar{t}$, W+jets and Z+jets events contribute as well. Separating events into categories based on the number of b-tagged jets improves the sensitivity in the MSSM. The $b\bar{b}$ annihilation process and radiation of a Higgs boson from a b quark give rise to events in which the Higgs boson is accompanied by a $b\bar{b}$ pair in the final state, sometimes with only one b within the detector acceptance. Requiring the presence of one or more b jets reduces the background from Z+jets. Data control samples are used to constrain background rates. The rates for jets to be identified as a hadronically decaying tau lepton are measured in dijet samples, and W+jets samples provide a measurement of the rate of events that, with a fake hadronic tau, can pass the signal selection requirements. Lepton fake rates are measured using samples of unisolated lepton candidates and same-sign lepton candidates. Constraints from ATLAS's and CMS's searches for $h \to \tau^+\tau^-$ are also shown in Fig. **@Fg.world-mssm@** in the m_h-max benchmark scenario, with $\mu = 200$ GeV. The neutral Higgs boson searches consider the contributions of both the CP-odd and CP-even neutral Higgs bosons with enhanced couplings to bottom quarks, as they were for the Tevatron results. As explained above, the di-tau inclusive search limits do not significantly change by considering other benchmark scenarios.

Due to the dependence of this production and decay mode on the SUSY radiative corrections there is complementarity between the $3b$ channel and the inclusive tau pair channel in exploring the supersymmetric parameter space.

The LHC has the potential to explore a broad range of SUSY parameter space through the search for non-SM-like Higgs bosons. Nevertheless, Fig. **@Fg.world-mssm@** shows a broad region with intermediate $\tan\beta$ and large values of m_A that is not tested by present neutral or charged Higgs boson searches, and which might be difficult to cover completely via these searches, even with much larger data sets. In this region of parameter space it is possible that only the SM-like Higgs boson can be within the LHC's reach. If a SM-like Higgs boson

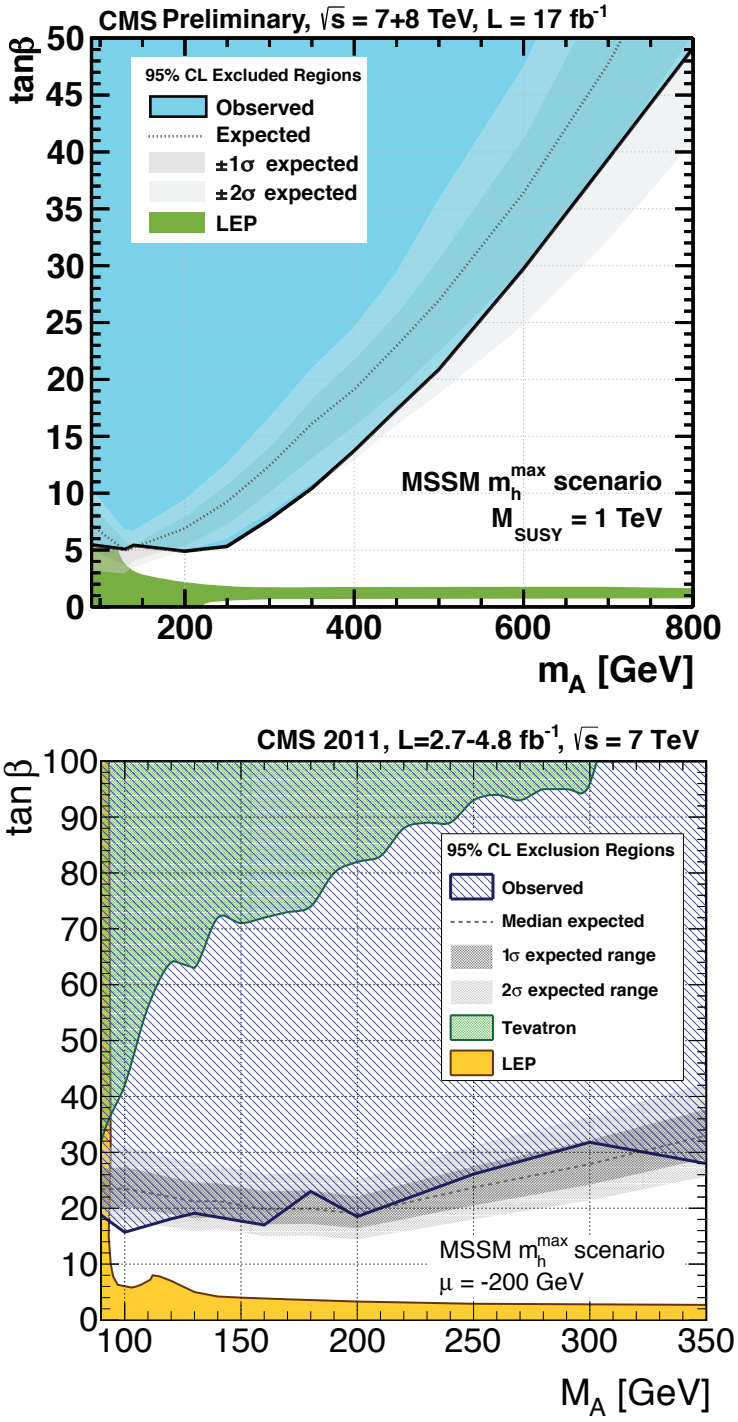

Figure 34: The 95% C.L.exclusion contours for. See full-color version on color pages at end of book.

is discovered, it may be challenging to determine only from the

Higgs sector whether there is a supersymmetric extension of the SM in nature.

(iii) Searches for Charged Higgs bosons $H^{\pm}$

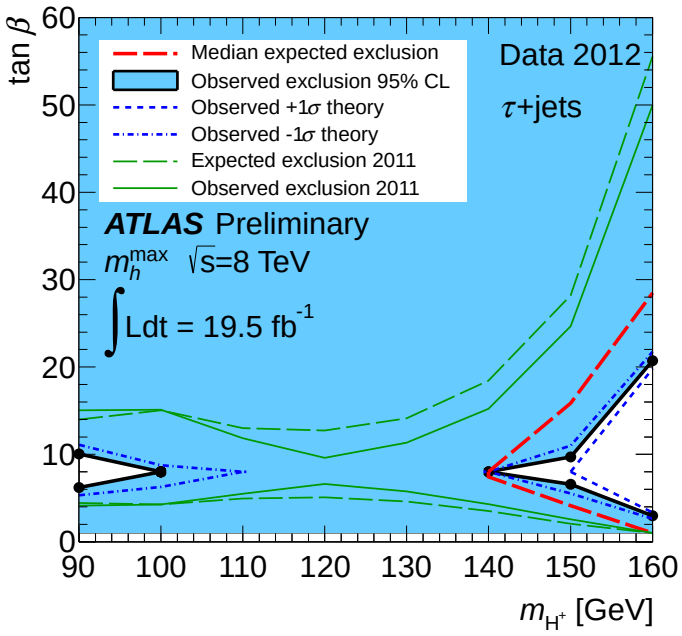

Figure 35: The 95% C.L.exclusion contours for. See full-color version on color pages at end of book.

The searches for charged Higgs bosons at the LHC have been made until recently in two channels,

(iv) Searches for the light CP-odd Higgs boson in the NMSSM a

The trilinear Higgs self coupling contributes to Higgs pair production which allows, in principle, its measurement. Many corresponding studies have been performed in the SM and its supersymmetric (Susy) extensions, notably at hadron colliders and considering gluon fusion [330], the production mode with the largest cross section.

Among the Susy extensions of the SM, the Next-to-Minimal Supersymmetric Standard Model (NMSSM) [31] has received considerable attention [3254], since a Higgs mass of 125 GeV is more natural within its parameter space than in the MSSM. Due to the ad- ditional gauge singlet superfield S compared to

the MSSM, the NMSSM contains CP-even Higgs states Hi, i = 1, 2, 3 (ordered in m

It is quite natural in the para of the NMSSM that the mostly SM-like state HSM is actually the second lightest state H2, wheras th te H1 is mostly singlet-like; then mixing effects cor increase of the mass of HSM. A lighter mostly sin H1 can well be compatible with the constraints fr (simultaneously with a SM-like state near 125 GeV ght even explain the mild (2) excess in e+e Zb b r 0 GeV [55].

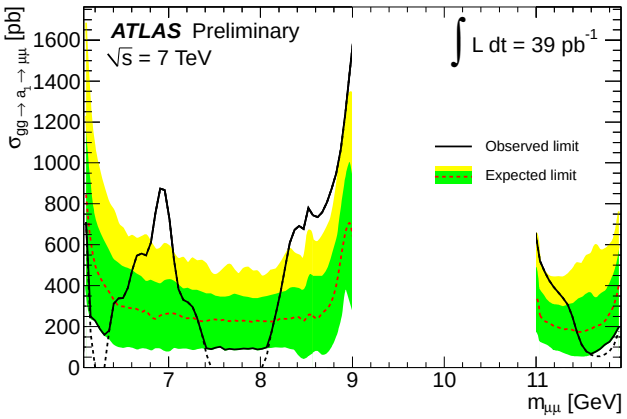

Figure 36: The 95% C.L.exclusion contours for. See full-color version on color pages at end of book.

(v) Searches for doubly charged Higgs bosons $H^{\pm\pm}$

The generation of small neutrino masses via the standard BEH mechanism described in Section II, requires unnaturally small Yukawa couplings, provided that neutrinos are Dirac-type fermions. A Majorana mass term with a see-saw mechanism for neutrinos, would allow for naturally small masses and yield a framework for the appealing scenario of leptogensis. However within the SM Majorana mass terms correspond to (non-renomalizable) dimension-5 operators. Such effective interactions can be generated via renormalizable interactions with an electroweak triplet of complex scalar fields (corresponding to

Table 15: Invisible and rare decay channels

	ATLAS	CMS	Other experiments
CP-even H			
$h, H \to \gamma\gamma$	–	[CMS-gamgam-degenerate]	–
$h, H \to ZZ \to 4\ell$	[1]	[2]	–
$h, H \to ZZ \to \ell\ell\nu\nu$	[1]	[2]	–
$h, H \to ZZ \to \ell\ell q\overline{q}$	–	[2]	[3] TEV/LEP
$h, H \to WW \to \ell\nu\ell\nu$	[1]	[2]	–
$h, H \to WW \to \ell\nu q\overline{q'}$	–	[2]	[3] TEV/LEP
CP-odd A			
$h, H, A \to \tau^+\tau^-$	[1]	[2]	–
$h, H, A \to \mu^+\mu^-$	[1]	[2]	–
$h, H, A \to b\overline{b}$	–	[2]	[3] TEV/LEP
Charged $H^\pm$			
$H^{\pm\pm}$	[1]	[2]	[3]
$H^\pm \to \tau^\pm\nu$	[1]	[2]	[3] TEV/LEP
$H^\pm \to cs$	[1]	[2]	[3] Tevatron/LEP
CP-odd NMSSM a			
$a \to \mu^+\mu^-$	[1]	[2]	–
$h \to aa \to 4\mu, 4\tau, 4\gamma$	[1]	[2]	[3]
$\Upsilon_{1s,3s} \to a\gamma$	–	–	[3] BaBar, Belle, LHCb
Doubly Charged $H^\pm$			

a type-II see-saw mechansim). Other models such as the Zee–Babu model, with the introduction of two $SU(2)_L$ singlets, also generate Majorana mass terms. The signature of such models would be the presence of doubly charged Higgs bosons $H^{\pm\pm}$.

The main production mechanisms of $H^{\pm\pm}$ bosons at hadron colliders are the pair production in the s-channel through the exchange of a Z boson or a photon and the associated production with a Charged Higgs boson through the exchange of a W boson.

(vi) Summary of the most recent searches for signatures of extended Higgs sector

(vi) Outlook of searches for additional states

Although the LHC program of searches for additionnal states covers a large variety of decay channels for additionnal

states, various important topologies are still not covered. In particular when searching for additionnal states the decays of heavy additionnal searches such as those of the neutral states decaying to a pair of H^0H^0 or to ZH^0, and searches for the $t\bar{t}$ decays are important. Similarly the search for charged Higgs bosons can be extended to include the search for H^0W and cover the high mass region with $t\bar{b}$ decays.

VI. Summary

The summary will be added at a later stage

VII. Outlook

The outlook will be added at a later stage

1. ATLAS Collab. Phys. Lett. **B716**, 1 (2012).
2. CMS Collab., Phys. Lett. **B716**, 30 (2012).
3. P.W. Higgs, Phys. Rev. Lett. **13**, 508 (1964);
   idem, Phys. Rev. **145**, 1156 (1966);
   F. Englert and R. Brout, Phys. Rev. Lett. **13**, 321 (1964);
   G.S. Guralnik, C.R. Hagen, and T.W. Kibble, Phys. Rev. Lett. **13**, 585 (1964).
4. S.L. Glashow, Nucl. Phys. **20**, 579 (1961);
   S. Weinberg, Phys. Rev. Lett. **19**, 1264 (1967);
   A. Salam, *Elementary Particle Theory*, eds.: Svartholm, Almquist, and Wiksells, Stockholm, 1968;
   S. Glashow, J. Iliopoulos, and L. Maiani, Phys. Rev. **D2**, 1285 (1970).
5. J.M. Cornwall, D.N. Levin, and G. Tiktopoulos, Phys. Rev. Lett. **30**, 1286 (1973); Phys. Rev. **D10**, 1145 (1974);
   C.H. Llewellyn Smith, Phys. Lett. **B46**, 233 (1973).
6. B.W. Lee, C. Quigg, and H.B. Thacker, Phys. Rev. **D16**, 1519 (1977).
7. K. Wilson, Phys. Rev. D 3,1818(1971).;
   G. t Hooft, in Proc. of 1979 Cargse Institute on Recent Developments in Gauge Theories, p. 135 Press, New York 1980.;

For a recent review, see G.F. Giudice, arXiv:1307.7879 [hep-ph] (2013)..

8. J. Wess and B. Zumino, Nucl. Phys. **B70**, 39 (1974);
idem. Phys. Lett. **49B**, 52 (1974);
H.P. Nilles, Phys. Rev. **C110**, 1984 (1);
S.P. Martin, `arXiv:hep-ph/9709356` (1997);
P. Fayet, Phys. Lett. **B69**, 489 (1977);
ibid., **B84**,421(1979);
ibid., **B86**,272(1979);
idem., Nucl. Phys. **B101**, 81 (2001).
9. E. Witten, Nucl. Phys. **B188**, 513 (1981);
R.K. Kaul, Phys. Lett. **B19**, 19 (1982);
R.K. Kaul, Pramana **19**, 183 (1982);
L. Susskind, Phys. Rev. **104**, 181 (1984).
10. H.E. Haber and G.L. Kane, Phys. Rev. **C117**, 75 (1985).
11. J.F. Gunion *et al.*, *The Higgs Hunter's Guide*, Addison-Wesley (1990).
12. P. Fayet, Phys. Lett. **B64**, 159 (1976);
F. Riva, C. Biggio and A. Pomarol, JHEP **1302**, 081 (2013)..
13. S. Weinberg, Phys. Rev. **D13**, 974 (1979); Phys. Rev. **D19**, 1277 (1979);
L. Susskind, Phys. Rev. **D20**, 2619 (1979);
E. Farhi and L. Susskind, Phys. Rev. **74**, 277 (1981);
R.K. Kaul, Rev. Mod. Phys. **55**, 449 (1983);
C. T. Hill and E. H. Simmons, Phys. Reports **381**, 235 (2003) [E: *ibid.*, **390**, 553 (2004)].
14. D. B. Kaplan and H. Georgi, Phys. Lett. **B136**, 183 (1984)..
15. T. van Ritbergen and R. G. Stuart, Phys. Rev. Lett. **82**, 488 (1999);
T. van Ritbergen and R. G. Stuart, Nucl. Phys. **B564**, 343 (2000);
M. Steinhauser and T. Seidensticker, Phys. Lett. **B467**, 271 (1999);
D. M. Webber *et al.*, Phys. Rev. Lett. **106**, 041803 (2011).
16. B.A. Kniehl, Phys. Rept. **240**, 211 (1994).

17. M. Carena and H.E. Haber, Prog. in Part. Nucl. Phys. **50**, 152 (2003).
18. A. Djouadi, Phys. Reports **457**, 1 (2008).
19. S. Dittmaier *et al.*, [LHC Higgs Cross Section Working Group], `arXiv:1101.0593[hep-ph]` (2011).
20. S. Dittmaier *et al.*, [LHC Higgs Cross Section Working Group], `arXiv:1201.3084 [hep-ph]` (2012).
21. S. Dittmaier *et al.*, [LHC Higgs Cross Section Working Group], `arXiv:1307.1347.0593[hep-ph]` (2013).
22. P. Sikivie, L. Suskind, M. Voloshin and V. Zakharov, Nucl. Phys. **B173**, 189 (1980);
H. Georgi, Ann, Rev. Nucl. Part. Sci. **43**, 209 (1993).
23. M. Veltmann, Diagrammatica, The Path to Feynman Rules (Cambridge, 199).
24. R. S. Chivukula, M. Dugan, M. Golden and E. Simmons, Ann, Rev. Nucl. Part. Sci. **45**, 255 (1995).
25. S. Willenbrock, `arXiv:0410370[hep-ph]` (2008).
26. N. Cabibbo *et al.*, Nucl. Phys. **B158**, 295 (1979);
G. Altarelli and G. Isidori, Phys. Lett. **B337**, 141 (1994);
J.A. Casas, J.R. Espinosa, and M. Quirós, Phys. Lett. **B342**, 171 (1995);
idem., Phys. Lett. **B382**, 374 (1996);
T. Hambye and K. Riesselmann, Phys. Rev. **D55**, 7255 (1997).
27. J.R. Espinosa and M. Quirós, Phys. Lett. **B353**, 257 (1995);
G. Isidori *et al.*, Nucl. Phys. **B609**, 387 (2001).
28. J. Elias-Miró *et al.*, Phys. Lett. **B709**, 222 (2012);
D. Buttazzo, G. Degrassi, P. P. Giardino, G. F. Giudice, F. Sala, A. Salvio and A. Strumia, arXiv:1307.3536 [hep-ph]..
29. J. Ellis, M.K. Gaillard, and D.V. Nanopoulos, Nucl. Phys. **B106**, 292 (1976);
B.L. Ioffe and V.A. Khoze. Sov. J. Nucl. Phys. **9**, 50 (1978).
30. D.R.T. Jones and S. Petcov, Phys. Lett. **B84**, 440 (1979);

R.N. Cahn and S. Dawson, Phys. Lett. **B136**, 196 (1984);
G.L. Kane, W.W. Repko, and W.B. Rolnick, Phys. Lett. **B148**, 367 (1984);
G. Altarelli, B. Mele, and F. Pitolli. Nucl. Phys. **B287**, 205 (1987);
W. Kilian, M. Krämer, and P.M. Zerwas, Phys. Lett. **B373**, 135 (1996).

31. B.A. Kniehl, Z. Phys. **C55**, 605 (1992).
32. J. Fleischer and F. Jegerlehner, Nucl. Phys. **B216**, 469 (1983);
A. Denner *et al.*, Z. Phys. **C56**, 261 (1992).
33. B.A. Kniehl, Int. J. Mod. Phys. **A17**, 1457 (2002).
34. K.J. Gaemers and G.J. Gounaris, Phys. Lett. **B77**, 379 (1978);
A. Djouadi, J. Kalinowski, and P. M. Zerwas, Z. Phys. **C54**, 255 (1992);
B.A. Kniehl, F. Madricardo, and M. Steinhauser, Phys. Rev. **D66**, 054016 (2002).
35. S. Dittmaier *et al.*, Phys. Lett. **B441**, 383 (1998);
S. Dittmaier *et al.*, Phys. Lett. **B478**, 247 (2000);
S. Dawson and L. Reina, Phys. Rev. **D59**, 054012 (1999).
36. H.M. Georgi, S.L. Glashow, M.E. Machacek and D. Nanopoulos, Phys. Rev. Lett. **40**, 692 (1978).
37. A. Djouadi, M. Spira, and P.M. Zerwas, Phys. Rev. **B264**, 440 (1991);
S. Dawson, Nucl. Phys. **B359**, 283 (1991).
38. A. Djouadi, M. Spira and P. Zerwas, Z. Phys. **C70**, 675 (1996).
39. M. Spira, et al. Nucl. Phys. **B453**, 17 (1995).
40. R.V. Harlander, Phys. Lett. **B492**, 74 (2000);
S. Catani, D. de Florian and M. Grazzini, JHEP **05**, 25 (2001);
R.V. Harlander and W.B. Kilgore, Phys. Rev. **D64**, 013015 (2001);
R.V. Harlander and W.B. Kilgore, Phys. Rev. Lett. **88**, 201801 (2002);

C. Anastasiou and K. Melnikov, Nucl. Phys. **B646**, 220 (2002);
V. Ravindran, J. Smith, and W.L. van Neerven, Nucl. Phys. **B665**, 325 (2003);
J. Blümlein and V. Ravindran, Nucl. Phys. **B716**, 128 (2005).

41. A. Djouadi and P. Gambino, Phys. Rev. Lett. **73**, 2528 (1994);
S. Actis *et al.*, Phys. Lett. **B670**, 12 (2008);
U. Aglietti *et al.*, Phys. Lett. **B595**, 432 (2004);
G. Degrassi and F. Maltoni, Phys. Lett. **B600**, 255 (2004);
U. Aglietti *et al.*, JHEP **0701**, 021 (2007);
S. Actis, G. Passarino, C. Sturm, and S. Uccirati, Nucl. Phys. **B811**, 182 (2009);
S. Actis *et al.*, Phys. Lett. **B670**, 12 (2008).

42. C. Anastasiou, R. Boughezal, and F. Petriello, JHEP **0904**, 003 (2009).

43. W.-Y. Keung and F. J. Petriello,Phys. Rev. **D80**, 01007 (2009);
O. Brein, Phys. Rev. **D81**, -93006 (2010).

44. M. Kramer, E. Laenen, and M. Spira, Nucl. Phys. **B511**, 523 (1998);
Chetyrkin et al, Nucl. Phys. **B510**, 61 (1998);
S. Catani *et al.*, JHEP **0307**, 028 (2003);
S. Moch and A. Vogt, Phys. Lett. **B631**, 48 (2005);
E. Laenen and L. Magnea, Phys. Lett. **B632**, 270 (2006);
A. Idilbi *et al.*, Phys. Rev. **D73**, 077501 (2006);
V. Ravindran, Nucl. Phys. **B746**, 291 (2006);
V. Ravindran, , Nucl. Phys. **B752**, 173 (2006).

45. S. Marzani, R. D. Ball, V. Del Duca, S. Forte, and A. Vicini, Nucl. Phys. **B800**, 127 (2008);
R. V. Harlander and K. J. Ozeren, Phys. Lett. **B679**, 467 (2009);
R. V. Harlander and K. J. Ozeren, JHEP **0911**, 088 (2009);

R. V. Harlander, H. Mantler, S. Marzani, and K. J. Ozeren, Eur. Phys. J. **C66**, 359 (2010);
A. Pak, M. Rogal, and M. Steinhauser, Phys. Lett. **B679**, 473 (2009);
A. Pak, M. Rogal, and M. Steinhauser, JHEP **1002**, 025 (2010).

46. D. de Florian and M. Grazzini, Phys. Lett. **B674**, 291 (2009);
D. de Florian and M. Grazzini, Phys. Lett. **B718**, 117 (2012).
47. C. Anastasiou, S. Buehler, F. Herzog, and A. Lazopoulos JHEP **1204**, 004 (2012).
48. J. Baglio and A. Djouadi, JHEP **1010**, 064 (2010).
49. V. Ahrens *et al.*, Phys. Rev. **D79**, 033013 (2009);
V. Ahrens *et al.*, Eur. Phys. J. **C62**, 333 (2009).
50. V. Ahrens *et al.*, Phys. Lett. **B698**, 271 (2011).
51. C.R. Schmidt, Phys. Lett. **B413**, 391 (1997).
52. D. de Florian, M. Grazzini, and Z. Kunszt, Phys. Rev. Lett. **82**, 5209 (1999).
53. Nucl. Phys. **B634**, 247 (2002).
54. C.J. Glosser and C. R. Schmidt, JHEP **0212**, 016 (2002).
55. J.M. Campbell, R.K. Ellis, and G. Zanderighi, JHEP **0610**, 028 (2006).
56. J.M. Campbell, R.K. Ellis, and C. Williams, Phys. Rev. **D81**, 074023 (2010).
57. R. Boughezal, F. Caola, K. Melnikov, F. Petriello, and M. Schulze, JHEP **1306**, 072 (2013),.
58. C. F. Berger, C. Marcantonini, I. W. Stewart, F. J. Tackmann, and W. J. Waalewijn, JHEP **1104**, 092 (2011);
A. Banfi, G. P. Salam, and G. Zanderighi, JHEP **1206**, 159 (2012);
T. Becher and M. Neubert, JHEP **1207**, 108 (2012);
F. J. Tackmann, J. R. Walsh, and S. Zuberi, Phys. Rev. **D86**, 053011 (2012);

A. Banfi, P. F. Monni, G. P. Salam, and G. Zanderighi, Phys. Rev. Lett. **109**, 202001 (2012);
X. Liu and F. Petriello, Phys. Rev. **D87**, 014018 (2013).

59. M. Dührssen et al., Phys. Rev. **D70**, 113009 (2004).

60. M. Spira, Fortschr. Phys. 46, 203 (1998);
T. Han, G. Valencia, and S. Willenbrock, Phys. Rev. Lett. **69**, 3274 (1992);
T. Figy, C. Oleari, and D. Zeppenfeld, Phys. Rev. **D68**, 073005 (2003);
T. Figy and D. Zeppenfeld, Phys. Lett. **B591**, 297 (2004);
E.L. Berger, J. Campbell, Phys. Rev. **D70**, 073011 (2004);
M. Ciccolini, A. Denner, and S. Dittmaier, Phys. Rev. Lett. **99**, 161803 (2007);
Ciccolini, A. Denner, and S. Dittmaier, Phys. Rev. **D77**, 103002 (2008);
A. Denner, S. Dittmaier, and A. Mck, HAWK: A Monte Carlo generator for the production of Higgs bosons Attached to WeaK bosons at hadron colliders, http://omnibus.uni-freiburg.de/ sd565/programs/hawk/hawk.html, 2010;
K. Arnold et al., VBFNLO: A parton level Monte Carlo for processes with electroweak bosons, Comput. Phys. Commun. 180 (2009) 16611670, arXiv:0811.4559 [hep-ph];
M. Spira, VV2H, http://people.web.psi.ch/spira/vv2h, 2007;
N. Adam, T. Aziz, J. Andersen, A. Belyaev, T. Binoth, et al., Higgs working group summary report, arXiv:0803.1154 [hep-ph];
T. Figy, S. Palmer, and G. Weiglein, JHEP **1202**, 105 (2012).

61. P. Bolzoni *et al.*, Phys. Rev. Lett. **105**, 011801 (2010).

62. S L. Glashow, D.V. Nanopoulos, and A. Yildiz, Phys. Rev. **D18**, 1724 (1978);
T. Han and S. Willenbrock, Phys. Lett. **B273**, 167 (1991);

T. Han, G. Valencia, and S. Willenbrock, Phys. Rev. Lett. **69**, 3274 (1992);
H. Baer, B. Bailey, and J. F. Owens, Phys. Rev. **D47**, 2730 (1993);
J. Ohnemus and W. J. Stirling, Phys. Rev. **D47**, 2722 (1993)..

63. A. Stange, W. Marciano, and S. Willenbrock, Phys. Rev. **D49**, 1354 (1994).

64. A. Stange, W. Marciano, and S. Willenbrock, Phys. Rev. **D50**, 4491 (1994).

65. M.L. Ciccolini, S. Dittmaier, and M. Krämer, Phys. Rev. **D68**, 073003 (2003);
A. Denner, S Dittmaier and S. Kalweit, JHEP **1203**, 075 (2012).

66. R. Hamberg, W. L. van Neerven, and T. Matsuura, Nucl. Phys. **B359**, 343 (1991)..

67. O. Brein, A. Djouadi, and R. Harlander, Phys. Lett. **B579**, 149 (2004);
L. Altenkamp, S. Dittmaier, R. V. Harlander, H. Rzehak, and T. J. Zirke, JHEP **1302**, 078 (2013).

68. O. Brein, R. Harlander, M. Wiesemann, and T. Zirke, Eur. Phys. J. **C72**, 1868 (2012).

69. O. Brein, R. V. Harlander, and T. J. Zirke, vh@nnlo - Higgs Strahlung at hadron colliders, Comput. Phys. Commun. 184, 998 (2013) 998.

70. G. Ferrera, M. Grazzini, and F. Tramontano, Phys. Rev. Lett. **107**, 152003 (2011).

71. A. Denner, S. Dittmaier, S. Kallweit, and A. Mck, Electroweak corrections to Higgs-strahlung off W/Z bosons at the Tevatron and the LHC with HAWK, 2011. arXiv:1112.5142 [hep-ph]..

72. R. Raitio and W. W. Wada, Phys. Rev. **D19**, 941 (1979);
J. N. Ng and P. Zakarauskas, Nucl. Phys. **B247**, 339 (1984);
J. F. Gunion, Phys. Lett. **B261**, 510 (1991);

W. J. Marciano and F. E. Paige, Phys. Rev. Lett. **66**, 2433 (1991).

73. W. Beenakker *et al.*, Phys. Rev. Lett. **87**, 201805 (2001); L. Reina and S. Dawson, Phys. Rev. Lett. **87**, 201804 (2001); S. Dawson *et al.*, Phys. Rev. **D67**, 071503 (2003); W. Beenakker *et al.*, Nucl. Phys. **B653**, 151 (2003).

74. R. Frederix et al., Phys. Lett. **B701**, 427 (2011); M. Garzelli, A. Kardos, C. Papadopoulos, and Z. Trocsanyi, Europhys. Lett. 96, 11001 (2011)..

75. http://www-d0.fnal.gov/Run2Physics/higgs/xsbr/xsb$r_J$an19$_2$012.pdf.

76. https://twiki.cern.ch/twiki/bin/view/LHCPhysics/CrossSections.

77. M. Spira, Fortschr. Phys.**46**, 203 (1998); A. Djouadi, J. Kalinowski, and M. Spira, Comput. Phys. Commun. **108**,56 (1998); A. Djouadi, J. Kalinowski, M. Mühlleitner, and M. Spira, An update of the program HDECAY, in The Les Houches 2009 workshop on TeV colliders: The tools and Monte Carlo working group summary report. 2010. arXiv:1003.1643 [hep-ph]..

78. S. Gorishnii, A. Kataev, S. Larin, and L. Surguladze, Mod. Phys. Lett. **A5**, 2703 (1990); [39] S. Gorishnii, A. Kataev, S. Larin, and L. Surguladze, Phys. Rev. **D43**, 1633 (1991); A. L. Kataev and V. T. Kim, Mod. Phys. Lett. **A9**,1309 (1994); L. R. Surguladze, Phys. Lett. **B341**, 60 (1994); S. Larin, T. van Ritbergen, and J. Vermaseren, Phys. Lett. **B362**, 134 (1995); K. Chetyrkin and A. Kwiatkowski, Nucl. Phys. **B461**, 3 (1996); K. Chetyrkin, Phys. Lett. **B390**, 309 (1997); P. A. Baikov, K. G. Chetyrkin, and J. H. Kuhn, Phys. Rev. Lett. **96**, 012003 (2006).

79. J. Fleischer and F. Jegerlehner, Phys. Rev. **D23**, 2001; D. Bardin, B. Vilensky, and P. Khristova, Sov. J. Nucl. Phys. **53**, 152 (1991);

A. Dabelstein and W. Hollik, Z. Phys. **C53**, 507 (1992);
B.A. Kniehl, Nucl. Phys. **B376**, 3 (1992);
A. Djouadi, D. Haidt, B. A. Kniehl, P. M. Zerwas, and B. Mele, Higgs in the Standard Model, . In *Munich/Annecy/Hamburg 1991, Proceedings, e+e? collisions at 500 GeV, pt. A* 11-30..

80. E. Braaten and J. P. Leveille, Phys. Rev. **D22**, 715 (1980);
N. Sakai, Phys. Rev. **D22**, 2220 (1980);
T. Inami and T. Kubota, Nucl. Phys. **B179**, 171 (1981);
S.G. Gorishniĭ, A.L. Kataev, and S.A. Larin, Sov. J. Nucl. Phys. **40**, 329 (1984) [Yad. Fiz. **40**, 517 (1984)];
M. Drees and K. Hikasa, Phys. Rev. **D41**, 1547 (1990);
M. Drees and K. Hikasa, Phys. Lett. **B240**, 455 (1990) [E: **B262** 497 (1991)].

81. T. Inami, T. Kubota, and Y. Okada, Z. Phys. **C18**, 69 (1983);
K.G. Chetyrkin, B.A. Kniehl, and M. Steinhauser, Phys. Rev. Lett. **79**, 353 (1997);
P.A. Baikov and K.G. Chetyrkin, Phys. Rev. Lett. **97**, 061803 (2006).

82. H.-Q. Zheng and D.-D. Wu, Phys. Rev. **D42**, 3760 (1990);
A. Djouadi, M. Spira, J. van der Bij, and P. Zerwas, Phys. Lett. **B257**, 187 (1991);
S. Dawson and R. Kauffman, Phys. Rev. **D47**, 1264 (1993);
A. Djouadi, M. Spira, and P. Zerwas, Phys. Lett. **B311**, 255 (1993);
K. Melnikov and O. I. Yakovlev, Phys. Lett. **B312**, 179 (1993);
M. Inoue, R. Najima, T. Oka, and J. Saito, Mod. Phys. Lett. **A9**, 1189 (1994).

83. U. Aglietti, R. Bonciani, G. Degrassi, and A. Vicini, Phys. Lett. **B595**, 432 (2004);
G. Degrassi and F. Maltoni, Phys. Lett. **B600**, 255 (2004);

S. Actis, G. Passarino, C. Sturm, and S. Uccirati, Phys. Lett. **B670**, 12 (2008);
U. Aglietti, R. Bonciani, G. Degrassi, and A. Vicini, Phys. Lett. **B600**, 57 (2004);
G. Degrassi and F. Maltoni, Nucl. Phys. **B724**, 183 (2005);
U. Aglietti et al., Tevatron for LHC report: Higgs, arXiv:hep-ph/0612172..

84. . A. Firan and R. Stroynowski, Phys. Rev. **D76**, 057301 (2007).

85. M. Spira, A. Djouadi, and P. M. Zerwas, Phys. Lett. **B276**, 350 (1992).

86. A. Bredenstein, A. Denner, S. Dittmaier, and M. M. Weber, Phys. Rev. **D74**, 013004 (2006);
A. Bredenstein, A. Denner, S. Dittmaier, and M. Weber, JHEP **0702**, 080 (2007);
A. Bredenstein, A. Denner, S. Dittmaier, A. Mück, and M. M. Weber, Prophecy4f: A Monte Carlo generator for a proper description of the Higgs decay into 4 fermions, http://omnibus.uni-freiburg.de/ sd565/programs/prophecy4f/prophecy4f.html, 2010..

87. A. Denner *et al.*, Eur. Phys. J. **C71**, 1753 (2011);
A. Djouadi, J. Kalinowski, and M. Spira, Comput. Phys. Commun. **108**, 56 (1998);
A. Djouadi *et al.*, `arXiv:1003.1643 [hep-ph]` (2010);
S. Actis *et al.*, Nucl. Phys. **B811**, 182 (2009);
K.G. Chetyrkin and M. Steinhauser, Phys. Lett. **B408**, 320 (1997);
E. Braaten and J.P. Leveille, Phys. Rev. **D22**, 715 (1980);
R. Harlander and M. Steinhauser, Phys. Rev. **D56**, 3980 (1997);
A. Ghinculov, Phys. Lett. **B337**, 137 (1994);
L. Durand, K. Riesselmann, and B.A. Kniehl, Phys. Rev. Lett. **72**, 2534 (1994);
A. Ghinculov, Nucl. Phys. **B455**, 21 (1995);
A. Frink *et al.*, Phys. Rev. **D54**, 4548 (1996);
E. Gross *et al.*, Z. Phys. **C63**, 417 (1994); [E: *ibid.*, **C66**, 32 (1995)];

A.L. Kataev, Sov. Phys. JETP Lett. **66**, 327 (1997) [*Pis'ma Zh. Éksp. Teor. Fiz.* **66** (1997) 308].

88. R.V. Harlander and W.B. Kilgore, Phys. Rev. **D68**, 013001 (2003);
J. Campbell *et al.*, Phys. Rev. **D67**, 095002 (2003);
S. Dawson *et al.*, Phys. Rev. Lett. **94**, 031802 (2005);
S. Dittmaier, M. Krämer, and M. Spira, Phys. Rev. **D70**, 074010 (2004);
S. Dawson *et al.*, Phys. Rev. **D69**, 074027 (2004).
89. W.J. Stirling and D.J. Summers, Phys. Lett. **B283**, 411 (1992);
F. Maltoni *et al.*, Phys. Rev. **D64**, 094023 (2001).
90. A. Ajaib et al., Snowmass 2013: Higgs working group report, (2013).
91. LEP Electroweak Working Group, status of March 2012, `http://lepewwg.web.cern.ch/LEPEWWG/`.
92. J. Erler and P. Langacker, *Electroweak Model and Constraints on New Physics*, in this volume.
93. ALEPH, DELPHI, L3, and OPAL Collabs., The LEP Working Group for Higgs Boson Searches, Phys. Lett. **B565**, 61 (2003).
94. CMS Collab., JHEP **06**, 081 (2013).
95. ALEPH, DELPHI, L3, and OPAL Collabs., The LEP Working Group for Higgs Boson Searches, Phys. Lett. **B565**, 61 (2003).
96. L. Lyons, *The Annals of Applied Statistics,* Vol. 2, No. 3, 887 (2008).
97. L. Demortier, "P-Values and Nuisance Parameters", *Proceedings of PHYSTAT 2007,* CERN-2008-001, p. 23 (2008).
98. CMS Collab. Phys. Lett. **B710**, 26 (2012).
99. ATLAS Collab. Phys. Rev. D 86, 032003 (2012).
100. CMS Collab., CMS-PAS-HIG-13-005 (2013).
101. ATLAS Collab. Phys. Lett. **B726**, 88 (2012).
102. CMS Collab., CMS-PAS-HIG-13-001 (2013).
103. CMS Collab., CMS-PAS-HIG-13-015 (2013).

104. CMS Collab., CMS-PAS-HIG-13-016 (2013).
105. CMS Collab., Phys. Rev. Lett. **110**, 081803 (2012).
106. CMS Collab., CMS-PAS-HIG-13-001 (2013).
107. CMS Collab., Phys. Rev. D TO BE SUBMITTED (2013).
108. ATLAS Collab. ATLAS-CONF-2013-030 (2013)..
109. ATLAS Collab. ATLAS-CONF-2013-075 (2013)..
110. CMS Collab., CMS-PAS-HIG-13-003 (2013).
111. CMS Collab., CMS-PAS-HIG-13-022 (2013).
112. CMS Collab., CMS-PAS-HIG-13-017 (2013).
113. J. M. Butterworth et al., Phys. Rev. Lett. **100**, 242001 (2008).
114. CDF & DØ Collab., Phys. Rev. Lett. **109**, 071804 (2012).
115. CDF & DØ Collab., Phys. Rev. D 88 ,052014 (2012).
116. CMS Collab., CMS-PAS-HIG-13-012 (2013).
117. CMS Collab., CMS-PAS-HIG-13-011 (2013).
118. CMS Collab., CMS-PAS-HIG-13-019 (2013).
119. CMS Collab., JHEP **05**, 145 (2013).
120. ATLAS Collab. ATLAS-CONF-2013-079 (2013)..
121. VS CMS Collab., VS CMS-PAS-HIG-13-004 (2013), CMS-PAS-HIG-12-053 (2013) VS.
122. ATLAS Collab., ATLAS-CONF-2012-160 (2012)..
123. CMS Collab., arXiv:1307.5515 (2013) . Submitted to Phys. Lett. (B)..
124. ATLAS Collab., ATLAS-CONF-2013-009 (2013)..
125. ATLAS Collab., ATLAS-CONF-2013-010 (2013)..
126. CMS-PAS-HIG-13-007 (2013).
127. W. Buchmuller and D. Wyler, Nucl. Phys. **B268**, 621 (1986).
128. B. Grzadkowski, M. Iskrzynski, M. Misiak and J. Rosiek, JHEP **1010**, 085 (2010).
129. R. Contino, M. Ghezzi, C. Grojean, M. Muhlleitner and M. Spira, JHEP **1307**, 035 (2013)..
130. J. Elias-Miro, J. R. Espinosa, E. Masso and A. Pomarol, arXiv:1308.1879 [hep-ph]..

131. K. Hagiwara, S. Ishihara, R. Szalapski and D. Zeppenfeld, Phys. Lett. **B283**, 353 (1992) and K. Hagiwara, S. Ishihara, R. Szalapski and D. Zeppenfeld, Phys. Rev. **D48**, 2182 (1993). K. Hagiwara, R. Szalapski and D. Zeppenfeld, Phys. Lett. **B318**, 155 (1993).

132. L.E. Ibáñez and G.G. Ross, Phys. Lett. **B110**, 215 (1982);
L.E. Ibáñez, Phys. Lett. **B118**, 73 (1982);
J. Ellis, D.V. Nanopoulos, and K. Tamvakis, Phys. Lett. **B121**, 123 (1983);
L. Alvarez-Gaumé, J. Polchinski, and M.B. Wise, Nucl. Phys. **B221**, 495 (1983).

133. H.E. Haber, *Supersymmetry*, in this volume.

134. S. Dimopoulos and H. Georgi, Nucl. Phys. **B193**, 150 (1981);
K. Harada and N. Sakai, Prog. Theor. Phys. **67**, 1877 (1982);
K. Inoue *et al.*, Prog. Theor. Phys. **67**, 1889 (1982);
L. Girardello and M.T. Grisaru, Nucl. Phys. **B194**, 65 (1982);
L.J. Hall and L. Randall, Phys. Rev. Lett. **65**, 2939 (1990);
I. Jack and D.R.T. Jones, Phys. Lett. **B457**, 101 (1999).

135. L.E. Ibáñez and G.G. Ross, Phys. Lett. **B105**, 439 (1981);
S. Dimopoulos, S. Raby, and F. Wilczek, Phys. Rev. **D24**, 1681 (1981);
M.B. Einhorn and D.R.T. Jones, Nucl. Phys. **B196**, 475 (1982);
W.J. Marciano and G. Senjanovic, Phys. Rev. **D25**, 3092 (1982).

136. J. Ellis, S. Kelley and D.V. Nanopoulos, Phys. Lett. **B249**, 441 (1990);
P. Langacker and M. Luo, Phys. Rev. **D44**, 817 (1991);
U. Amaldi, W. de Boer, and H.Fürstenau, Phys. Lett. **B260**, 447 (1991);
P. Langacker and N. Polonsky, Phys. Rev. **D52**, 3081 (1995);
S. Pokorski, *Act. Phys. Pol.* **B30**, 1759 (1999);

For a recent review, see R.N. Mohapatra, in *Particle Physics 1999, Proceedings of the ICTP Summer School in Particle Physics,* Trieste, Italy, 21 June–9 July, 1999, edited by G. Senjanovic and A.Yu. Smirnov. (World Scientific, Singapore, 2000) pp. 336–394.

137. Y. Okada, M. Yamaguchi, T. Yanagida, Prog. Theor. Phys. **85**, 1 (1991);
J. Ellis, G. Ridolfi, F. Zwirner, Phys. Lett. **B257**, 83 (1991).

138. H.E. Haber and R. Hempfling, Phys. Rev. Lett. **66**, 1815 (1991).

139. S.P. Li and M. Sher, Phys. Lett. **B140**, 339 (1984);
R. Barbieri and M. Frigeni, Phys. Lett. **B258**, 395 (1991);
M. Drees and M.M. Nojiri, Phys. Rev. **D45**, 2482 (1992);
J.A. Casas *et al.*, Nucl. Phys. **B436**, 3 (1995) [E: **B439** (1995) 466];
J. Ellis, G. Ridolfi, and F. Zwirner, Phys. Lett. **B262**, 477 (1991);
A. Brignole *et al.*, Phys. Lett. **B271**, 123 (1991) [E: **B273** (1991) 550].

140. R.-J. Zhang, Phys. Lett. **B447**, 89 (1999);
J.R. Espinosa and R.-J. Zhang, JHEP **0003**, 026 (2000);
J.R. Espinosa and R.-J. Zhang, Nucl. Phys. **B586**, 3 (2000);
A. Brignole *et al.*, Nucl. Phys. **B631**, 195 (2002), Nucl. Phys. **B643**, 79 (2002);
A. Dedes, G. Degrassi, and P. Slavich, Nucl. Phys. **B672**, 144 (2003).

141. J.F. Gunion and A. Turski, Phys. Rev. **D39**, 2701 (1989), Phys. Rev. **D40**, 2333 (1989);
M.S. Berger, Phys. Rev. **D41**, 225 (1990);
A. Brignole, Phys. Lett. **B277**, 313 (1992), Phys. Lett. **B281**, 284 (1992);
M.A. Díaz and H.E. Haber, Phys. Rev. **D45**, 4246 (1992);
P.H. Chankowski, S. Pokorski, and J. Rosiek, Phys. Lett. **B274**, 191 (1992), Nucl. Phys. **B423**, 437 (1994);

A. Yamada, Phys. Lett. **B263**, 233 (1991), Z. Phys. **C61**, 247 (1994);
A. Dabelstein, Z. Phys. **C67**, 496 (1995);
R. Hempfling and A.H. Hoang, Phys. Lett. **B331**, 99 (1994);
S. Heinemeyer, W. Hollik, and G. Weiglein, Phys. Rev. **D58**, 091701 (1998), Phys. Lett. **B440**, 296 (1998), Eur. Phys. J. **C9**, 343 (1999).

142. D.M. Pierce *et al.*, Nucl. Phys. **B491**, 3 (1997).

143. R. Barbieri, M. Frigeni, and F. Caravaglios, Phys. Lett. **B258**, 167 (1991);
Y. Okada, M. Yamaguchi, and T. Yanagida, Phys. Lett. **B262**, 45 (1991);
J.R. Espinosa and M. Quirós, Phys. Lett. **B266**, 389 (1991);
D.M. Pierce, A. Papadopoulos, and S. Johnson, Phys. Rev. Lett. **68**, 3678 (1992);
K. Sasaki, M. Carena, and C.E.M. Wagner, Nucl. Phys. **B381**, 66 (1992);
R. Hempfling, in *Phenomenological Aspects of Supersymmetry*, edited by W. Hollik, R. Rückl, and J. Wess (Springer-Verlag, Berlin, 1992) pp. 260–279;
J. Kodaira, Y. Yasui, and K. Sasaki, Phys. Rev. **D50**, 7035 (1994);
H.E. Haber and R. Hempfling, Phys. Rev. **D48**, 4280 (1993);
M. Carena *et al.*, Phys. Lett. **B355**, 209 (1995).

144. H.E. Haber, R. Hempfling, and A.H. Hoang, Z. Phys. **C75**, 539 (1997);
M. Carena *et al.*, Nucl. Phys. **B580**, 29 (2000).

145. M. Carena, M. Quirós, and C.E.M. Wagner, Nucl. Phys. **B461**, 407 (1996).

146. S. Martin, Phys. Rev. **D67**, 095012 (2003); Phys. Rev. **D71**, 016012 (2005); Phys. Rev. **D75**, 055005 (2007).

147. M. Carena, S. Mrenna, and C.E.M. Wagner, Phys. Rev. **D60**, 075010 (1999);
ibid., Phys. Rev. **D62**, 055008 (2000).

148. S. Heinemeyer, W. Hollik, and G. Weiglein, Phys. Lett. **B455**, 179 (1999);
J.R. Espinosa and I. Navarro, Nucl. Phys. **B615**, 82 (2001);
G. Degrassi, P. Slavich, and F. Zwirner, Nucl. Phys. **B611**, 403 (2001);
S. Heinemeyer *et al.*, Eur. Phys. J. **C39**, 465 (2005).

149. S. P. Martin, Phys. Rev. **D75**, 055005 (2007);
P. Kant, R. V. Harlander, L. Mihaila and M. Steinhauser, JHEP **1008**, 104 (2010);
J. L. Feng, P. Kant, S. Profumo and D. Sanford, Phys. Rev. Lett. **111**, 131802 (2013).

150. E. Accomando, *et al.*, `hep-ph/0608079`.

151. U. Ellwanger and C. Hugonie, Mod. Phys. Lett. **A22**, 1581 (2007).

152. P. Batra *et al.*, JHEP **0402**, 043 (2004);
P. Batra *et al.*, JHEP **0406**, 032 (2004);
R. Huo, G. Lee, A. M. Thalapillil and C. E. M. Wagner, Phys. Rev. **D87**, 055011 (2013).

153. M. Dine, N. Seiberg, and S. Thomas, Phys. Rev. **D76**, 095004 (2007) and refs. therein.

154. J.R. Espinosa and M. Quirós, Phys. Rev. Lett. **81**, 516 (1998).

155. M. Carena *et al.*, Phys. Rev. **D81**, 015001 (2010);
W. Altmannshofer *et al.*, Phys. Rev. **D84**, 095027 (2011).

156. I. Antoniadis *et al.*, Nucl. Phys. **B831**, 133 (2010).

157. S. Dimopoulos and D.W. Sutter, Nucl. Phys. **B452**, 496 (1995);
D.W. Sutter, Stanford Ph. D. thesis, `hep-ph/9704390` (1997);
H.E. Haber, *Nucl. Phys. B* (Proc. Suppl.) **62A-C** (1998) 469.

158. A. Djouadi, Phys. Reports **459**, 1 (2008).

159. H.E. Haber and Y. Nir, Nucl. Phys. **B335**, 363 (1990);
A. Dobado, M. J. Herrero, and S. Penaranda, Eur. Phys. J. **C17**, 487 (2000);

J.F. Gunion and H.E. Haber, Phys. Rev. **D67**, 075019 (2003).

160. L.J. Hall and M.B. Wise, Nucl. Phys. **B187**, 397 (1981).

161. T.D. Lee, Phys. Rev. **D8**, 1226 (1973);
P. Fayet, Nucl. Phys. **B78**, 14 (1974);
R.D. Peccei and H.R. Quinn, Phys. Rev. Lett. **38**, 1440 (1977);
P. Fayet and S. Ferrara, Phys. Rept. 32, 249 (1977);
V.D. Barger, J.L. Hewett, and R.J.N. Phillips, Phys. Rev. **D41**, 3421 (1990).

162. S.L. Glashow and S. Weinberg, Phys. Rev. **D15**, 1958 (1977);
E.A. Paschos, Phys. Rev. **D15**, 1966 (1977);
H. Georgi, Hadronic J. **1,** 1227 (1978);
H. Haber, G Kane and T Sterling Nucl. Phys. **B161**, 493 (1979);
A. G. Akeroyd, Phys. Lett. **B368**, 89 (1996);
A.G. Akeroyd, Nucl. Phys. **B544**, 557 (1999);
A. G. Akeroyd, A. Arhrib, and E. Naimi, Eur. Phys. J. **C20**, 51 (2001).

163. M. Carena, S. Heinemeyer, O. Stl, C. E. M. Wagner and G. Weiglein, Eur. Phys. J. **C73**, 2552 (2013).

164. M. Carena *et al.*, `hep-ph/9912223` (1999); *idem*, Eur. Phys. J. **C26**, 601 (2003).

165. G. Degrassi *et al.*, Eur. Phys. J. **C28**, 133 (2003).

166. S. Heinemeyer *et al.*, J. High Energy Phys. **0808**, 087 (2008).

167. M. Carena S. Gori, N. R. Shah, C. E. M. Wagner, JHEP **1203**, 014 (2012);
M. Carena, S. Gori, N. R. Shah, C. E. M. Wagner and L. -T. Wang, JHEP **1207**, 175 (2012).

168. K. Blum, R. DAgnolo and J. Fan, JHEP 1301 (2013) 057;
M. Buckley and D. Hooper, Phys. Rev. D 86 (2012) 075008;
J. Espinosa, C. Grojean, V. Sanz and M. Trott, JHEP 1212 (2012) 077 [.

169. A. Arbey *et al.*, Phys. Lett. **B708**, 162 (2012);

A. Arbey, M. Battaglia, A. Djouadi and F. Mahmoudi, JHEP **1209**, 107 (2012).

170. L.J. Hall, D. Pinner, and J.T. Ruderman, JHEP **1204**, 131 (2012).

171. H. Baer, V. Barger, and A. Mustafayev, Phys. Rev. **D85**, 075010 (2012).

172. P. Draper, P. Meade, M. Reece and D. Shih, Phys. Rev. D **85**, 095007 (2012).

173. S. Heinemeyer, O. Stal, and G. Weiglein, Phys. Lett. **B710** , 201 (2012).

174. M. Kadastik, K. Kannike, A. Racioppi and M. Raidal, JHEP **1205**, 061 (2012).

175. XXXXXXXXXXXX.

176. G. Degrassi, S. Di Vita, J. Elias-Miro, J. R. Espinosa, G. F. Giudice, G. Isidori and A. Strumia, JHEP **1208**, 098 (2012);
A. Arvanitaki, N. Craig, S. Dimopoulos and G. Villadoro, JHEP **1302**, 126 (2013);
G. Kane, P. Kumar, R. Lu and B. Zheng, Phys. Rev. D **85**, 075026 (2012).

177. J. F. Gunion and H. E. Haber, Phys. Rev. D 67, 075019 (2003) [hep-ph/0207010].;
N. Craig, J. Galloway and S. Thomas, arXiv:1305.2424 [hep-ph].;
D. Asner et al, arXiv:1310.0763[hep-ph].

178. M. Carena, I. Low, N. R. Shah and C. E. M. Wagner, arXiv:1310.2248 [hep-ph]..

179. T. Kitahara, JHEP 1211, 021 (2012) [arXiv:1208.4792 [hep-ph]].;
M. Carena, S. Gori, I. Low, N. R. Shah and C. E. M. Wagner, JHEP **1302**, 114 (2013).

180. B. Batell, S. Jung and C. E. M. Wagner,.

181. M. Carena, S. Gori, N. R. Shah, C. E. M. Wagner and L. -T. Wang, JHEP **1308**, 087 (2013).

182. P. Batra, A. Delgado, D. E. Kaplan and T. M. P. Tait, JHEP **0402**, 043 (2004).

183. P. Batra, A. Delgado, D. E. Kaplan and T. M. P. Tait, JHEP **0406**, 032 (2004).

184. A. Maloney, A. Pierce and J. G. Wacker, JHEP **0606**, 034 (2006).

185. Y. Zhang, H. An, X. -d. Ji and R. N. Mohapatra, Phys. Rev. D **78**, 011302 (2008).

186. C. -W. Chiang, N. G. Deshpande, X. -G. He and J. Jiang, Phys. Rev. D **81**, 015006 (2010).

187. A. D. Medina, N. R. Shah and C. E. M. Wagner, Phys. Rev. D **80**, 015001 (2009).

188. M. Endo, K. Hamaguchi, S. Iwamoto, K. Nakayama and N. Yokozaki, Phys. Rev. D **85**, 095006 (2012).

189. C. Cheung and H. L. Roberts, arXiv:1207.0234 [hep-ph]..

190. H. An, T. Liu and L. -T. Wang, Phys. Rev. D **86**, 075030 (2012).

191. R. Huo, G. Lee, A. M. Thalapillil and C. E. M. Wagner, Phys. Rev. D **87**, 055011 (2013).

192. R.V. Harlander and W.B. Kilgore, Phys. Rev. **D68**, 013001 (2003);
J. Campbell *et al.*, Phys. Rev. **D67**, 095002 (2003);
S. Dawson *et al.*, Phys. Rev. Lett. **94**, 031802 (2005);
S. Dittmaier, M. Krämer, and M. Spira, Phys. Rev. **D70**, 074010 (2004);
S. Dawson *et al.*, Phys. Rev. **D69**, 074027 (2004).

193. W.J. Stirling and D.J. Summers, Phys. Lett. **B283**, 411 (1992);
F. Maltoni *et al.*, Phys. Rev. **D64**, 094023 (2001).

194. V. Barger, H. E. Logan, G. Shaughnessy, Phys. Rev. **D79**, 115018 (2009).

195. M. Carena *et al.*, Phys. Lett. **B495**, 155 (2000);
M. Carena *et al.*, Nucl. Phys. **B625**, 345 (2002).

196. A. Dabelstein, Nucl. Phys. **B456**, 25 (1995);
F. Borzumati *et al.*, Nucl. Phys. **B555**, 53 (1999);
H. Eberl *et al.*, Phys. Rev. **D62**, 055006 (2000).

197. J.A. Coarasa, R.A. Jiménez, and J. Solà, Phys. Lett. **B389**, 312 (1996);

R.A. Jiménez and J. Solà, Phys. Lett. **B389**, 53 (1996);
A. Bartl *et al.*, Phys. Lett. **B378**, 167 (1996).

198. S. Heinemeyer, W. Hollik, and G. Weiglein, Eur. Phys. J. **C16**, 139 (2000).
199. H.E. Haber *et al.*, Phys. Rev. **D63**, 055004 (2001).
200. L. Hall, R. Rattazzi, and U. Sarid, Phys. Rev. **D50**, 7048 (1994);
R. Hempfling, Phys. Rev. **D49**, 6168 (1994).
201. M. Carena *et al.*, Nucl. Phys. **B426**, 269 (1994).
202. M. Carena *et al.*, Phys. Lett. **B499**, 141 (2001).
203. E. Berger *et al.*, Phys. Rev. **D66**, 095001 (2002).
204. A. Brignole *et al.*, Nucl. Phys. **B643**, 79 (2002); R. Dermisek and I. Low, Phys. Rev. **D77**, 035012 (2008).
205. A. Djouadi, Phys. Lett. **B435**, 101 (1998).
206. E. Boos *et al.*, Phys. Rev. **D66**, 055004 (2002).
207. A. Djouadi, J. Kalinowski, and P.M. Zerwas, Z. Phys. **C57**, 569 (1993);
H. Baer *et al.*, Phys. Rev. **D47**, 1062 (1993);
A. Djouadi *et al.*, Phys. Lett. **B376**, 220 (1996);
A. Djouadi *et al.*, Z. Phys. **C74**, 93 (1997);
S. Heinemeyer and W. Hollik, Nucl. Phys. **B474**, 32 (1996).
208. J.F. Gunion, Phys. Rev. Lett. **72**, 199 (1994);
D. Choudhury and D.P. Roy, Phys. Lett. **B322**, 368 (1994);
O.J. Eboli and D. Zeppenfeld, Phys. Lett. **B495**, 147 (2000);
B.P. Kersevan, M. Malawski, and E. Richter-Was, Eur. Phys. J. **C29**, 541 (2003).
209. J.F. Gunion *et al.*, Phys. Rev. **D38**, 3444 (1988).
210. S.H. Zhu, `hep-ph/9901221` (1999);
S. Kanemura, Eur. Phys. J. **C17**, 473 (2000);
A. Arhrib *et al.*, Nucl. Phys. **B581**, 34 (2000).
211. H.E. Logan and S. Su, Phys. Rev. **D66**, 035001 (2002).
212. A. Gutierrez-Rodriguez and O.A. Sampayo, Phys. Rev. **D62**, 055004 (2000).;

A. Gutierrez-Rodriguez, M.A. Hernandez-Ruiz, and O.A. Sampayo, J. Phys. Soc. Jap. **70**, 2300 (2001);
S. Moretti, EPJdirect **C15**, 1 (2002).

213. S. Kanemura, S. Moretti, and K. Odagiri, JHEP **0102**, 011 (2001).

214. J.F. Gunion and H.E. Haber, Nucl. Phys. **B278**, 449 (1986) [E: **B402**, 567 (1993)];
S. Dawson, A. Djouadi, and M. Spira, Phys. Rev. Lett. **77**, 16 (1996);
A. Djouadi *et al.*, Phys. Lett. **B318**, 347 (1993);
R.V. Harlander and W.B. Kilgore, JHEP **0210**, 017 (2002);
C. Anastasiou and K. Melnikov, Phys. Rev. **D67**, 037501 (2003);
J. Guasch, P. Hafliger and M. Spira, Phys. Rev. **D68**, 115001 (2003);
R.V. Harlander and M. Steinhauser, JHEP **0409**, 066 (2004);
S. Dawson *et al.*, Mod. Phys. Lett. **A21**, 89 (2006);
A. Djouadi and M. Spira, Phys. Rev. **D62**, 014004 (2000);
M. Mühlleitner and M. Spira, Nucl. Phys. **B790**, 1 (2008);
T. Hahn *et al.*, `arXiv:hep-ph/0607308` (2006).

215. D. Dicus *et al.*, Phys. Rev. **D59**, 094016 (1999).

216. C. Balázs, H.-J. He, and C.P. Yuan, Phys. Rev. **D60**, 114001 (1999).

217. J.A. Coarasa *et al.*, Eur. Phys. J. **C2**, 373 (1998).

218. C.S. Li and T.C. Yuan, Phys. Rev. **D42**, 3088 (1990);
[E: Phys. Rev. **D47**, 2156 (1993);
A. Czarnecki and S. Davidson, Phys. Rev. **D47**, 3063 (1993);
C.S. Li, Y.-S. Wei, and J.-M. Yang, Phys. Lett. **B285**, 137 (1992).

219. J. Guasch, R.A. Jiménez. and J. Solà, Phys. Lett. **B360**, 47 (1995).

220. M. Carena *et al.*, Nucl. Phys. **B577**, 88 (2000).

221. M. Guchait and S. Moretti, JHEP **0201**,001 (2002).

222. R.M. Barnett, H.E. Haber, and D.E. Soper, Nucl. Phys. **B306**, 697 (1988).

223. F. Olness and W.-K. Tung, Nucl. Phys. **B308**, 813 (1988).

224. F. Borzumati, J.-L. Kneur, and N. Polonsky, Phys. Rev. **D60**, 115011 (1999).

225. A. Belyaev *et al.*, JHEP **0206**, 059 (2002).

226. L.G. Jin *et al.*, Eur. Phys. J. **C14**, 91 (2000); Phys. Rev. **D62**, 053008 (2000);
A. Belyaev *et al.*, Phys. Rev. **D65**, 031701 (2002);
G. Gao *et al.*, Phys. Rev. **D66**, 015007 (2002).

227. S.-H. Zhu, Phys. Rev. **D67**, 075006 (2005);
T. Plehn, Phys. Rev. **D67**, 014018 (2003).

228. A.A. Barrientos Bendezú and B.A. Kniehl, Phys. Rev. **D59**, 015009 (1999); Phys. Rev. **D61**, 015009 (2000; Phys. Rev. **D63**, 015009 (2001).

229. A.A. Barrientos Bendezú and B.A. Kniehl, Nucl. Phys. **B568**, 305 (2000).

230. A. Krause *et al.*, Nucl. Phys. **B519**, 85 (1998).

231. O. Brein and W. Hollik, Eur. Phys. J. **C13**, 175 (2000).

232. ALEPH Collab., Phys. Lett. **B526**, 191 (2002).

233. DELPHI Collab., Eur. Phys. J. **C32**, 145 (2004).

234. OPAL Collab., Eur. Phys. J. **C37**, 49 (2004).

235. L3 Collab., Phys. Lett. **B545**, 30 (2002).

236. OPAL Collab., Eur. Phys. J. **C23**, 397 (2002).

237. DELPHI Collab., Eur. Phys. J. **C38**, 1 (2004).

238. M. Carena *et al.*, Eur. Phys. J. **C45**, 797 (2006).

239. DØ Collab., Phys. Lett. **B698**, 97 (2011).

240. CDF Collab., Phys. Rev. **D85**, 032005 (2012).

241. DØ Collab., Phys. Rev. Lett. **104**, 151801 (2010);
DØ Collab., Phys. Rev. Lett. **107**, 121801 (2011).

242. (***) DØ Collab., DØ Note 5974-CONF, "Search for neutral Higgs bosons $\phi b \to \tau_e \tau_{\rm had} b$ with 3.7 fb^{-1} of DØ data" (2011).

243. CDF Collab., Phys. Rev. Lett. **103**, 201801 (2009).

244. DØ Collab., Phys. Rev. Lett. **101**, 071804 (2008);
DØ Collab., Phys. Lett. **B707**, 323 (2012).

245. DØ Collab., Phys. Lett. **B710**, 569 (2012).

246. M. Carena *et al.*, `arXiv:1203.1041 [hep-ph]` (2012).

247. ATLAS Collab., "Search for neutral MSSM Higgs bosons decaying to $\tau^+\tau^-$ pairs in proton-proton collisions at $\sqrt{s} = 7$ TeV with the ATLAS detector", ATLAS-CONF-2011-132 (2011).

248. ATLAS Collab., Phys. Lett. **B705**, 174 (2011).

249. ATLAS Collab., `arXiv:0901.0512 [hep-ex]` (2009).

250. ALEPH Collab., Phys. Lett. **B543**, 1 (2002);
DELPHI Collab., Phys. Lett. **B525**, 17 (2002);
L3 Collab., Phys. Lett. **B575**, 208 (2003);
OPAL Collab., Eur. Phys. J. **C7**, 407 (1999).

251. (*) ALEPH, DELPHI, L3 and OPAL Collabs., The LEP Working Group for Higgs Boson Searches, *Search for Charged Higgs Bosons: Preliminary ...*, LHWG-Note/ 2001-05.

252. DØ Collab., Phys. Rev. Lett. **82**, 4975 (1999);
idem, **88**, 151803 (2002);
CDF Collab., Phys. Rev. **D62**, 012004 (2000);
idem, Phys. Rev. Lett. **79**, 357 (1997).

253. CDF Collab., Phys. Rev. Lett. **96**, 042003 (2006).

254. DØ Collab., Phys. Lett. **B682**, 278 (2009).

255. ATLAS Collab., `arXiv:1204.2760 [hep-ex]` (2012).

256. ATLAS Collab., "A Search for a light charged Higgs boson decaying to $c\bar{s}$ in pp collisions at $\sqrt{s} = 7$ TeV with the ATLAS detector", ATLAS-CONF-2011-094 (2011).

257. CMS Collab., "Search for the light charged Higgs boson in top quark decays in pp collisions at $\sqrt{s} = 7$ TeV CMS-PAS-HIG-11-019.

258. A. D. Sakharov, JETP Lett. **5**, 24 (1967).

259. M. Carena *et al.*, Nucl. Phys. **B599**, 158 (2001).

260. S. Dimopoulos and S. Thomas, Nucl. Phys. **B465**, 23, (1996);
S. Thomas, Int. J. Mod. Phys. **A13**, 2307 (1998).

261. A. Pilaftsis and C.E.M. Wagner, Nucl. Phys. **B553**, 3 (1999).

262. M. Carena *et al.*, Nucl. Phys. **B586**, 92 (2000).

263. A. Pilaftsis, Phys. Rev. **D58**, 096010 (1998); Phys. Lett. **B435**, 88 (1998);
K.S. Babu *et al.*, Phys. Rev. **D59**, 016004 (1999).

264. G.L. Kane and L.-T. Wang, Phys. Lett. **B488**, 383 (2000);
S.Y. Choi, M. Drees and J.S. Lee, Phys. Lett. **B481**, 57 (2000);
S.Y. Choi and J.S. Lee, Phys. Rev. **D61**, 015003 (2000);
S.Y. Choi, K. Hagiwara and J.S. Lee, Phys. Rev. **D64**, 032004 (2001); Phys. Lett. **B529**, 212 (2002);
T. Ibrahim and P. Nath, Phys. Rev. **D63**, 035009 (2001);
T. Ibrahim, Phys. Rev. **D64**, 035009 (2001);
S. Heinemeyer, Eur. Phys. J. **C22**, 521 (2001);
S.W. Ham *et al.*, Phys. Rev. **D68**, 055003 (2003).

265. M. Frank *et al.*, JHEP **0702**, 047 (2007);
S. Heinemeyer *et al.*, Phys. Lett. **B652**, 300 (2007);
T. Hahn *et al.*, `arXiv:0710.4891` (2007).

266. D.A. Demir, Phys. Rev. **D60**, 055006 (1999);
S. Y. Choi *et al.*, Phys. Lett. **B481**, 57 (2000).

267. E. Christova *et al.*, Nucl. Phys. **B639**, 263 (2002) [E: Nucl. Phys. **B647**, 359 (2002)].

268. P. Draper, T. Liu, and C.E.M. Wagner, Phys. Rev. **D81**, 015014 (2010).

269. W. de Boer and C. Sander, Phys. Lett. **B585**, 276 (2004);
S. Heinemeyer *et al.*, JHEP **0608**, 052 (2006);
A. Djouadi *et al.*, Phys. Rev. Lett. **78**, 3626 (1997);
A. Djouadi *et al.*, Phys. Rev. **D57**, 4179 (1998);
S. Heinemeyer and G. Weiglein, JHEP 10 (2002) 072,;
J. Haestier *et al.*, JHEP **0512**, 027, (2005).;
S. Heinemeyer, W. Hollik, and G. Weiglein, Phys. Rept. **425**, 265 (2006);
S. Heinemeyer *et al.*, JHEP **0804**, 039 (2008).

270. O. Buchmueller *et al.*, Phys. Rev. **D81**, 035009 (2010).

271. O. Buchmueller *et al.*, Eur. Phys. J. **C72**, 1878 (2012).

272. G. D'Ambrosio *et al.*, Nucl. Phys. **B645**, 155 (2002).

273. M. Carena, A. Menon, and C.E.M. Wagner, Phys. Rev. **D76**, 035004 (2007);
P. Draper, T. Liu, and C.E.M. Wagner, Phys. Rev. **D80**, 035025 (2009).

274. J.R. Ellis *et al.*, JHEP **0708**, 083 (2007).

275. E. Lunghi, W. Porod, and O. Vives, Phys. Rev. **D74**, 075003 (2006).

276. M. Carena *et al.*, Phys. Rev. **D74**, 015009 (2006).

277. G. Buchalla, A.J. Buras, and M.E. Lautenbacher, Rev. Mod. Phys. **68**, 1125 (1996).

278. A. Dedes and A. Pilaftsis, Phys. Rev. **D67**, 015012 (2003).

279. A.J. Buras *et al.*, Phys. Lett. **B546**, 96 (2002).

280. A. J. Buras *et al.*, Nucl. Phys. **B659**, 2 (2003).

281. K.S. Babu and C.F. Kolda, Phys. Rev. Lett. **84**, 228 (2000).

282. (**) CDF Collab., "A Search for $B^0_{s(d)} \to \mu^+\mu^-$ Decays using 9.7 fb^{-1} of Data", CDF Note 10701 (2012);
CDF Collab., Phys. Rev. Lett. **107**, 191801 (2011);
LHCb Collab., `arXiv:1203.4493 [hep-ex]` (2012);
CMS Collab., "Search for $B_s \to \mu^+\mu^-$ and $B^0 \to \mu^+\mu^-$ decays", `arXiv:1203.3976` (2012). Submitted to JHEP.

283. A. G. Akeroyd, F. Mahmoudi, and D. Martinez Santos, JHEP **1112**, 088 (2011);
A. Arbey, M. Battaglia, and F. Mahmoudi, Eur. Phys. J. **C72**, 1906 (2012).

284. M. Misiak *et al.*, Phys. Rev. Lett. **98**, 022002 (2007), and refs. therein.

285. T. Becher and M. Neubert, Phys. Rev. Lett. **98**, 022003 (2007).

286. Heavy Flavor Averaging Group (HFAG), `http://www.slac.stanford.edu/xorg/hfag/rare/leppho09/radll/btosg.pdf`.

287. Belle Collab., `arXiv:0809.3834 [hep-ex]` (2008).

288. Belle Collab., Phys. Rev. **D82** 071101 (2010).

289. BaBar Collab., Phys. Rev. D **81**, 051101 (2010).

290. BaBar Collab., arXiv:1008.0104 [hep-ex].

291. M. Bona *et al.* [UTfit Collab.], Phys. Lett. **B687**, 61 (2010), http://ckmfitter.in2p3.fr/www/html/ckm_results.html.

292. G. Isidori and P. Paradisi, Phys. Lett. **B639**, 499 (2006).

293. BaBar Collab., Phys. Rev. Lett. **100**, 021801 (2008); Belle Collab., arXiv:0910.4301 [hep-ex] (2009).

294. U. Nierste, S. Trine and S. Westhoff, Phys. Rev. **D78**, 015006 (2008).

295. S. Trine, arXiv:0810.3633 [hep-ph] (2008).

296. LHCb Collab., Phys. Rev. Lett. **108**, 111602 (2012).

297. CDF Collab., "Improved Measurement of the Difference between Time Integrated CP Asymmetries in $D^0 \to K^+K^-$ and $D^0 \to \pi^+\pi^-$ Decays at CDF", CDF Note 10784 (2012).

298. W. Altmannshofer *et al.*, JHEP **1204**, 049 (2012).

299. M. Carena, A. Menon, and C.E.M. Wagner, Phys. Rev. **D79**, 075025 (2009).

300. W. Altmannshofer and D.M. Straub, JHEP **1009**, 078 (2010).

301. J. Ellis *et al.*, Phys. Lett. **B653**, 292 (2007).

302. N. Cabibbo, G.R. Farrar, and L. Maiani, Phys. Lett. **B105**, 155 (1981);
H. Goldberg, Phys. Rev. Lett. **50**, 1419 (1983);
J. R. Ellis *et al.*, Nucl. Phys. **B238**, 453 (1984);
G. Bertone, D. Hooper, and J. Silk, Phys. Reports **405**, 279 (2005).

303. M. Carena, D. Hooper, and A. Vallinotto, Phys. Rev. **D75**, 055010 (2007);
M. Carena, D. Hooper, and P. Skands, Phys. Rev. Lett. **97**, 051801 (2006).

304. A. Djouadi and Y. Mambrini, JHEP **0612**, 001 (2006).

305. J. Ellis, K.A. Olive, and Y. Santoso, Phys. Rev. **D71**, 095007 (2005).

306. N.G. Deshpande and E. Ma Phys. Rev. **D18**, 2574 (1978);
R. Barbieri, L.J. Hall, and V. Rychkov Phys. Rev. **D74**, 015007 (2006);
L. Lopez-Honorez *et al.*, JCAP **0702,** 028 (2007);
E. Lundstrom, M Gustafsson, and J. Edjo, Phys. Rev. **D79**, 035013 (2009);
E. Dolle *et al.*, Phys. Rev. **D8**, 035003 (2010);
X. Miao, S. Su, and B. Thomas, Phys. Rev. **D82**, 035009 (2010);
L. Lopez-Honorez and C.Yaguna, JCAP **1101,** 002 (2011).

307. H.E. Haber, *Proceedings of the 1990 Theoretical Advanced Study Institute in Elementary Particle Physics,* edited by M. Cvetič and Paul Langacker (World Scientific, Singapore, 1991) pp. 340–475, and references therein.

308. S. Glashow and S. Weinberg, Phys. Rev. **D15**, 1958 (1977).

309. P. Fayet, Phys. Lett. **B90**, 104 (1975);
H.-P. Nilles, M. Srednicki, and D. Wyler, Phys. Lett. **B120**, 346 (1983);
J.-M. Frere, D.R.T. Jones, and S. Raby, Nucl. Phys. **B222**, 11 (1983);
J.-P. Derendinger and C.A. Savoy, Nucl. Phys. **B237**, 307 (1984);
B.R. Greene and P.J. Miron, Phys. Lett. **B168**, 226 (1986);
J. Ellis *et al.*, Phys. Lett. **B176**, 403 (1986);
L. Durand and J.L. Lopez, Phys. Lett. **B217**, 463 (1989);
M. Drees, Int. J. Mod. Phys. **A4**, 3635 (1989);
U. Ellwanger, Phys. Lett. **B303**, 271 (1993);
U. Ellwanger, M. Rausch de Taubenberg, and C.A. Savoy, Phys. Lett. **B315**, 331 (1993); Z. Phys. **C67**, 665 (1995); Phys. Lett. **B492**, 21 (1997);
P.N. Pandita, Phys. Lett. **B318**, 338 (1993); Z. Phys. **C59**, 575 (1993);
T. Elliott, S.F. King, and P.L.White, Phys. Lett. **B305**, 71 (1993); Phys. Lett. **B314**, 56 (1993); Phys. Rev. **D49**, 2435 (1994); Phys. Lett. **B351**, 213 (1995);

K.S. Babu and S.M. Barr, Phys. Rev. **D49**, R2156 (1994);
S.F. King and P.L. White, Phys. Rev. **D52**, 4183 (1995);
N. Haba, M. Matsuda, and M. Tanimoto, Phys. Rev. **D54**, 6928 (1996);
F. Franke and H. Fraas, Int. J. Mod. Phys. **A12**, 479 (1997);
S.W. Ham, S.K. Oh, and H.S. Song, Phys. Rev. **D61**, 055010 (2000);
D.A. Demir, E. Ma, and U. Sarkar, J. Phys. **G26**, L117 (2000);
R. B. Nevzorov and M. A. Trusov, Phys. Atom. Nucl. **64**, 1299 (2001);
U. Ellwanger and C. Hugonie, Eur. Phys. J. **C25**, 297 (2002);
U. Ellwanger *et al.*, `arXiv:hep-ph/0305109` (2003);
D.J. Miller and S. Moretti, `arXiv:hep-ph/0403137` (2004).

310. A. Dedes *et al.*, Phys. Rev. **D63**, 055009 (2001);
A. Menon, D. Morrissey, and C.E.M. Wagner, Phys. Rev. **D70**, 035005, (2004).

311. R. Dermisek and J.F. Gunion, Phys. Rev. **D76**, 095006 (2007);
R. Dermisek and J.F. Gunion, Phys. Rev. **D81**, 075003 (2010);
G. Degrassi and P. Slavich, Nucl. Phys. **B825**, 119 (2010);
M. Maniatis, Int. J. Mod. Phys. **A25**, 3505 (2010);
U. Ellwanger, G. Espitalier-Noel and C. Hugonie, JHEP **1109**, 105 (2011);
U. Ellwanger, JHEP **1203**, 044 (2012);
J.F. Gunion, Y. Jiang, and S. Kraml, Nucl. Phys. **B710**, 454 (2012);
S.F. King, M. Muhlleitner, and R. Nevzorov, Nucl. Phys. **B860**, 207 (2012).

312. J. R. Espinosa and M. Quirós, Phys. Lett. **B279**, 92 (1992).

313. P. Batra and E. Ponton, Phys. Rev. **D79**, 035001 (2009).

314. M. Schmaltz and D. Tucker-Smith, Ann. Rev. Nucl. Part. Sci. **55**, 229 (2005).

315. M. Perelstein, Prog. Part. Nucl. Phys. **58**, 247 (2007).

316. H.C Cheng, I. Low, and L.T. Wang, Phys. Rev. **D74**, 055001 (2006).

317. C.R. Chen, K. Tobe, and C. P. Yuan, Phys. Lett. **B640**, 263 (2006).

318. G.F. Giudice *et al.*, JHEP **0706**, 045 (2007).

319. J. Hubisz *et al.*, JHEP **0601**, 135 (2006).

320. G. F. Giudice, R. Rattazzi, and J. D. Wells, Nucl. Phys. **B595**, 250 (2001);
M. Chaichian *et al.*, Phys. Lett. **B524**, 161 (2002);
D. Dominici *et al.*, Acta Phys. Polon. **B33**, 2507 (2002);
J. L. Hewett and T. G. Rizzo, JHEP **0308**, 028 (2003).

321. OPAL Collab., Phys. Lett. **B609**, 20 (2005). [E: *ibid.*, **637**, 374 (2006)].

322. B. Grzadkowski and J. F. Gunion, `arXiv:1202.5017 [hep-ph]` (2012);
B. Coleppa, T. Gregoire, and H. Logan, Phys. Rev. **D85**, 055001 (2012).

323. S. Casagrande *et al.*, JHEP **1009**, 014 (2010);
A. Azatov, M. Toharia, and L. Zhu, Phys. Rev. **D82**, 056004 (2010);
A. Azatov and J. Galloway, Phys. Rev. **D85**, 055013 (2012);
F. Goertz, U. Haisch, and M. Neubert, arXiv:1112.5099 [hep-ph] (2012);
M. Carena *et al.*, `arXiv:1204.0008 [hep-ph]` (2012).

324. T. Appelquist, H. -C. Cheng, and B. A. Dobrescu, Phys. Rev. **D64**, 035002 (2001).

325. F.J. Petriello, JHEP **0205**, 003 (2002).

326. A. Azatov *et al.*, `arXiv:1204.4817 [hep-ph]` (2012);
J. R. Espinosa *et al.*, `arXiv:1202.3697 [hep-ph]` (2012).

327. M. J. Strassler and K. M. Zurek, Phys. Lett. **B651**, 374 (2007).

328. M. J. Strassler and K. M. Zurek, Phys. Lett. **B661**, 263 (2008).

329. T. Han *et al.*, JHEP **0807**, 008 (2008).

330. A. Falkowski *et al.*, JHEP **1005**, 077 (2010);
A. Falkowski *et al.*, Phys. Rev. Lett. **105**, 241801 (2010).

331. S. Chivukula *et al.*, *Dynamical Electroweak Symmetry Breaking*, in this volume.

332. S. Schael *et al.*, [ALEPH Collab.], JHEP **1005**, 049 (2010).

333. (*) DELPHI Collab., Interpretation of the searches for Higgs bosons in the MSSM with an additional scalar singlet, CERN-OPEN-99-438 (1999).

334. DØ Collab., Phys. Rev. Lett. **103**, 061801 (2009).

335. CDF Collab., Phys. Rev. Lett. **107**, 031801 (2011).

336. CMS Collab., "Search for a light pseudoscalar boson in the dimuon channel", CMS-PAS-HIG-12-004 (2012).

337. ATLAS Collab., "A Search for Light CP-Odd Higgs Bosons Decaying to $\mu^+\mu^-$ in ATLAS", ATLAS-CONF-2011-020 (2012).

338. E.L. Berger *et al.*, Phys. Rev. **D66**, 095001 (2002).

339. W. Loinaz and J. Wells, Phys. Lett. **B445**, 178 (1998);
X. Calmet and H. Fritzsch, Phys. Lett. **B496**, 190 (2000).

340. ALEPH Collab., Phys. Lett. **B544**, 25 (2002);
DELPHI Collab., Eur. Phys. J. **C44**, 147 (2005);
L3 Collab., Phys. Lett. **B583**, 14 (2004);
OPAL Collab., Eur. Phys. J. **C18**, 425 (2001).

341. (*) The LEP Working Group for Higgs Boson Searches, *Flavour Independent Search for Hadronically Decaying Neutral Higgs Bosons at LEP*, LHWG Note 2001-07.

342. OPAL Collab., Eur. Phys. J. **C18**, 425 (2001);
DELPHI Collab., Eur. Phys. J. **C38**, 1 (2004).

343. DELPHI Collab., Eur. Phys. J. **C34**, 399 (2004).

344. OPAL Collab., `arXiv:0812.0267 [hep-ex]` (2008).

345. Y. Chikashige *et al.*, Phys. Lett. **B98**, 265 (1981);

A.S. Joshipura and S.D. Rindani, Phys. Rev. Lett. **69**, 3269 (1992);
F. de Campos *et al.*, Phys. Rev. **D55**, 1316 (1997).

346. DELPHI Collab., Eur. Phys. J. **C32**, 475 (2004);
L3 Collab., Phys. Lett. **B609**, 35 (2005);
OPAL Collab., Phys. Lett. **B377**, 273 (1996).

347. (*) ALEPH, DELPHI, L3 and OPAL Collabs., The LEP Working Group for Higgs Boson Searches, *Search for Invisible Higgs Bosons: Preliminary ...*, LHWG-Note/ 2001-06.

348. (**) CDF Collab., "Search for heavy metastable particles decaying to quark pairs in $p\bar{p}$ collisions at $\sqrt{s} = 1.96$ TeV", CDF Note 10356 (2010).

349. DØ Collab., Phys. Rev. Lett. **103**, 071801 (2009).

350. (**) CDF Collab., "Search for Anomalous Production of Events with a W or Z boson and Additional Leptons", CDF Note 10526 (2011).

351. A. Abbasabadi *et al.*, Phys. Rev. **D52**, 3919 (1995);
K. Hagiwara, R. Szalapski, and D. Zeppenfeld, Phys. Lett. **B318**, 155 (1993);
O.J.P. Éboli *et al.*, Phys. Lett. **B434**, 340 (1998).

352. L3 Collab, Phys. Lett. **B589**, 89 (2004).

353. ALEPH Collab., Phys. Lett. **B544**, 16 (2002);
DELPHI Collab., Eur. Phys. J. **C35**, 313 (2004);
L3 Collab., Phys. Lett. **B534**, 28 (2002);
OPAL Collab., Phys. Lett. **B544**, 44 (2002).

354. (*) ALEPH, DELPHI, L3 and OPAL Collabs., The LEP Working Group for Higgs Boson Searches, *Search for Higgs Bosons Decaying into Photons: Combined ...*, LHWG Note/2002-02.

355. L3 Collab., Phys. Lett. **B568**, 191 (2003).

356. ALEPH Collab., Eur. Phys. J. **C49**, 439 (2007).

357. DØ Collab., Phys. Rev. Lett. **107**, 151801 (2011).

358. (***) DØ Collab., DØ Note 6297-CONF, "Search for a Fermiophobic Higgs Boson in the di-photon final state using using 9.7 fb^{-1} of DØ data" (2012).

359. CDF Collab., Phys. Rev. Lett. **103**, 061803 (2009).

360. (**) CDF Collab., CDF Note 10731, "Search for a Fermiophobic Higgs Boson in the Di-photon Final State Using 10.0 fb^{-1} of CDF Data" (2012).

361. The CDF and DØ Collabs. and the Tevatron New Physics and Higgs Working Group, "Combined CDF and DØ upper limits on Fermiophobic Higgs Boson Production with up to 8.2 fb^{-1} of $p\bar{p}$ data", `arXiv:1109.0576` (2011).

362. (***) DØ Collab., DØ Note 5067-CONF, "Search for Fermiophobic Higgs Boson in $3\gamma + X$ Events" (2007).

363. ATLAS Collab., "Search for a fermiophobic Higgs boson in the diphoton decay channel with 4.9 fb^{-1} of ATLAS data at $\sqrt(s) = 7$ TeV", ATLAS-CONF-2012-013 (2012).

364. CMS Collab., "Search for the fermiophobic model Higgs boson decaying into two photons", CMS-PAS-HIG-12-002 (2012).

365. G.B. Gelmini and M. Roncadelli, Phys. Lett. **B99**, 411 (1981);
R.N. Mohapatra and J.D. Vergados, Phys. Rev. Lett. **47**, 1713 (1981);
V. Barger *et al.*, Phys. Rev. **D26**, 218 (1982).

366. B. Dutta and R.N. Mohapatra, Phys. Rev. **D59**, 015018 (1999);
C.S. Aulakh *et al.*, Phys. Rev. **D58**, 115007 (1998);
C.S. Aulakh, A. Melfo, and G. Senjanovic, Phys. Rev. **D57**, 4174 (1998).

367. DELPHI Collab., Phys. Lett. **B552**, 127 (2003).

368. OPAL Collab., Phys. Lett. **B295**, 347 (1992);
idem, **B526**, 221 (2002).

369. L3 Collab., Phys. Lett. **B576**, 18 (2003).

370. OPAL Collab., Phys. Lett. **B577**, 93 (2003).

371. DØ Collab., Phys. Rev. Lett. **93**, 141801 (2004);
DØ Collab., Phys. Rev. Lett. **101**, 071803 (2008).

372. CDF Collab., Phys. Rev. Lett. **93**, 221802 (2004);
CDF Collab., Phys. Rev. Lett. **101**, 121801 (2008).

373. CDF Collab., Phys. Rev. Lett. **95**, 071801 (2005).

374. CMS Collab., "Inclusive search for doubly charged Higgs in leptonic final states with the 2011 data at 7 TeV", CMS-PAS-HIG-12-005 (2012).

375. ATLAS Collab., Phys. Rev. **D88**, 032004 (2012).

376. F. Gianotti, on behalf of the ATLAS Collaboration, "Status of Standard Model Higgs Searches in ATLAS", presentation given July 4, 2012 at CERN.

377. ATLAS Collab., ATLAS-CONF-2012-093 (2012).

378. J. Incandela, on behalf of the CMS Collaboration, "Status of the CMS SM Higgs Search", presentation given July 4, 2012 at CERN.

379. CMS Collab., CMS-PAS-HIG-12-020 (2012).

380. ATLAS Collab., ATLAS-CONF-2012-091, ATLAS-CONF-2012-092 (2012).

381. ATLAS Collab, `arXiv:1205.6744 [hep-ex]`, submitted to Phys. Lett. B (2012); ATLAS Collab., `arXiv:1206.2443 [hep-ex]`, submitted to Phys. Lett. B (2012); ATLAS Collab., `arXiv:1206.0756 [hep-ex]`, submitted to Phys. Lett. B (2012); ATLAS Collab., `arXiv:1206.0756 [hep-ex]`, submitted to Phys. Lett. B (2012); ATLAS Collab., `arXiv:1206.6074 [hep-ex]`, submitted to Phys. Lett. B (2012); ATLAS Collab., `arXiv:1206.5971 [hep-ex]`, submitted to JHEP (2012); ATLAS Collab., `arXiv:1207.0210 [hep-ex]`, submitted to Phys. Lett. B (2012).

382. ATLAS Collab., `arXiv:1207.0319 [hep-ex]`, submitted to Phys. Rev. D (2012).

383. CMS Collab., CMS-PAS-HIG-12-015, CMS-PAS-HIG-12-016, CMS-PAS-HIG-12-023, CMS-PAS-HIG-12-023, CMS-PAS-HIG-11-024, CMS-PAS-HIG-12-017, CMS-PAS-HIG-12-003, CMS-PAS-HIG-12-021, CMS-PAS-HIG-12-019, CMS-PAS-HIG-12-018, CMS-PAS-HIG-12-012, CMS-PAS-HIG-12-006, CMS-PAS-HIG-12-025 (2011, 2012).

384. CMS Collab., CMS-PAS-HIG-12-001 (2012).

385. CMS Collab., Phys. Lett. B **710**, 91 (2012).

386. The CDF and D0 Collaborations and the Tevatron New Physics and Higgs Working Group, arXiv:1207.0449 [hep-ex] (2012).

387. D0 Collab., arXiv:1207.0422 [hep-ex] (2012).

388. D0 Collab., D0 Note 6302-CONF, (2012).

389. CDF Collab., CDF Note 10804, (2012); CDF Collab., arXiv:1207.1707, submitted to Phys. Rev. Lett. (2012).

390. H. Georgi and D. B. Kaplan, Phys. Lett. **B145**, 216 (1984).

391. J. Mrazek, A. Pomarol, R. Rattazzi, M. Redi, J. Serra and A. Wulzer, Nucl. Phys. **B853**, 1 (2011).

392. D. B. Kaplan, Nucl. Phys. **B365**, 259 (1991).

393. N. Arkani-Hamed, A. G. Cohen, E. Katz and A. E. Nelson, JHEP **0207**, 034 (2002).

394. N. Arkani-Hamed, A. G. Cohen and H. Georgi, Phys. Lett. **B513**, 232 (2001).

395. M. Perelstein, Prog. Part. Nucl. Phys. **58**, 247 (2007).

396. M. Schmaltz and D. Tucker-Smith, Ann. Rev. Nucl. Part. Sci. **55**, 229 (2005).

397. J. A. Casas, J. R. Espinosa and I. Hidalgo, JHEP **0503**, 038 (2005).

398. H. -C. Cheng and I. Low, JHEP **0309**, 051 (2003).

399. M. S. Carena, J. Hubisz, M. Perelstein and P. Verdier, Phys. Rev. **D75**, 091701 (2007).

400. ATLAS Collab., ATLAS-CONF-2012-147, ATLAS-CONF-2012-109 and ATLAS-CONF-2013-024. CMS Collab., CMS-PAS-EXO-12-048 and CMS-SUS-12-028.

401. CMS Collab., CMS-PAS-B2G-12-015. ATLAS Collab., ATLAS-CONF-2013-060.

402. R. S. Chivukula, M. Narain, and J. Womersley, in this review.

403. H. Georgi, A. E. Nelson and A. Manohar, Phys. Lett. **B126**, 169 (1983). A. E. Nelson and M. J. Strassler, JHEP **0009**, 030 (2000) S. Davidson, G. Isidori and S. Uhlig, Phys. Lett. **B663**, 73 (2008).

404. C. Csaki, A. Falkowski and A. Weiler, JHEP **0809**, 008 (2008). B. Keren-Zur, P. Lodone, M. Nardecchia, D. Pappadopulo, R. Rattazzi and L. Vecchi, Nucl. Phys. **B867**, 429 (2013).

405. K. Agashe, R. Contino and A. Pomarol, Nucl. Phys. **B719**, 165 (2005).

406. O. Matsedonskyi, G. Panico and A. Wulzer, JHEP **1301**, 164 (2013). M. Redi and A. Tesi, JHEP **1210**, 166 (2012). D. Marzocca, M. Serone and J. Shu, JHEP **1208**, 013 (2012). A. Pomarol and F. Riva, JHEP **1208**, 135 (2012).

407. R. Contino and G. Servant, JHEP **0806**, 026 (2008). J. Mrazek and A. Wulzer, Phys. Rev. **D81**, 075006 (2010).

408. A. De Simone, O. Matsedonskyi, R. Rattazzi and A. Wulzer, JHEP **1304**, 004 (2013). A. Azatov, M. Salvarezza, M. Son and M. Spannowsky, arXiv:1308.6601 [hep-ph].

409. A. Falkowski, Phys. Rev. **D77**, 055018 (2008). I. Low and A. Vichi, Phys. Rev. **D84**, 045019 (2011). A. Azatov and J. Galloway, Phys. Rev. **D85**, 055013 (2012). C. Delaunay, C. Grojean and G. Perez, JHEP **1309**, 090 (2013).

410. A. Banfi, A. Martin and V. Sanz, arXiv:1308.4771 [hep-ph]. A. Azatov and A. Paul, arXiv:1309.5273 [hep-ph]. C.Grojean, E.Salvioni, M.Schlaffer, A.Weiler, arXiv:1311.xxxx [hep-ph].

411. R. Contino, L. Da Rold and A. Pomarol, Phys. Rev. **D75**, 055014 (2007).

412. K. Agashe, R. Contino and A. Pomarol, Nucl. Phys. **B719**, 165 (2005).

413. D. Pappadopulo, A. Thamm and R. Torre, JHEP **1307**, 058 (2013). M. Montull, F. Riva, E. Salvioni and R. Torre, arXiv:1308.0559 [hep-ph].

414. M. Ciuchini, E. Franco, S. Mishima and L. Silvestrini, JHEP **1308**, 106 (2013).

415. C. Grojean, O. Matsedonskyi and G. Panico, arXiv:1306.4655 [hep-ph].